

# **Assessment of Seismic Risk for Subsea Production Systems in the Gulf of Mexico**

by

**Laura Ann Brown, M.S., Texas A&M University  
Joseph M. Bracci, Mary Beth Hueste, J. Don Murff, Texas A&M University**

**Final Project Report Prepared for the Minerals Management Service  
Under the MMS/OTRC Cooperative Research Agreement  
1435-01-99-CA-31003  
Task Order 18204  
Project Number 422**

**December 2003**

OTRC Library Number: 12/03A136

“The views and conclusions contained in this document are those of the authors and should not be interpreted as representing the opinions or policies of the U.S. Government. Mention of trade names or commercial products does not constitute their endorsement by the U. S. Government”.



*For more information contact:*

**Offshore Technology Research Center**

Texas A&M University  
1200 Mariner Drive  
College Station, Texas 77845-3400  
(979) 845-6000

or

**Offshore Technology Research Center**

The University of Texas at Austin  
1 University Station C3700  
Austin, Texas 78712-0318  
(512) 471-6989

*A National Science Foundation Graduated Engineering Research Center*

## ABSTRACT

The number of subsea production systems placed in deepwater locations in the Gulf of Mexico (GOM) has increased significantly in the last ten to fifteen years. Currently, API-RP2A (2000 a,b) designates the GOM as a Zone 0 seismic risk area, indicating an area of low seismic activity with an expected horizontal ground motion of less than 0.05g, and thus does not require seismic effects to be considered during the design process. However, there have been a number of seismic events with Richter magnitudes between 3.0 and 4.9 that have occurred in this region. As a result, questions have been raised regarding the seismic performance of deepwater subsea systems.

This study presents an analytical parametric study where a prototype subsea structure was selected based on a survey of subsea systems. The baseline analytical model consisted of a single casing embedded in soft clay soils, which supported a lumped mass at a cantilevered height above the soil. A number of the model characteristics were varied in the parametric study to simulate the structural response of a range of subsea structures. This study examined the impact of API-RP2A Zone 1 and 2 design seismic demands for the performance of subsea structures to provide a conservative bound for the performance of a Zone 0 area such as the Gulf of Mexico. The results from the subsequent analyses show that the stresses and deflections produced by the Zone 1 and 2 peak ground accelerations fall within the allowable design limits.

## TABLE OF CONTENTS

	Page
ABSTRACT .....	ii
TABLE OF CONTENTS .....	iii
LIST OF FIGURES.....	vi
LIST OF TABLES .....	x
1. INTRODUCTION .....	1
1.1. Background .....	1
1.2. Objectives and Methodology .....	4
1.3. Thesis Outline .....	8
2. LITERATURE REVIEW .....	9
2.1. Introduction .....	9
2.2. Modeling and Analysis.....	9
2.2.1. General .....	9
2.2.2. Hydrodynamic Effects.....	12
2.2.3. Forces Due to Waves and Currents .....	14
2.2.4. Soil-Casing Interaction for Soft Clays .....	15
2.2.5. Spectral Analysis Method .....	19
2.2.6. Time History Analysis .....	23
2.3. Previous Seismic Research of Offshore Systems.....	24
2.3.1. Offshore Ground Motions .....	24
2.3.2. Seismic Analysis of Fixed Platforms .....	27
2.3.3. Pile Behavior Under Seismic Loading .....	31
2.3.4. Subsea Pipelines Under Seismic Loading.....	34
2.3.5. Conclusion.....	37
3. SEISMIC DESIGN CRITERIA AND SEISMIC ACTIVITY IN THE GULF OF MEXICO.....	39
3.1. Introduction .....	39
3.2. Seismic Design Criteria.....	39
3.2. Seismicity of the Gulf of Mexico.....	42
4. SUBSEA SYSTEMS .....	48
4.1. Introduction .....	48
4.2. Overview of Subsea Systems .....	48

	Page
4.2.1. General .....	48
4.2.2. Wellhead Completion Equipment .....	49
4.2.3. Templates .....	52
4.2.4. Manifold Systems.....	54
4.2.5. Subsea Systems in the Gulf of Mexico .....	55
5. STRUCTURAL MODELS AND ANALYSIS PROCEDURES.....	60
5.1. Introduction .....	60
5.2. Description of Analytical Model.....	60
5.2.1. Prototype Structure.....	60
5.2.2. Baseline Analytical Model .....	62
5.2.3. Modeling Parameters.....	67
5.2.4. Details of the Time History Analysis Model .....	70
5.3. Analysis Procedures .....	72
5.3.1. General .....	72
5.3.2. Calculation of Equivalent Soil-Casing Stiffness.....	73
5.3.3. Time History Analysis Method.....	79
5.3.4. Calculation of Force and Stress Values.....	79
6. ANALYTICAL RESULTS .....	84
6.1. Introduction .....	84
6.2. Parametric Study .....	84
6.2.1. Results for the Baseline Model .....	84
6.2.2. Variation of Soil-Casing Stiffness.....	85
6.2.3. Variation of Casing Size .....	90
6.2.4. Variation of Mudline Strength and Strength Gradient of the Soil .....	94
6.2.5. Variation of Mass Height Above the Mudline .....	101
6.2.6. Variation of Mass .....	105
6.2.7. Variation of Mass and Mass Height Above the Mudline.....	109
6.2.8. Fixity Variation .....	114
6.2.9. Summary of Parametric Study Results.....	118
6.3. Time History Analysis Results.....	126
6.4. Conclusion.....	130
7. SUMMARY AND CONCLUSIONS .....	131
7.1. Summary .....	131
7.2. Conclusions .....	133
7.3. Recommendations .....	135
REFERENCES.....	136
APPENDIX A. SAMPLE CALCULATIONS .....	143

	Page
A.1. Introduction .....	143
A.2. Calculation of Input Values for BMCOL 76.....	143
A.3. Calculation of Soil-Casing Stiffness .....	145
A.4. Calculation of Stresses and Displacements.....	147

## LIST OF FIGURES

FIGURE	Page
2.1. Simplified Structural Model.....	10
2.2. Response Spectra, El Centro Earthquake, May 18, 1940 (Newmark and Hall 1987).....	20
2.3. Design Spectra Taken from API-RP2A (API 2000 a,b) .....	23
2.4. Elevation View of Model Platform for Ground Motion Comparison Study (Smith 1997).....	26
2.5. Illustration of Computer Model F (Boote et al. 1998) .....	30
2.6. Impact of Earthquake Magnitude and Proximity on Pipeline (Jones 1985) .....	35
3.1. API-RP2A Seismic Risk of Map of Coastal Waters in Contiguous United States (API 2000 a,b) .....	42
3.2. Recorded Earthquakes in GOM Region and Bay of Campeche Region (Latitude Range 18°- 32° and Longitude Range -98° to -82°) .....	45
4.1. Subsea Wellhead System (API 1996) .....	49
4.2. Tubing Hangar Installation (API 1996) .....	51
4.3. Subsea Completion Loads and Reactions (API 1996) .....	51
4.4. Diagram of Well Spacer/Support Template (API 1996).....	52
4.5. Deepwater Subsea Systems and Recorded Earthquake Epicenters in the Gulf of Mexico.....	57
4.6. Gemini Subsea Development (Beer and Jeffries 2000) .....	58
4.7. Zinc Template/Manifold – Elevation (Bednar 1993).....	59
5.1. Advertisement for Kvaerner Subsea Christmas Tree (Kvaerner 2001) .....	62
5.2. Free-Headed and Fixed-Headed Analytical Models .....	63

FIGURE	Page
5.3. Lumped Mass Model for Time History Analysis.....	71
5.4. 1940 El Centro, California Earthquake Acceleration Record (COSMOS 2003).....	72
5.5. Force Versus Displacement Curve.....	76
5.6. API Design Spectra (API 2000 a,b).....	78
6.1. Change in Period Due to Variation of Soil-Casing Stiffness.....	88
6.2. Change in Displacement Due to Variation of Soil-Casing Stiffness.....	88
6.3. Change in Shear Stress Due to Variation of Soil-Casing Stiffness.....	89
6.4. Change in Bending Stress Due to Variation of Soil-Casing Stiffness.....	89
6.5. Change in Period Due to Variation of Casing Size.....	92
6.6. Change in Deflections Due to Variation of Casing Size.....	92
6.7. Change in Shear Stress Due to Variation of Casing Size.....	93
6.8. Change in Bending Stress Due to Variation of Casing Size.....	93
6.9. Change in Period Due to Variation of Mudline Strength.....	97
6.10. Change in Deflection Due to Variation of Mudline Strength.....	97
6.11. Change in Shear Stress Due to Variation of Mudline Strength.....	98
6.12. Change in Bending Stress Due Variation of Mudline Strength.....	98
6.13. Change in Period Due to Variation of Strength Gradient.....	99
6.14. Change in Deflection Due to Variation of Strength Gradient.....	99
6.15. Change in Shear Stress Due to Variation of Strength Gradient.....	100
6.16. Change in Bending Stress Due Variation of Strength Gradient.....	100
6.17. Change in Period Due to Variation of Mass Height.....	103

FIGURE	Page
6.18. Change in Displacement Due to Variation of Mass Height .....	103
6.19. Change in Shear Stress Due to Variation of Mass Height .....	104
6.20. Change in Bending Stress Due to Variation of Mass Height .....	104
6.21. Change in Period Due to Variation of Mass.....	107
6.22. Change in Displacement Due to Variation of Mass .....	107
6.23. Change in Shear Stress Due to Variation of Mass .....	108
6.24. Change of Bending Stress Due to Variation of Mass.....	108
6.25. Change in Period Due to Variation of Mass and Height.....	112
6.26. Change in Displacement Due to Variation of Mass and Height .....	112
6.27. Change in Shear Stress Due to Variation of Mass and Height.....	113
6.28. Change in Bending Stress Due to Variation of Mass and Height .....	113
6.29. Comparison of Period Values Obtained from Free-Headed and Fixed-Headed Casings.....	116
6.30. Comparison of Displacement Values Obtained from Free-Headed and Fixed-Headed Casings.....	116
6.31. Comparison of Shear Stress Values Obtained from Free-Headed and Fixed- Headed Casings .....	117
6.32. Comparison of Bending Stress Values Obtained from Free-Headed and Fixed-Headed Casings.....	117
6.33. Range of Period Values for Parameter Variations – Free Headed Pile.....	119
6.34. Range of Maximum Displacement Values for Parameter Variations .....	122
6.35. Range of Shear Stress Values for Parameter Variations. ....	124
6.36. Range of Bending Stress Values for Parameter Variations.....	126

FIGURE	Page
6.37. Acceleration Record from 1940 El Centro, CA Earthquake .....	128
6.38. Response Spectra and API Design Spectra .....	128
6.39. Accelerations Obtained from Time History Analysis .....	129
6.40. Shear Forces Obtained from Time History Analysis .....	129
A.1. Force-Displacement Curve for Baseline Analytical Model .....	146
A.2. Zone 1 Casing Displacement Profile.....	150
A.3. Zone 2 Casing Displacement Profile.....	150
A.4. Zone 1 Casing Shear Profile.....	151
A.5. Zone 2 Casing Shear Profile.....	151
A.6. Zone 1 Casing Moment Profile .....	152
A.7. Zone 2 Casing Moment Profile .....	152

## LIST OF TABLES

TABLE	Page
3.1. Recorded Earthquakes in the Gulf of Mexico Region (Latitude Range 20° to 32° and Longitude Range -98° to -82°) (USGS 2003).....	43
3.2. Recorded Earthquakes in Bay of Campeche Region (Latitude Range 18° to 20° and Longitude Range -98° to -90°) (USGS 2003).....	44
4.1. Dimensions and Weights of Modules (Goodfellow Associates 1990) .....	53
4.2. Partial Listing of Some Deepwater Subsea Systems Located in GOM .....	56
5.1. Characteristics of the Baseline Analytical Model .....	64
5.2. Loadings and Stresses Due to Current with Specified Velocities .....	67
5.3. Variation of Range of Soil-Casing Stiffness .....	68
5.4. Variation of Casing Size .....	69
5.5. Variation of Mudline Strength .....	69
5.6. Variation of Strength Gradient.....	69
5.7. Variation of Mass and Height .....	70
5.8. Variations for Fixed-Headed Casing Models.....	70
5.9. Values of <i>p-y</i> Curve for Soft Clays (API 2000 a,b) .....	74
6.1. Baseline Model (CC) Results.....	85
6.2. Response Spectra Calculations for Variation of Soil-Casing Stiffness.....	87
6.3. Force and Stress Values for Variation of Soil-Casing Stiffness .....	87
6.4. BMCOL76 and Response Spectra Calculations for Variations of Casing Size .....	91
6.5. Resulting Force and Stress Values for Variation of Casing Size .....	91

TABLE	Page
6.6. BMCOL76 and Response Spectra Calculations for Variation of Mudline Strength .....	95
6.7. Force and Stress Values for Variation of Mudline Strength .....	95
6.8. BMCOL76 and Response Spectra Calculations for Variation of Strength Gradient .....	96
6.9. Force and Stress Values for Variation of Strength Gradient.....	96
6.10. BMCOL76 and Response Spectra Calculations for Variation of Mass Height ....	102
6.11. Resulting Force and Stress Values for Height Variations.....	102
6.12. BMCOL 76 and Response Spectra Calculations for Variation of Mass .....	106
6.13. Force and Stress Values for Variation of Mass.....	106
6.14. BMCOL76 and Response Spectra Calculations for Variation of Mass and Height .....	110
6.15. Force and Stress Values for Variation of Mass and Height .....	111
6.16. BMCOL76 and Response Spectra Calculations for Fixed-Headed Casing .....	115
6.17. Force and Stress Values for Fixed-Headed Casing.....	115
6.18. Summary of Results for Parameter Variation .....	118
6.19. Summary of Period Data from Parametric Study – Fixed-Headed Pile.....	119
6.20. Summary of Period Data from Parametric Study – Free-Headed Pile.....	120
6.21. Summary of Deflection Data from Parametric Study – Free-Headed Pile .....	121
6.22. Summary of Deflection Data from Parametric Study – Fixed-Headed Pile .....	122
6.23. Summary of Shear Stresses from Parametric Study – Free-Headed Pile.....	123

TABLE	Page
6.24. Summary of Shear Stresses from Parametric Study – Fixed-Headed Pile.....	124
6.25. Summary of Bending Stresses from Parametric Study – Free-Headed Pile .....	125
6.26. Summary of Bending Stresses from Parametric Study – Fixed-Headed Pile .....	126
6.27. Time History Analysis Results (SAP2000 1999).....	127
A.1. Required Soil and Casing Properties for BMCOL76 Analysis.....	144
A.2. <i>P-y</i> Curve Values for Soft Clays (API 2000 a,b).....	144
A.3. Lateral Soil Resistance Properties for BMCOL76 Input .....	145
A.4. Deflections Obtained from BMCOL76.....	146
A.5. Soil-Casing Calculations for Zone 1 .....	147
A.6. Soil-Casing Calculations for Zone 2 .....	147
A.7. Summary of Results from Soil-Casing Calculations.....	147
A.8. Summary of Displacement and Stress Results .....	149

# 1. INTRODUCTION

## 1.1. BACKGROUND

The use of subsea systems at deep water sites in the Gulf of Mexico has become increasingly popular in recent years due to the growing demand for energy and continuing advances in the construction, placement and maintenance of subsea systems (Deluca 2002). With this increase, questions have been raised about the performance of these deep water subsea systems during earthquakes. The potential vulnerabilities of subsea systems during earthquakes are created by the earthquake shaking itself, liquefaction potential, and dynamic impact from soil sliding due to nearby slope instability. The focus of this research is to evaluate the shaking performance of subsea systems placed in deep water environments in the Gulf of Mexico during potential earthquakes.

Historically, the Gulf of Mexico (GOM) has played a key role in providing energy resources for the United States. Even as the exploration and development of other regions has slowed, the GOM continues to see new construction throughout the region. In addition, the technological advances in the construction, placement, and maintenance of offshore structures have kept pace with the increasing demand for energy. These advances have provided energy companies with a means of producing

---

This report follows the style and format of the *ASCE Journal of Structural Engineering*.

oil and gas from sites which were previously inaccessible because of their extreme water depths. Critical improvements in technology include the development of subsea systems capable of retrieving and pre-processing oil and gas at sites located miles away from the host platform. As a result, resources can be accessed at sites where the expected production, water depth, or other conditions would not justify the construction of a platform.

As companies employ new technologies in order to extend developments out into deeper waters, it is important to assess their seismic adequacy. For this reason, research in areas such as seabed technology and deepwater construction is necessary to study their seismic performance. The Minerals Management Service funded several projects that researched different aspects of offshore systems in deepwater environments (Smith 1997).

Currently, the use of these deep water systems is primarily concentrated in the eastern GOM, south of Louisiana. A few examples of these developments include Gemini, Zinc, Mensa, and Canyon Express. The Gemini development is located at a water depth of approximately 1040 m at a site 145 km southeast of New Orleans (Coleman and Isenmann 2000). Zinc is located in the Mississippi Canyon in 445 m of water at a site with highly unconsolidated soil (Bednar 1993). Also located in the Mississippi Canyon, at a water depth of 1615 m, Mensa consists of a manifold with a template base set on the seafloor (McLaughlin 1998). To date, one of the deepest

subsea tiebacks is Canyon Express (extending through the Mississippi and Desoto Canyon areas), which collects and transports gas from fields with depths ranging from 2015 to 2215 m (Deluca 2002).

One of the controlling factors in the design of offshore structures is the effect of environmental loads due to wave, current, wind and geologic activity. According to the American Petroleum Institute (API) in document API-RP2A (API 2000 a,b); earthquake shaking, fault movement, and sea floor instability are all geologic processes that must be accounted for in the design. Because subsea systems are located directly on the seafloor, the processes mentioned above could play an important role in the design and placement of these systems. The focus of this research is directed exclusively toward the evaluating the performance of subsea systems during potential earthquake shaking.

API outlines the loads to be considered for the design of subsea structural systems in RP17A (API 1996) and RP2A (API 2000 a,b). These loads include gravity loads, externally applied loads caused by risers or pipelines, thermal stresses, and environmental loads. The guidelines in RP2A, for both the WSD and the LRFD versions, specify the procedures for determining expected environmental loads, such as those produced by earthquakes.

The seismic risk map presented in API-RP2A (API 2000 a,b) indicates that the majority of the GOM is zoned at a peak ground acceleration of less than 0.05g. Although the seismic risk is low, earthquakes have occurred in the GOM. The strongest measured event for this region since 1978 was a magnitude 4.9 earthquake, which occurred near the Mississippi Fan region of the GOM. Crustal subsidence due to sedimentation loading, measured at a rate of 0.2 inches per year, was the most probable cause of this particular event (Frohlich 1982). Seismic events taking place in other areas of the GOM seem to be associated with the plate boundaries in Mexico, Central America, and the Caribbean (Frohlich 1982). Based on the information shown, the GOM has a low level of seismic activity. As a result, the seismic data available in this region is very limited. Although this is the case, there have been seismic events in the region and such events may impact the operability, stability and safety of subsea systems. Therefore, investigating the response and vulnerability of subsea structures under probable seismic loading in the GOM is appropriate.

## **1.2. OBJECTIVES AND METHODOLOGY**

The focus of this research is to assess the vulnerability of subsea production systems in the GOM when subjected to earthquake motions. In order to accomplish this objective, a parametric study of a prototype subsea structure was conducted for a number of structural and geologic variations. The information used to establish the

parameter variations was based on results from research of seismic conditions in the region, information provided by API guidelines, and publications about deep water subsea production systems in the GOM. The parametric study and subsequent analyses were achieved by utilizing a methodology consisting of five basic tasks. The tasks performed to complete this research are outlined below.

### **Task 1: Review of Seismic Activity in the Gulf of Mexico**

The first task is focused on gathering information on the historical seismicity and identifying current seismic risk for the GOM. The scope of information to be gathered for this study includes the frequency, intensity and location of recorded events; and geological features that would affect the seismicity of a given site within the region. This information is needed to characterize the overall seismic risk for subsea structures. One important consideration is the concentration of seismic activity relative to the areas undergoing the most development. The primary source of information for recorded earthquakes in the GOM is the website for the National Earthquake Information Center (USGS 2003), which contains recorded events for this region dating back to 1973.

### **Task 2: Conduct a Survey of Subsea Structures**

Conduct a survey to identify subsea structures currently located in deep water sites in the GOM and search for general information on subsea structures. The information gathered from the survey of existing subsea structures in the GOM

includes location, water depth at the site, type of structure, geometric properties, function, site conditions, and any other available details that may be pertinent for this research. The knowledge accumulated from this portion of the research is used to select the prototype structures for the parametric study. Load cases considered for the design of these structures, such as externally applied loads from connecting elements, gravity loads, thermal stresses, and environmental loads, are also identified.

### **Task 3: Identify Design Criteria**

The third task involves identifying currently accepted practice for assessing the adequacy of an offshore structure for seismic loading. It should be noted that most of the literature that addresses the issue of seismic design for offshore structures is intended for the design of large fixed platforms. The guidelines provided by API are generally accepted standards for the design of offshore structures. API-RP17A, a publication that is focused on the design of subsea production systems, provides general information about the loads experienced by subsea structures (API 1996). As specified by API-RP17A, API-RP2A provides criteria for calculating expected environmental loads in an offshore environment.

### **Task 4: Develop Prototype Model and Analysis Procedures**

Based on the literature review and API guidelines, models and analysis procedures are developed to assess subsea systems under seismic loads. The baseline model

used in the parametric study is a free-headed single casing system with characteristics derived from an advertisement for a subsea Christmas tree (Kvaerner 2001) in a trade magazine. Parameters are varied to simulate the behavior of a range of subsea structures. The BMCOL76 program (BMCOL76 1981) is used to obtain deflections and forces for an embedded casing with specific geometry, loads, and soil conditions. Soil casing spring values are derived based on the results from the BMCOL76 program and the design response spectra shown in Figure C2.3.6-2 of API-RP2A for both Zone 1 and Zone 2 accelerations and soil type C (API 2000 a,b).

#### **Task 5: Evaluation of Results**

The final task is focused on evaluating the seismic vulnerability of deep water subsea structures in the GOM. Results from the parametric study using elastic analysis provide a range of displacements, accelerations, and applied stresses describing the overall behavior of the model under earthquake loading. The results from the study of free-headed casings are applicable to single casing systems such as a subsea Christmas tree. Analyses of fixed head models are conducted to evaluate structures with multiple casings such as subsea templates. A comparison is made between the resulting stresses and the allowable design stresses for each structure.

### **1.3. REPORT OUTLINE**

This section provides a general background of the development of subsea production systems for deepwater applications and the overall seismic risk associated with the GOM. The second section of this report gives an overview of the theory related to the analysis procedures used for this study and outlines some of the past research associated with offshore seismic design and subsea production systems. Section 3 summarizes the API guidelines for offshore seismic design and presents information gathered on the seismic activity in the GOM. A brief overview of subsea systems is presented in the fourth section, along with some examples of deepwater subsea systems used in the GOM. Section 5 presents information regarding the structural models and analyses used for the parametric study. The results of the parametric study, as well as a discussion of the findings, are given in Section 6. Section 7 contains the conclusions and recommendations derived from this study.

## **2. LITERATURE REVIEW**

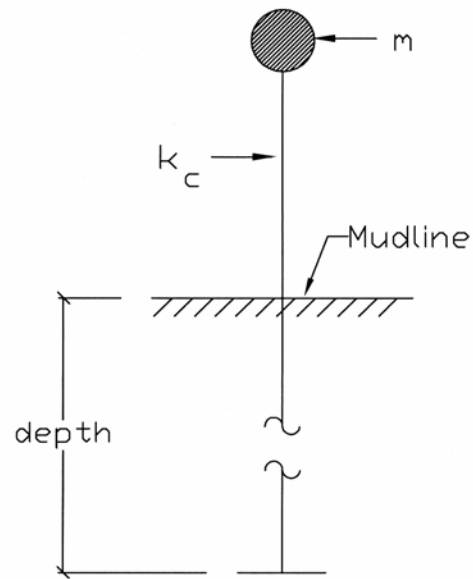
### **2.1. INTRODUCTION**

This section presents an overview of topics related to seismic risk assessment of deepwater subsea systems. Literature specific to this area is extensive; so a limited number of publications that address topics pertinent to the modeling and analysis procedures were selected for this study. In addition, literature addressing previous research related to offshore structures subjected to seismic loading is discussed.

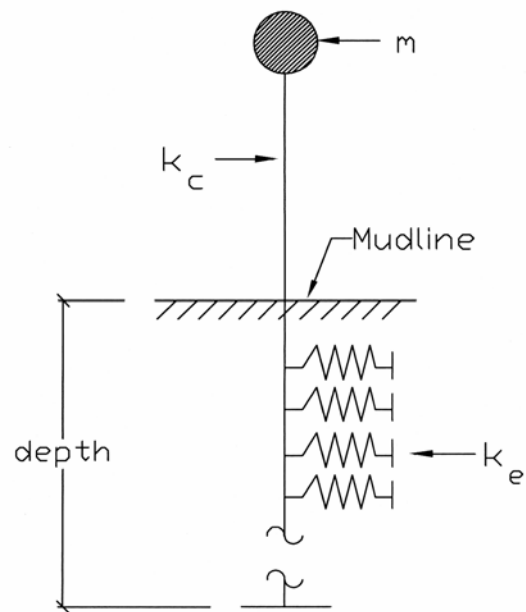
### **2.2. MODELING AND ANALYSIS**

#### **2.2.1. General**

Information describing a structure, its surrounding soil conditions, and the expected seismic demands are crucial for modeling and predicting the expected structural response during earthquakes. Fig. 2.1 depicts the basic simplified physical and analytical models of a structure with lumped mass,  $m$ , structural stiffness,  $k_c$ , and soil properties shown as a series of equivalent soil springs,  $k_e$ . Structural and soil properties, along with the intensity and frequency characteristics of the ground motions, play important roles in the performance of a structure during earthquakes.



**(a) Physical Model**



**(b) Analytical Model**

**FIG. 2.1 Simplified Structural Model**

The basic equation of motion for a single degree of freedom (SDOF) linear elastic system is shown below (Chopra 1995).

$$f_I + f_D + f_S = 0 \quad (2.1)$$

Where:

$$\begin{aligned} f_I &= m\ddot{u}_i(t) = \text{Inertia force (kN)} \\ f_D &= c\dot{u}(t) = \text{Damping force (kN)} \\ f_S &= ku(t) = \text{Spring force (kN)} \\ \ddot{u}_i(t) &= \ddot{u}(t) + \ddot{u}_g(t) = \text{Total acceleration of the mass (m/s}^2\text{)} \\ m &= \text{Mass of the system (see Sect. 2.2.1 for more details) (kg)} \\ c &= \text{Equivalent linear viscous damping coefficient of the system (kg/s)} \\ k &= \text{Stiffness of the system (kN/mm)} \\ u(t) &= \text{Relative displacement between the mass and ground (mm)} \\ \dot{u}(t) &= \text{Relative velocity of the mass with respect to the ground (m/s)} \\ \ddot{u}(t) &= \text{Relative acceleration of the mass with respect to the ground (m/s}^2\text{)} \\ \ddot{u}_g(t) &= \text{Acceleration of the ground from the earthquake (m/s}^2\text{)} \end{aligned}$$

Substituting these terms into Eq. 2.1 and rearranging the inertia force terms yields the following expression:

$$m\ddot{u}(t) + c\dot{u}(t) + ku(t) = -m\ddot{u}_g(t) \quad (2.2)$$

Further manipulation of the expression will produce the following equation:

$$\ddot{u}(t) + 2\zeta\omega_n\dot{u}(t) + \omega_n^2u(t) = -\ddot{u}_g(t) \quad (2.3)$$

Where:

$$\begin{aligned}\zeta &= \text{Damping ratio} \\ \omega_n &= \text{Natural frequency of the system, which is defined as } \sqrt{k/m} \text{ (rad/s)}\end{aligned}$$

The overall stiffness, damping and mass of an offshore system are dependent upon the properties of the structure, the soil upon which the structure is founded, and the water surrounding the structure. These properties, as well as the characteristics of a given ground motion record, influence the stresses and displacements acting on the structure during an earthquake. The response spectrum and time history analyses are two methods commonly employed to estimate the elastic response of structural systems during earthquakes. The following subsections provide information on these methods, as well as the procedures used to estimate hydrodynamic effects, wave and current loads, and the soil casing interaction in soft clays.

### **2.2.2. Hydrodynamic Effects**

The lateral motion of a structure placed in water is influenced by the effect of hydrodynamic interaction, which can impact the mass and damping characteristics of the structure (Liaw and Reimer 1975). An object submerged in fluid will be subjected to forces generated by the movement of the object through fluid (Han and Xu 1996). The method used to estimate hydrodynamic effects is dependent upon the shape and size of the object as well as the nature of the forces causing the object to move.

The added mass method is a simplified approach to approximate the effects of hydrodynamic interaction. Because it is assumed that the motion of an object or structure in water corresponds to a steady periodic motion, the acceleration of this structure will also be periodic. In addition, because this method assumes that the hydrodynamic pressure is in phase with respect to the periodic acceleration of the structure, the impact on the damping characteristics is negligible (Liaw and Reimer 1975). In this approach, the force is the product of the mass of the fluid displaced by the movement of the object (“added mass”) and the acceleration of the object. As stated in API-RP2A, the mass used for the dynamic analysis of an offshore structure should include the mass of the structure, fluids contained within the structure, appurtenances, and the added mass (API 2000a,b). In other words, mass is added to the mass of the structure and its contents for dynamic analysis in order to account for hydrodynamic effects. The total mass to be used for dynamic analysis can be described using the following expression:

$$m = m_s + m_c + m_a + m_f \quad (2.4)$$

Where:

- $m$  = Mass of the system (kg)
- $m_s$  = Mass of the structure (kg)
- $m_c$  = Mass of the contents contained within structure (kg)
- $m_a$  = Mass of appurtenances (kg)
- $m_f$  = Mass of the volume of fluid displaced by the structure (added mass) (kg)

### 2.2.3. Forces Due to Waves and Currents

Another important environmental factor in the structural design of offshore structures is the force generated by waves and currents. API-RP17A indicates that loads generated by currents affect the structural design of subsea systems (API 1996). The direction, strength and other characteristics of these forces are influenced by a number of different factors. The height, shape, and velocity of surface waves are influenced primarily by wind characteristics (API 2000 a,b). Three common types of currents are storm-generated currents, tidal currents, and circulatory currents. Because of the various ways these forces are created, predicting the direction, wave height, and velocity is complicated. A thorough evaluation of the installation site is necessary in order to gain the necessary information required to estimate wave and current characteristics for structural design of an offshore structure.

There are several methods available for estimating the wave and current profiles used to determine the forces acting on an offshore structure. The method used to estimate water particle velocity and acceleration due to waves and currents includes the contributions of the observed conditions at the installation site and the complexity of the proposed offshore structure. Once these quantities are known, the expression known as Morison's equation (Dean and Borgman 1986) can be used to obtain the forces experienced by individual elements in the structure. This expression, seen in Eq. 2.5, is typically used to quantify the wave or current forces acting on slender cylindrical elements.

$$f(t) = \left[ \frac{C_D \rho D}{2} v |v| + \frac{C_m \rho \pi D^2}{4} \dot{v} \right] \Delta S \quad (2.5)$$

Where:

- $C_D$  = Drag coefficient
- $C_m$  = Inertia coefficient
- $v$  = Velocity of the water (m/s)
- $\dot{v}$  = Acceleration of the water (m/s<sup>2</sup>)
- $\Delta S$  = Length of the element (m)
- $\rho$  = Density of water (kN/m<sup>3</sup>)

Both the drag coefficient and the inertia coefficient are dependent upon the shape of the structural element.

It should be noted that the subsea systems included in this study are located at deepwater sites, where wave interaction is negligible. On the other hand, mudline currents at these depths can be significant. Although this is the case, the mudline currents are neglected in this work.

#### **2.2.4. Soil-Casing Interaction for Soft Clays**

Structural response to lateral loading is heavily dependent upon the soil conditions, the foundation type, and the interaction between the structure and soil. Modeling soil-structure interaction for the casings (herein referred to as piles) is critical in determining the seismic response of a subsea structure. The characteristics of the soil-pile behavior

are dependent upon the soil and structural geometry, along with the elastic behavior of the pile.

The relationship between the pile and surrounding soil can be modeled as a complex beam-column placed on an inelastic foundation. The soil is represented as a series of uncoupled springs which act along the pile to resist lateral forces applied to the structure (refer to Fig. 2.1). The governing equation which describes the lateral response of the pile to static loads (Cox and McCann 1986).

$$EI \frac{d^4 y}{dx^4} - \frac{d}{dx} \left( \frac{Rf'_0(x)}{dx} \right) + \frac{d^2(Qy)}{dx^2} + E_s y = p_0 + \frac{d}{dx} \left( \frac{T}{dx} \right) \quad (2.6)$$

Where:

- $E$  = Modulus of elasticity of the pile (kPa)
- $I$  = Moment of inertia of the pile (mm<sup>4</sup>)
- $y$  = Lateral displacement of the pile at some point  $x$  along the length of the pile (mm)
- $x$  = Coordinate along the pile axis (mm)
- $R$  = Load-displacement rate for a rotational restraint (kN/mm)
- $Q$  = Axial load acting on the pile (kN)
- $T$  = Applied moment (kN-m)
- $E_s$  = Load displacement rate for the soil (kPa)
- $p_0$  = Applied distributed lateral load along the pile (shown as  $p$  in Fig. 2.2) (kN/mm)
- $f'_0(x) = \frac{dy}{dx} = \text{slope}$

The solution to this equation can be obtained through the use of difference equation techniques (Reese and Wang 1986), which includes the use of the expression shown in Eq. 2.7, with each term described in Eqs. 2.8 through 2.13.

$$a_i y_{i-2} + b_i y_{i-1} + c_i y_i + d_i y_{i+1} + e_i y_{i+2} = f_i \quad (2.7)$$

$$a_i = F_{i-1} - 0.25hR_{i-1} \quad (2.8)$$

$$b_i = -2(F_{i-1} + F_i) + h^2 Q_{i-1} \quad (2.9)$$

$$c_i = F_{i-1} + 4F_i + F_{i+1} + 0.25h(R_{i-1} + R_{i+1}) - 2h^2 Q_{i-1} + h^4 E_s \quad (2.10)$$

$$d_i = -2(F_i + F_{i+1}) + h^2 Q_{i+1} \quad (2.11)$$

$$e_i = F_{i+1} - 0.25hR_{i+1} \quad (2.12)$$

$$f_i = h^3 P_i + 0.5h^2 (T_{i+1} - T_{i-1}) \quad (2.13)$$

Where:

- $h$  = Increment length along the pile (m)
- $F_i$  =  $EI$  (kN/mm)
- $P_i$  = Applied concentrated load,  $h \cdot p$  (kN)

Gaussian elimination can be used to obtain the solution of the expression in Eq. 2.7 with the appropriate boundary conditions and a sufficient number of increments along the length of the pile since the soil stiffness varies with displacement, the equations are nonlinear and an iterative solution technique are used (Reese and Wang 1986). The beam-column solution is used to calculate the displacement, slope, moment, shear, and lateral loading at each specified increment along the length of the pile (Cox and McCann

1986). These quantities are then used to determine the maximum axial, bending and combined stresses in the pile, which are in turn compared to the allowable stresses in a design procedure. It should be mentioned that in this idealization, the mass of the pile and soil are ignored, i.e. the pile response is treated as quasi-static behavior. This assumption is based on the fact that the soil pile system has very high natural frequencies relative to the primary exciting frequencies of the earthquakes. Thus the soil-pile system can be approximated by a simple non-linear spring system.

The soil resistance characteristics are described through the use of  $p$ - $y$  curves, which represent the soil resistance to pile displacement at a given location along the length of the pile. A few different approaches can be used to construct  $p$ - $y$  curves. Typically these curves are site specific and are constructed using stress-strain data obtained from soil samples taken from the location under consideration. In addition,  $p$ - $y$  curve construction is dependent upon the soil type (API 2000 a,b). Typically, the soils found in the GOM consist of soft clays; therefore, the corresponding  $p$ - $y$  curves for this soil type should be used. API-RP2A refers designers to “Correlations for Design of Laterally Loaded Piles in Soft Clay” (Matlock 1970) to obtain further information on the construction of  $p$ - $y$  curves for soft clay. This publication states that the shape of the  $p$ - $y$  curve is dependent upon the type of lateral load applied to the structure, as well as the pile stiffness, geometry and soil characteristics. For the research presented in Matlock’s paper,  $p$ - $y$  curves were developed using a combination of laboratory experiments, field testing, and numerical analysis. The objective was to confirm that a reasonable model of the soil-pile interaction could be

developed that was consistent with experiments and analysis. Based on the results of the study, Matlock concluded that soil resistance – deflection characteristics are nonlinear and inelastic, and that within a practical range, the characteristics of the  $p$ - $y$  curve were unaffected by the type of pile head restraint.

### **2.2.5. Spectral Analysis Method**

One approach to approximate the response of a structure during an earthquake event is the spectral analysis, or response spectrum, method. An elastic response spectrum shows the peak elastic response of a SDOF oscillator with constant damping as a function of natural period (or frequency) when subjected to a specified ground motion (Chopra 1995). A response spectrum plot typically consists of peak deformation, velocity, acceleration, or a combination of these values with respect to the natural period of the structure. The shape of a response spectrum of an actual earthquake record is often somewhat erratic. However, when the spectra are plotted on a logarithmic scale, as shown in Fig. 2.2, the general shape of the plot begins to resemble a trapezoid (Newmark and Hall 1987).

Use of the spectral analysis method for structural design is most appropriate for cases when the structure is expected to behave elastically (Chopra 1995). In general, available ground motion records are insufficient for the construction of a site specific design spectra. For this reason, the analysis is performed using a generalized design spectrum. The design spectrum is a smoothed curve based on statistical analysis of a variety of different ground motions. In order to perform the design of a structure at a specific

location, the spectrum is modified according to the characteristics of the area, including the soil type and the expected intensity of ground motions.

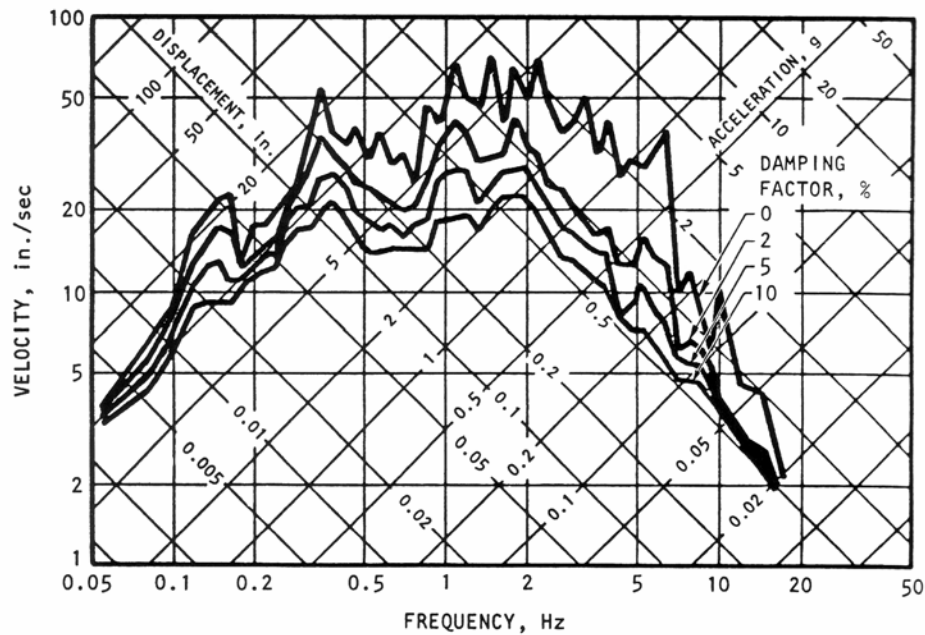


**FIG. 2.2. Response Spectra, El Centro Earthquake, May 18, 1940 (Newmark and Hall 1987)**

The design spectra in Fig. 2.3 are smooth idealized response spectra used to conduct spectral analysis when there is insufficient seismic data available for the development of a site specific response spectrum for the region of interest (API 2000 a,b). The plot depicts the relationship between  $S_A/G$  and the period of the structure, where  $S_A$  is the spectral acceleration and  $G$  is the acceleration of gravity. Three different soil classifications are represented on this plot. Soil type A is designated as a rock material with a shear wave velocity of 914 m/s or higher. Soil type B is designated as shallow strong alluvium or sands, silts and stiff clays with a shear strength greater than 72 kPa, that are limited to

depths of 61 m, with an overlying rock-like material. Soil type C is described as deep strong alluvium or sands, silts, and stiff clays with depths greater than 61 m. The spectrum is constructed for a critical damping ratio of five percent. This standardized response spectrum is adapted to the site through the use of an amplification factor related to the expected peak ground acceleration for the location. API-RP2A specifies that in the horizontal plane, the design response spectrum accelerations are to be applied to the structure equally in directions perpendicular to each other and half of the acceleration should be applied in the vertical plane of the structure (API 2000 a,b). The acceleration value obtained from the design spectra can then be used to calculate the spectral displacement, spectral velocity, shear force and overturning moment or shear and bending stresses, as shown below.

$$S_v = \frac{T}{2\pi} S_A \quad (2.14)$$

$$S_D = \frac{T^2}{4\pi^2} S_A \quad (2.15)$$

$$F = m * S_A \quad (2.16)$$

$$f_v = \frac{F}{A} \quad (2.17)$$

$$M = F * d \quad (2.18)$$

$$f_b = \frac{Mc}{I} \quad (2.19)$$

Where:

- $S_V$  = Spectral Velocity (m/s)
- $S_D$  = Spectral Displacement (m)
- $T$  = Fundamental period (s)
- $F$  = Shear force applied to structural element (kN)
- $f_v$  = Shear stress acting on structural element (kPa)
- $A$  = Area of structural element (m<sup>2</sup>)
- $M$  = Overturning moment acting on structural element (kN-m)
- $d$  = Length of the moment arm (m)
- $f_b$  = Bending stress acting on structural element (kPa)
- $I$  = Moment of inertia of structural element (mm<sup>4</sup>)
- $c$  = Distance from extreme edge to the centroid of structural element (mm)

Finally, the stress and displacement values obtained are compared to the allowable stresses and displacements to determine the adequacy of the element for the seismic demand.

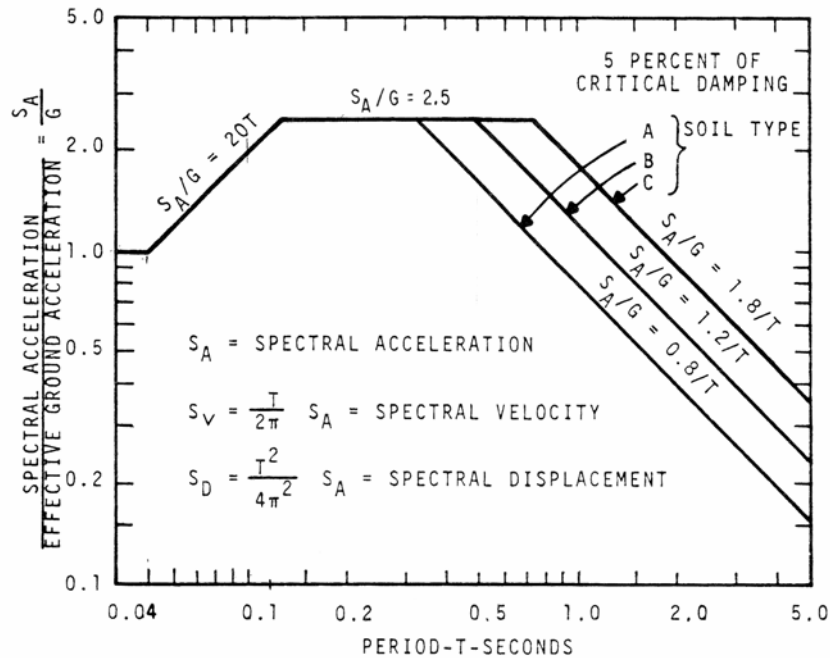


**FIG. 2.3. Design Spectra Taken from API-RP2A (API 2000 a,b)**

### 2.2.6. Time History Analysis

Time history analysis employs ground motion acceleration records of actual or synthetic earthquakes as a means of evaluating structural response. As with the response spectrum method, the ground motion records are scaled according to the seismicity of the region for design. With proper modeling, this analysis can be used to evaluate the response of structures that are behaving either linearly or nonlinearly during a seismic event. For this method, the records are scaled so that the corresponding response spectrum approximately matches the design spectrum for the region at the fundamental period of the structure. API-RP2A specifies that the acceleration time histories used in each orthogonal direction should be scaled in the same manner as the accelerations used for the spectral analysis (API 2000 a,b). The selection of the acceleration records is important because the

response of the structure is sensitive to the frequency content and magnitude of the accelerations (Nair and Kallaby 1986). Therefore, records should be used that contain characteristics representative of the conditions at the proposed installation site.

### **2.3. PREVIOUS SEISMIC RESEARCH OF OFFSHORE SYSTEMS**

The literature contains many studies on various aspects of earthquake analysis for offshore structures. The following subsections present research findings related to this study, including studies of the seismic behavior of fixed offshore platforms, piles, and subsea pipelines. Also included in this section is a summary of research related to the characteristics of ground motions at offshore locations. Although the topics covered by the studies cited in the following subsections are somewhat varied, each provides useful guidelines and insight for the investigation of the deepwater subsea systems considered in this study.

#### **2.3.1. Offshore Ground Motions**

Smith (1997) studied the differences between onshore and offshore ground motions. A comparison was made between measurements taken during the September 1981 Santa Barbara Island, California earthquake at nearby onshore and offshore locations. This event was selected because of the comparable epicentral distances to the land based instruments and the Seafloor Earthquake Measurement System (SEMS) instruments. The onshore site, SBVictor, was located 98 km from the epicenter of the earthquake and the

offshore site, SBHenry, was approximately 85 km. The platform model used for this study was approximately 185 m in height and located in 145 m of water (see Fig 2.4). The jacket was supported by a group of four piles at each of the four corners. A seismic response analysis was performed on the platform using the Santa Barbara Island records scaled to match the API spectrum with an acceleration of 0.25g. In addition, the soil stiffness was varied to simulate stiff clay, soft clay, and dense sand conditions.

Comparisons between the different soil types show that the periods obtained for the models founded in soft clays were between 101 and 162 percent of the values obtained from the models located in either stiff clay or dense sand. The vertical deflections observed for the offshore earthquake record were between 24.8 and 61.1 percent of the values observed for the onshore records. The total vertical accelerations generated by the offshore records were between 25.8 and 46.2 percent of those observed in the platform models subjected to the onshore accelerations. A comparison between the results from the onshore records and the results from the offshore records show that the differences in the vertical component are due to the presence of the water layer over the offshore site. In conclusion, this study demonstrates that the vertical component of the measurement recorded at the offshore location was significantly smaller than that of the onshore record.

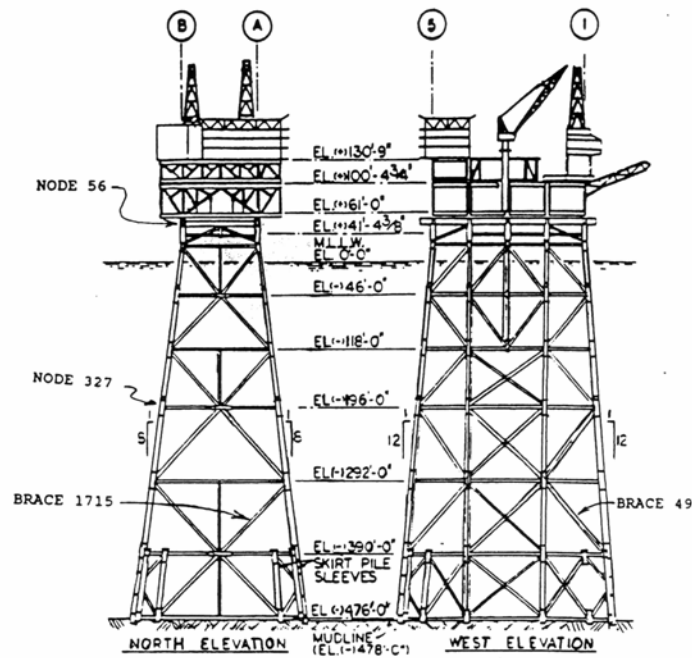


**FIG. 2.4. Elevation View of Model Platform for Ground Motion Comparison Study (Smith 1997)**

Boore and Smith (1999) observed the characteristics of ground shaking on the seafloor and compared them with observed characteristics of onshore ground motions. The offshore ground motions were measured using SEMS, which has units at six different offshore sites off the coast of Southern California, recording seismic activity in the area. During a 20 year period, eight earthquakes, with Richter magnitudes ranging between 4.7 and 6.1, were recorded at these sites. The distance from the epicenters of these events to measurement sites ranged between 49.4 km and 309 km. The recorded motions were compared with those taken from onshore locations as equidistant as possible from the epicenter. The results from this study show that the effect of ground motions on a given structure is dependent on a number of different factors including earthquake magnitude, distance from the epicenter, fault type and the site conditions for the structure in question

(Boore and Smith 1999). In general, ground motions at an offshore site were found to be the same as ground motions at an onshore site. In other words, the effects of a given earthquake are considered to be the same for onshore and offshore sites. However, results from this study show that the sediment layer and the water volume over the site dampen the vertical component of the ground motion. As a result, the V/H ratios (vertical to horizontal component of motion) for offshore locations are smaller than those with comparable characteristics at onshore locations. In addition, the amount of damping is proportional to the period of the ground motions, such that the difference between the vertical component of the onshore motions and the offshore motions increased as the periods became shorter and decreased as the periods became longer. Finally, the results also showed that the horizontal component of the motion did not vary much between offshore and onshore sites having comparable characteristics.

### **2.3.2. Seismic Analysis of Fixed Platforms**

Boote and Mascia (1994) studied the application of the response spectra method and the time history analysis method for evaluating the seismic behavior of a fixed offshore platform. Both methods were designed to represent an envelope of seismic excitation of the platform consistent with the seismicity of the region. Typically, several ground motion records from different earthquakes should be used for the analysis in order to formulate a comprehensive picture of the effects of different input motions on variations in the response of the platform (API 2000 a,b).

The fixed platform analytical model used in the above study was a four-leg jacket with bracing in the vertical and horizontal planes of the jacket. The jacket was modeled with and without foundation piles. To analyze the model without foundation piles, the jacket was assumed to be fixed at the ground level. In the jacket model with foundation piles, the piles were modeled as a series of horizontal springs with varying stiffness values, which accounted for the soil-pile interaction with linear elastic behavior. An added mass, taken as a percentage of the water volume displaced by the submerged portion of the structure, was used to account for the water-structure interaction. For the hypothetical location of the platform, the soil type was assumed to be “rock”, represented by curve “A” in the API design spectrum, with Zone 2 seismicity, corresponding to accelerations of 0.1g. For both analysis methods, ground accelerations recorded from the 1952 Taft, CA and 1940 El Centro, CA earthquakes were applied to the model and scaled down for Zone 2 seismicity. For both events, earthquake durations of 20 seconds were selected for the study, as specified in the Eurocode. These records were chosen because they are both Class II earthquakes typical for compact ground with irregular movements and extended duration, although the accelerations from the El Centro record are approximately 19 percent higher than that of the Taft record (Boote and Mascia 1994). In addition, the damping ratios were varied from 0.005 to 0.05 to observe the influence of damping on the stresses and deflections estimated by the model.

The results from the analyses were presented in the form of structural displacements and forces produced by the ground motions. The results from the spectral analyses show that

the spectra from the scaled Taft and El Centro earthquakes produced higher stresses and deflections than those produced by the design spectrum. The time history analyses, which used Taft and El Centro measured ground accelerations, yielded force and deflection values smaller than those produced by the spectral analyses. Based on the results from this study, the authors concluded that the use of the spectral analysis method for evaluating seismic response of offshore structures is a conservative approach.

Boote et al. (1998) continued to study response spectra and time history analysis methods with varying design spectra and time history accelerations. The model used for the study was based on a platform located in the Adriatic Sea. The jacket consisted of eight legs, braced horizontally and vertically, supporting the main deck (46 m by 21 m) and the cellar deck (36 m by 12 m). The structure was approximately 46 m high and was located in 30 m of water. The foundation piles were 70 m deep and the soil consisted of five distinct layers, which were assumed to behave elastically for the analysis. Analyses of the platform were conducted using five different numerical models with varying parameters for the soil-structure interaction, added mass, presence of conductors, and foundation. The first model, Model A, was constructed by schematizing all of the structural components of the jacket and platform. Model B included consideration of added mass in the portion of the jacket under water. Models C and D included the conductors, which run vertically from the deck down through the jacket to the seafloor. Model D included the added mass of the submerged portion of the structure and Model C excluded consideration for hydrodynamic effects. Fig. 2.5 illustrates the numerical model used for Model F, which

included the simplified method of modeling the pile foundations for the jacket. This method, known as “stub piling”, involves the use of “stubs” in the computer model to replace modeling of the actual pile properties. In this study, the pile foundations were simulated by lengthening the jacket legs to six times the leg diameter and fixing the ends of these legs.

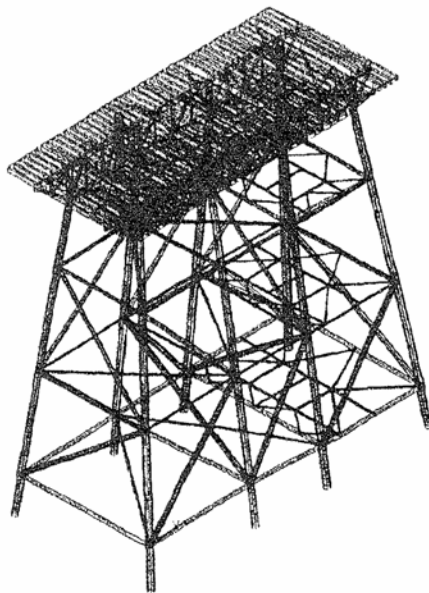


**FIG. 2.5. Illustration of Computer Model F (Boote et al. 1998)**

For this study, the primary focus centered on the spectral analysis and time history analysis of Model F (Boote et al. 1998). The spectral analyses included the design spectrum presented by API, a response spectrum developed from a ground motion evaluation (GME) of the site, and spectra derived from two different acceleration time histories. A peak ground acceleration (PGA) of 0.22g was assumed for the horizontal motions applied to the structure. Response of the structure for each seismic direction was

calculated using both the Square Root of the Sum of the Squares (SRSS) combination method and the Complete Quadratic Combination (CQC) method for each response spectra studied. The time history analyses were conducted using two different acceleration records, labeled TH1 and TH2. These records were also used to construct the response spectra used for the spectral analysis of the platform. As with the response spectra analyses, both records were scaled to a PGA value of 0.22g.

For each of the different analyses, spectra, and combination methods, a comparison was made of the stresses obtained at the seabed level for each of the platform legs (Boote et al. 1998). The results indicate that the API spectrum yields more severe results than the GME spectrum. In addition, the CQC method yields higher stress values than that of the SRSS combination method for all of the spectral analysis results. Finally, the differences between the results obtained by spectral analysis and those obtained from time history analysis are less than six percent, demonstrating the suitability of the spectral analysis method for linear analysis.

### **2.3.3. Pile Behavior Under Seismic Loading**

Michalopoulos et al. (1984) examined the process of designing the foundations of offshore structures to resist earthquake loads. Because of the differences that exist between onshore and offshore buildings and site conditions, building codes typically used for onshore structures are not applicable for the design of offshore structures (Michalopoulos et al. 1984). The process used for foundation design involves several

different steps, which include the development of time history records appropriate to the seismicity of the site, conducting a soil-pile-structure-water analysis, determining the static stiffness of the pile, and determining the pile loads from the structure and the soil.

The type of mathematical model used to simulate a structure and foundation subjected to ground motions heavily influences the analysis results (Michalopoulos et al. 1984). Four important characteristics considered for the selection of these models were the foundation type, water depth, required efficiency during the design phase, and the influence of higher modes on member forces. To demonstrate the importance of proper model selection, the paper cites the example of a fixed platform, 117 m high, located in a depth of 106 m in the Mediterranean Sea (Michalopoulos et al. 1984). Each of the four jacket legs was supported by a group of four 83 m long piles. Modal analyses were conducted on a lumped mass model and a structural frame model of the platform. The seismic risk for this model was based on the seismicity of a site near Viking Graben in the North Sea. According to the probabilistic analysis of the seismic risk of this region, the strength level earthquake (SLE) was 0.25g, and the ductility level earthquake (DLE) was greater than 0.4g, based on earthquake data recorded in this area between 1970 and 1981.

Because the lumped mass model was only two dimensional, the analysis produced frequencies for one lateral direction (Michalopoulos et al. 1984). However, frequency values for both lateral components of motion were obtained for the structural frame model. A comparison of the results from the two models indicated that the frequency

values for the lumped mass model were approximately 37 to 137 percent larger than the frequencies obtained for either lateral component of the structural frame model.

Rao and O'Neill (1997) studied the response of piles to earthquake loads and evaluated the effect of variations in the earthquake magnitude. In order to study the response of seismically loaded piles, a scaled laboratory model was subjected to three different horizontal accelerations corresponding to California-type earthquakes. The model consisted of a steel pipe driven into fine sand inside a chamber filled with water. The pipe dimensions were 25.4 mm outer diameter with a 1.4 mm wall thickness and 405 mm in length. Tension loads, varying between approximately 45 to 90 percent of the pile static capacity, were applied at the top of the pile. The magnitude of the motions were 7.0, 7.5, and 8.0 Richter magnitudes scaled up from ground accelerations recorded for the Upland 1990 and Oceanside 1986 earthquakes events in California, both records were for Richter magnitude 5.0 events. The accelerograms were obtained from an offshore deep sand site near Long Beach, California, approximately 75 km from both events.

Results from thirteen of the horizontal shaking tests were reported, displaying the behavior of the pile under various seismic and static tension loads. For the range of tension load values used in this experiment, the pile did not experience failure under the Richter magnitude 7.0 seismic loading (Rao and O'Neill 1997). Pullout of the pile occurred at 91 percent of the static capacity under the magnitude Richter magnitude 7.5 loading and 78 percent of the static axial tension capacity for the Richter magnitude 8.0

loading. In addition, the pile remained stable up to 65, 60, and 45 percent of the static capacity for the magnitude 7.0, 7.5, and 8.0 seismic events, respectively. Therefore, it was found that as the magnitude of the seismic event increases, the pile will lose stability for increasingly smaller tension loads, consistent with expectations.

#### **2.3.4. Subsea Pipelines Under Seismic Loading**

Jones (1985) discussed some of the environmental considerations that impact the loading for deepwater pipelines as part of a feasibility study conducted for Shell Development Company. The pipe sizes included in this study ranged from 305 mm up to 1067 mm outside diameter for water depths ranging from 183 m to 914 m. Two of the environmental factors examined in the study were bottom currents and earthquakes.

Research on deepwater bottom currents consisted of gathering general background information, including a list of all available measured current velocities for deepwater locations at the time of the study. In addition, a design current velocity of 0.91 m/s was recommended for situations where information on the currents is unavailable. Jones (1985) developed two diagrams (shown in Fig. 2.6) to illustrate the impact of ground motions on a pipeline with respect to earthquake magnitude and proximity.

Bruschi et al. (1996) reviewed current procedures for seismic design of offshore pipelines placed in seismically active areas. Some of the problems encountered as a result of an earthquake are the loss of soil stability due to seismic excitation, steep discontinuities in

the seabed at active fault locations, loss of structural integrity of pipeline and supports during a seismic event, and increased earthquake response at subsea connections due to structural discontinuities or changes in stiffness. The process of pipeline design must include consideration for these possibilities and corrective measures included where necessary (Bruschi et al. 1996).

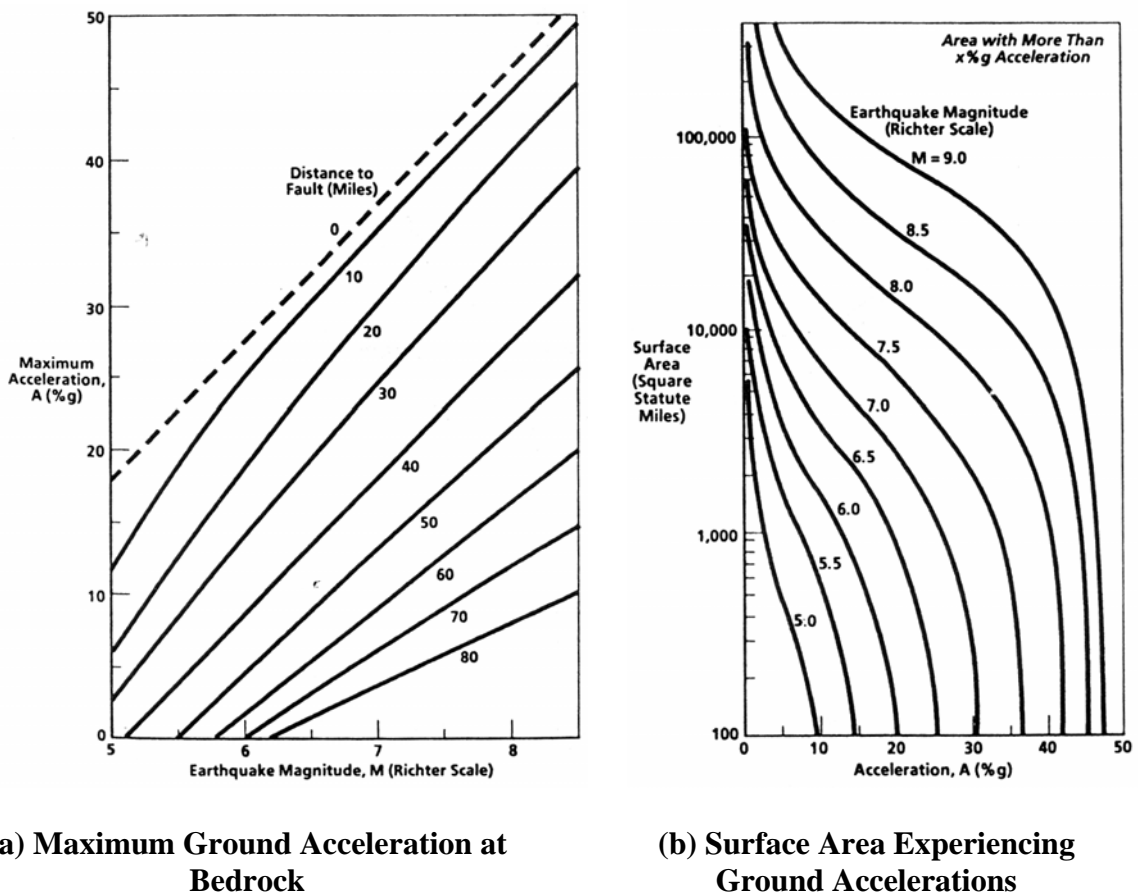


**FIG. 2.6. Impact of Earthquake Magnitude and Proximity on a Pipeline (Jones 1985)**

The first step in the design process is to evaluate the seismic hazard and soil stability for the proposed installation site (Bruschi et al. 1996). The next step is to examine the pipeline integrity. The pipeline deforms with the soil because it acts as one body with the soil. The response of the pipeline to earthquake loading is affected by the pipe properties, suspended pipe lengths, characteristics of the seabed, soil-pipeline interaction, and the axial load applied to the pipeline prior to the seismic event. Of primary concern in seismic design for pipelines is the stress experienced by the pipeline at the support locations. If the stresses exceed the allowable limit, then additional supports must be added to shorten the unsupported span length. Except for instances where a number of risk factors are present in the pipeline and site conditions, seismic excitations alone will not cause significant damage (Bruschi et al. 1996).

According to Kershenbaum et al. (1998), the behavior of subsea pipelines under seismic loading is dependent on the magnitude of the seismic event, seabed characteristics, geometry and properties of the pipeline prior to the seismic event. Although the pipeline is straight at the time of installation, snaking, or bending in the pipeline, caused by thermal and internal pressure on the pipe, will eventually change the shape of the line over time. The amount of bending increases at points in the line where the ends are restrained.

The authors present a method of earthquake analysis for unburied pipelines subjected to fault dislocation, which includes consideration of the initial shape of the pipeline

(Kershenbaum et al. 1998). The factors used to quantify the behavior of the seismically loaded pipeline include the earthquake magnitude, shape of the overall pipeline, soil properties, and the type of fault over which the pipeline has been placed. For this study, several different pipeline models with varying fault types and various degrees of bending were subjected to earthquake loading equivalent to Richter magnitude 6 and 7 seismic events.

The final results from the analysis of several different models show that increasing the magnitude of ground motions causes small increases in the stresses measured in the pipelines. Snaking, or deformation from the original pipeline shape, resulted in an amplification of the stress equal to 1.65 when the earthquake strength changed from Richter magnitude 6 to 7 (Kershenbaum et al. 1998). The stress amplification for the vertical component of reverse-slip fault movement was 1.2 and 1.05 for oblique slip fault movement. The final conclusion of the study was to recommend that the design of pipelines include consideration for snaking.

### **2.3.5. Conclusion**

The studies presented by Smith (1997) and Boore and Smith (1999) indicate that the horizontal component of ground motions observed at offshore locations are similar to those observed at onshore locations, while the vertical component of the offshore ground motions are often significantly lower. These results indicate that the current practice of using onshore ground motions for the design of offshore structures is acceptable. As

shown in the studies listed above, the use of spectral analysis and time history analysis methods are reasonable methods for evaluating the response of offshore structures to earthquake loadings. The study presented by Jones (1985) provides information on the type of environmental loads that deepwater pipelines will experience, which are similar to the loads applied to subsea structures. Finally, the research presented by Bruschi et al. (1996) and Kershenbaum et al. (1998) indicate that the primary points of concern along the pipeline section are at the supports and locations where the pipeline connects to subsea systems. Therefore consideration should be given to the loads that pipelines incur on these systems during seismic events.

### **3. SEISMIC DESIGN CRITERIA AND SEISMIC ACTIVITY IN THE GULF OF MEXICO**

#### **3.1. INTRODUCTION**

The purpose of this section is to outline the design criteria for earthquake loading on offshore structures. Section 3.2 presents the criteria and procedures proposed for the seismic design of subsea structures. Part of the design process involves identifying site characteristics, including local seismicity and site conditions, in order to evaluate the seismic risk. A summary of the earthquakes recorded for the GOM region is also presented.

#### **3.2. SEISMIC DESIGN CRITERIA**

Preliminary design procedures for offshore structures outlined by API-RP2A (API 2000 a,b) include the evaluation of seismicity at and near the proposed installation site. The evaluation should encompass an investigation of local site conditions, as well as the surrounding area, in order to make a thorough assessment of the risk to the proposed structure. The purpose of studying the surrounding area is to determine the location of potential sources of seismic activity, such as faults, and to gauge the source-to-site transmission and attenuation properties (API 2000 a,b). The type of faulting and local soil conditions play an important role in the ground motions transmitted to the structure, as well as the response of the structure to these motions. Finally, the accelerations or measured ground motions used for structural design are based upon the seismic

intensity, potential duration, frequency content of strong ground motions, and recurrence interval of previously recorded events for the location.

Offshore structures are designed for two types of seismic events: a strength level earthquake and a ductility level earthquake. The strength level earthquake is the strongest event expected to occur at the site within the span of operation for the offshore structure (API 2000 a,b). The purpose of using the strength level event is to design the structure so that it will respond to these motions primarily in the elastic region. The ductility level earthquake is a rare seismic event with a return period of a thousand years or more. Since this event can be rather large, structures must be designed to withstand the earthquake without collapsing, although nonlinear response and significant damage may occur.

The seismicity of the installation site governs the method of analysis used to evaluate the performance of subsea systems. If the expected earthquake strength is very small, then the earthquake effects can be neglected in the design process. If the horizontal accelerations are small but greater than 0.05g, then the structure should be analyzed by the spectral analysis method for earthquake force demands (API 2000 a,b). Although the use of the time history analysis method is applicable for these accelerations, this method can also be used for situations where the strength of the ground motions causes the structure to behave nonlinearly.

Because predicting the occurrence of earthquakes is highly uncertain, offshore systems can be expected to be operating if a seismic event does in fact occur (API 2000 a,b). Therefore, the loads under consideration for a seismic event will include operating loads, as well as dead loads. For subsea production systems, the mass used for the analysis should include the mass of the structure, attached equipment, fluids contained within the equipment, and the added mass, typically taken as a fraction of the mass of the volume of water displaced by the structure. The equivalent linear viscous damping ratio to be used for an elastic analysis of offshore structures is five percent (API 2000 a,b).

As specified by API-RP2A, the seismicity of an area under scrutiny can be rated according to relative zone factors (see Fig. 3.1). The effective horizontal ground acceleration is the product of the zone factor and five percent of the gravitational acceleration ( $Z \cdot 0.05g$ ). For instance, the strength level design for structures located within areas rated as Zone 2 will have a predicted peak ground acceleration of  $0.10g$ . However, the GOM is currently zoned as aseismic and has a relative seismic zone factor of 0, which means that the effective horizontal ground accelerations for the strength level earthquake can be neglected since they are less than  $0.05g$  (API 2000 a,b). This assumption is discussed in the next section.



**FIG. 3.1. API-RP2A Seismic Risk of Map of Coastal Waters in Contiguous United States (API 2000 a,b)**

### **3.3. SEISMICITY OF THE GULF OF MEXICO**

Since the GOM near the United States coastline is not a very seismically active region, there is not a great deal of information available on the seismicity of this region. Although the GOM is designated as a Zone 0 region by API-RP2A, there have been at least eight earthquakes with Richter magnitudes ranging from 4.0 to 4.9 recorded in this region. Fig. 3.2 and Tables 3.1 and 3.2 provide information on earthquakes recorded in the GOM region since 1974 according to the National Earthquake Information Center (USGS 2003).

**TABLE 3.1. Recorded Earthquakes in the Gulf of Mexico Region (Latitude Range 20° to 32° and Longitude Range -98° to -82°) (USGS 2003)**

<b>Date</b>	<b>Time UTC (hhmmss.mm)</b>	<b>Lat. (degrees)</b>	<b>Long. (degrees)</b>	<b>Mag. (Richter)</b>	<b>Depth (km)</b>	<b>Comments</b>
07/24/1978	080617.60	26.73	-88.74	4.9	33	Miss. Fan
06/12/1979	155959.60	21.78	-93.20	4.2	33	N. B. of Camp.
01/10/1980	191619.60	24.35	-85.38	3.9	10	Florida Scarp
05/12/1986	041802.47	27.70	-88.73	3.6	10	Miss. Fan
12/21/1988	130917.10	21.57	-94.65	4.5	33	N. B. of Camp.
03/18/1990	054232.14	20.49	-96.23	N.A.	33	N. B. of Camp.
03/31/1992	145939.60	26.02	-85.73	3.8	5	Florida Scarp
08/31/1992	194216.20	20.11	-94.39	4.2	10	N. B. of Camp.
09/27/1992	170234.30	28.17	-88.44	3.8	10	Miss. Fan
09/12/1993	155132.20	20.19	-96.53	N.A.	33	N. B. of Camp.
06/30/1994	010824.22	27.91	-90.18	4.2	10	Miss. Fan
06/07/1996	003026.77	20.77	-92.32	4.0	10	N. B. of Camp.
03/03/1997	054704.51	20.45	-94.33	3.8	10	N. B. of Camp.
04/18/1997	145735.40	25.78	-86.55	3.9	33	Florida Scarp
07/06/1998	065403.79	25.02	-93.63	3.4	10	S. of Texas
12/09/2000	064609.12	28.03	-90.17	4.3	10	Miss. Fan
03/16/2001	043907.68	28.36	-89.03	3.6	10	Miss. Fan
03/16/2001	053641.79	28.31	-89.42	N.A.	10	Miss. Fan
05/27/2002	002816.99	27.12	-94.44	3.8	10	S. of Texas
07/28/2002	232329.89	21.76	-96.15	4.0	10	N. B. of Camp.
09/19/2002	144436.15	27.82	-89.14	3.7	10	Miss. Fan
04/13/2003	045253.92	26.09	-86.08	3.2	10	Florida Scarp

**TABLE 3.2. Recorded Earthquakes in Bay of Campeche Region (Latitude Range 18° to 20° and Longitude Range -98° to -90°) (USGS 2003)**

<b>Year</b>	<b>Time UTC (hhmmss.mm)</b>	<b>Latitude (degrees)</b>	<b>Longitude (degrees)</b>	<b>Magnitude (Richter)</b>	<b>Depth (km)</b>
07/25/1974	095338.90	19.37	-96.25	4.5	76
09/20/1974	113326.00	18.91	-93.49	4.1	45
08/28/1977	235738.40	18.61	-94.39	3.8	33
12/31/1983	202132.00	18.77	-95.69	4.4	33
10/07/1985	195819.40	19.75	-96.17	N.A.	33
06/09/1986	214222.10	18.57	-95.46	N.A.	33
04/07/1987	020246.58	19.58	-92.09	4.7	10
08/14/1987	094032.46	19.01	-96.11	4.4	130
07/31/1990	073010.71	18.52	-94.51	4.7	33
11/23/1990	201737.90	18.50	-95.79	N.A.	10
11/27/1991	120033.30	19.22	-95.78	3.6	33
06/05/1992	034252.19	18.94	-95.82	4.4	39
04/12/1993	202034.00	18.74	-95.31	3.7	33
04/30/1993	114856.80	19.39	-96.06	N.A.	33
04/30/1993	150538.70	19.34	-96.08	3.4	33
11/10/1994	210315.70	19.31	-95.27	N.A.	33
04/11/1995	014231.51	18.77	-95.28	N.A.	33
03/14/1996	091211.94	19.53	-92.00	4.3	33
10/31/1996	021223.20	19.30	-95.33	3.6	10
03/18/1997	015944.66	19.64	-91.99	3.9	33
04/15/1997	011234.04	19.63	-95.76	3.8	250
07/11/1997	210830.70	19.39	-92.15	4.1	33
09/01/1997	105019.50	18.94	-95.84	4.3	33
09/23/1997	004716.77	19.66	-91.76	4.1	10
01/14/2000	222254.20	19.46	-92.01	4.3	10
03/24/2000	175830.80	18.91	-95.58	4.1	26
06/05/2000	115931.50	19.01	-95.68	4.4	20
08/11/2000	081955.30	19.55	-96.41	4.1	4
04/19/2001	214250.80	19.24	-95.90	4.1	16
07/09/2001	134642.80	19.24	-96.28	3.7	25
07/21/2001	000951.19	19.42	-92.14	4.2	33
07/23/2001	065921.10	18.50	-95.47	4.0	26

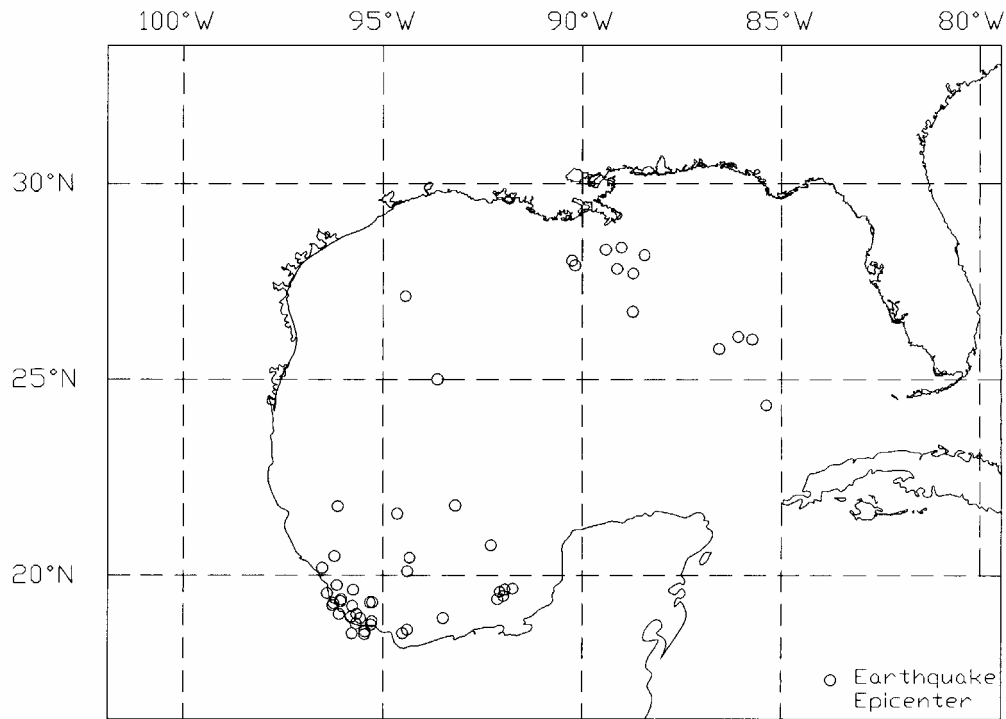


**FIG. 3.2. Recorded Earthquakes in GOM Region and Bay of Campeche Region (Latitude Range 18°- 32° and Longitude Range -98° to -82°)**

The earthquakes listed in Table 3.1 are located within a rectangular area extending from 20° to 32° latitude and -98° to -82° longitude. Table 3.2 lists the events that have occurred in the Bay of Campeche area, contained within a rectangular area extending from 18° to 20° latitude and -98° to -90° longitude. Each table gives information on the date, time, magnitude, and location of the seismic event. Fig. 3.2 was constructed using the data from both tables and the information provided by the mapping program GEODAS (GEODAS 1998). The expression used to denote the time of the recorded event lists the hour, minutes and seconds as the digits on the left side of the decimal

point, and milliseconds as the digits on the right side of the decimal point. The intensity of the record is expressed in terms of Richter magnitude, the location of the epicenter of the earthquake is given in terms of latitude and longitude, and the depth from the ground surface.

The information in Table 3.1 indicates that the measured earthquakes in the GOM are not very large and have relatively infrequent occurrences. The earliest recorded earthquakes for this region date back to 1974. Of the 22 recorded earthquakes, eleven of the earthquakes had Richter magnitudes falling within the range of 3.0 and 3.9, eight had Richter magnitudes ranging from 4.0 to 4.9, and three of the events do not have a recorded magnitude. Of these, eight of the events occurred in the Mississippi Fan area at depths of 10 km and 33 km. Four of the epicenters were located further south and east of this area, closer to the Florida Scarp. The depths of these events varied from 5 km to 33 km and the Richter magnitudes ranged between 3.2 and 3.9. Another grouping of eight events is approximately north of the Bay of Campeche and two events were located in the area south of the Texas coastline. The strongest measured event for this region was a magnitude 4.9 earthquake, which occurred in 1978 near the Mississippi Fan region of the Gulf. Crustal subsidence due to sedimentation loading, measured at a rate of 5.1 mm per year, is the most probable cause of this particular event (Frohlich 1982).

As indicated by the information for the Bay of Campeche presented in Table 3.2, there are eight seismic events with Richter magnitudes that fall between 3.1 and 3.9 and 18

events with Richter magnitudes that fall between 4.1 and 4.7. Most of these events were located close to the coastline in the Bay of Campeche with depths less than 33 km, although some of the epicenters of these events were as deep as 250 km. Finally, some of the seismic events taking place in areas other than the Mississippi Fan seem to be associated with the plate boundaries in Mexico, Central America, and the Caribbean (Frohlich 1982).

## **4. SUBSEA SYSTEMS**

### **4.1. INTRODUCTION**

The use of subsea systems in the GOM for retrieving, transporting, and processing oil and gas resources has increased significantly in recent years. As such, there are several different types of structures and systems currently used in this region to obtain and transport oil and gas to offshore platforms or onshore locations. In general, each structure is designed to fit the specific criteria set by site conditions and performance requirements as set forth by API-RP2A. The purpose of this section is to give an overview of the types of systems in use and provide basic information on the prototype system selected for this study.

### **4.2. OVERVIEW OF SUBSEA SYSTEMS**

#### **4.2.1. General**

Information regarding the details of specific subsea systems is largely proprietary. However, there are a few publications available which identify primary components and functions of these systems. One of these publications is API-RP17A (API 1996) which provides general descriptions of the basic types of subsea systems and their corresponding components. The basic types of systems are subsea wellheads, subsea wellhead trees, manifolds and templates. Descriptions provided by these publications

include information about the structural configuration, expected loads and function. The following paragraphs provide a summary of these descriptions and figures.

#### 4.2.2. Wellhead Completion Equipment

The components of wellhead completion equipment include subsea wellheads and subsea tubing hanger/tree systems. The primary function of subsea wellheads is to provide support for casing strings, blowout preventer (BOP) stack, and the subsea tree (API 1996). Fig. 4.1 highlights the basic components of this wellhead system, which includes a temporary guide base, a permanent guide base, conductor and wellhead housings and casing hangers. The temporary guide supports the permanent guide base and provides a flat horizontal surface above the seabed upon which the wellhead rests (Goodfellow Associates 1990). The permanent guide base supports the wellhead system

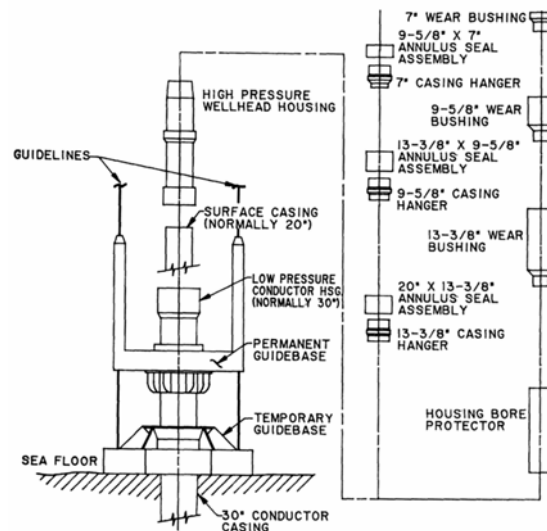


**FIG. 4.1. Subsea Wellhead System (API 1996)**

and acts as a template for the placement of the BOP stack and subsea tree. The casing hangers are used to support casing strings inside the wellhead. The conductor housing attaches to the permanent guide base and extends down to attach to the conductor casing and the wellhead housing, which fits inside the conductor housing, and maintains constant pressure inside the well.

As shown in Fig. 4.2, the subsea tubing hanger system provides support for the tubing inside the wellhead and maintains pressure between the tubing and the wellhead. Subsea Christmas trees control the flow for production and injection wells through a series of valves (see Fig. 4.3) (Goodfellow Associates 1990). These structures can be installed in remote locations in order to retrieve resources from “marginal fields” or can be installed with templates to aid with retrieval and production in locations where the oil reserves are large.

Structural design considerations for these systems include soil-structure interaction, environmental loads such as earthquake and current, thermal loads, and externally applied loads originating from connecting pipelines and risers. The largest loads are generated by the risers, applying moment and tension to the wellhead. The flowline connections also provide a significant amount of loading in the form of shear and applied moment. The subsea tubing hanger/wellhead connection is subjected to the same loads as the wellhead systems (see Fig. 4.3).

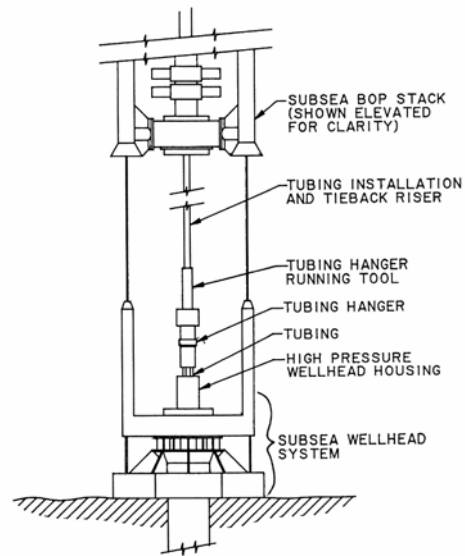


**FIG. 4.2. Tubing Hanger Installation (API 1996)**

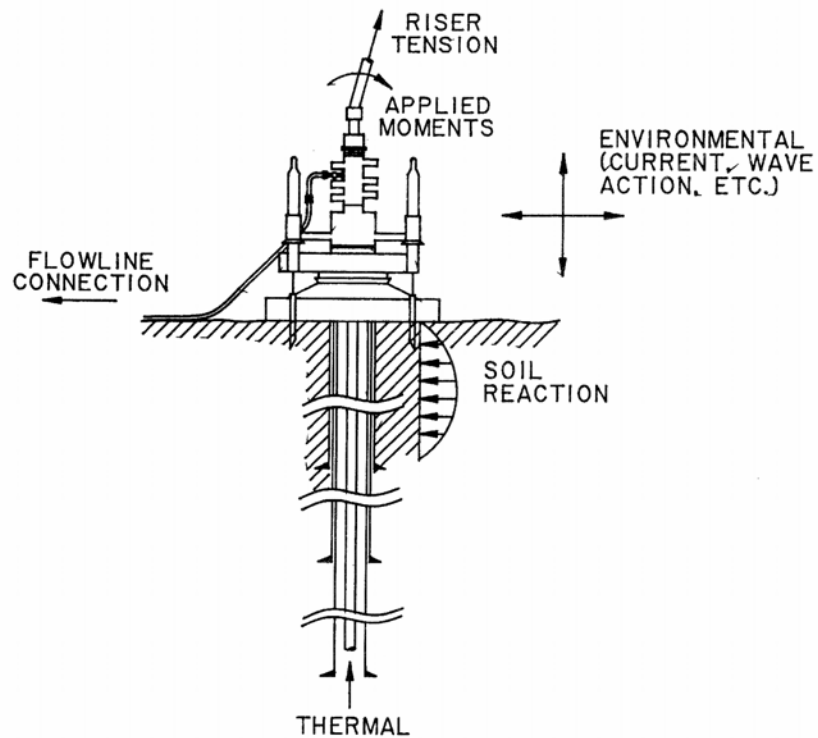


**FIG. 4.3. Subsea Completion Loads and Reactions (API 1996)**

### 4.2.3. Templates

Templates, as shown in Fig. 4.4, are welded steel frames that generally serve as drilling guides and provide support for other equipment (API 1996). The different types of templates listed by the recommended practice, based on the equipment supported in the frame, are the manifold templates, well spacer/tieback templates, multi-well/manifold templates, riser support templates and modular templates. In addition, templates can be categorized as either unit or modular templates based on the configuration of the well spacing (Goodfellow Associates 1990).

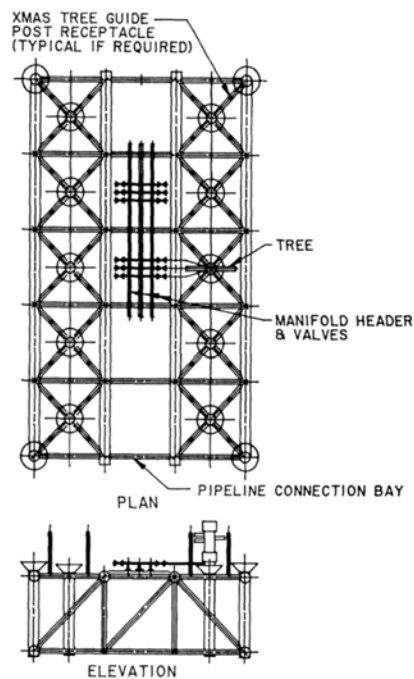


**FIG. 4.4. Diagram of Well Spacer/Support Template (API 1996)**

Frame sizes for unit templates range between 15 m by 15 m up to 60 m by 45 m, and are capable of supporting several well casings, subsea trees, the BOP stack, as well as other associated equipment (Goodfellow Associates 1990). On the other hand, modular templates consist of a series of smaller frames that are attached to a base structure to form one large unit (API 1996). These modules can be installed on an as needed basis when the full details of demand requirements are unknown during the initial design phases. Table 4.1 lists some typical weights and dimensions of the modules supported by templates.

**TABLE 4.1. Dimensions and Weights of Modules (Goodfellow Associates 1990)**

<b>Equipment</b>	<b>Overall Size (m) (length by width by height)</b>	<b>Weight (kg)</b>
Christmas tree	5.2 x 2.6 x 5.0	15,000
Valve Module	4.0 x 3.6 x 2.3	6,000
Choke Module	1.3 x 1.8 x 1.4	2,000
Isolation Module	2.3 x 2.6 x 3.0	3,000
Controls Module	1.0 x 1.0 x 2.0	2,000
Pigging Cross-Over Module	4.5 x 2.0 x 2.0	7,500
Piping and Control Trunking Module	21.0 x 2.0 x 1.5	18,000
Insert Valve	0.6 x 0.6 x 1.2	450
Flowline Connection Module (8" Pipe)	2.4 x 2.2 x 3.6	14,693
Riser Manifold	6.5 x 6.5 x 5.0	70,000
Water Injection Manifold	5.0 x 5.0 x 4.5	60,000

Structural considerations for the design of templates include environmental, installation, operation, piping, and riser loads. The primary environmental forces that affect the design of these frames are earthquakes and hydrostatic loads. Some loads associated with the operation of subsea systems include thermal expansion, supporting maintenance equipment, pipe movement, and drilling loads. Finally, as with the subsea wellhead

completion systems, the soil conditions play a critical role in the design of these structures.

#### **4.2.4. Manifold Systems**

The primary function of a manifold system is to collect or distribute produced fluids. Additional functions, such as well testing and servicing, may also be performed using the manifold if the appropriate equipment is provided. The size and type of manifold used for each application is dependent upon the number of wells located in each field (Goodfellow Associates 1990). Some of the same loads used in template design are applicable to the design of manifolds as well (API 1996). These loads may include seismic effects and thermal expansion.

Template well manifolds and satellite well manifolds are two types of manifold systems available for subsea applications (Goodfellow Associates 1990). The oil or gas is collected from reservoirs or wells and distributed to riser lines by template manifolds. In addition, these systems are responsible for injecting water back into the wells and transmitting riser loads to the template, and providing a means of releasing the subsea system from the risers in case of emergency. Satellite well manifolds are capable of controlling the flow of fluids from reservoirs or wells.

#### 4.2.5. Subsea Systems in the Gulf of Mexico

One of the tasks of this research was to conduct a survey of deepwater subsea systems in the GOM for the purpose of developing a prototype system for the analytical study. A listing of some deepwater subsea systems found in the Gulf of Mexico is provided in Table 4.2.

Fig. 4.5 depicts the approximate locations of the subsea systems listed in Table 4.2, based on the lease block location information provided by MMS (2003). The epicenters of recorded earthquakes in this region are also shown (USGS 2003). As shown in the map, a number of the subsea systems are located in the Mississippi Fan region where several earthquake epicenters are concentrated. The information on deepwater subsea systems was obtained from a number of sources, including the Shell Exploration and Production Company (SEPCo) and *Offshore Technology*. Further details for two specific subsea projects, Gemini and Zinc, are provided below.

**TABLE 4.2. Partial Listing of Deepwater Subsea Systems Located in the GOM**

<b>Project</b>	<b>Location</b>	<b>Depth (m)</b>	<b>No. of Wells</b>	<b>Description</b>
Canyon Express	Three separate fields - Aconcagua (TotalFina) in MC 305, King's Peak (bp) in Desoto Canyon 177 & 133, Camden Hills MC 348	2210	N.A.	Pipeline
Diana Hoover	East Breaks Blocks 945,946, 988, and 989 - 160 miles S of Galveston, Texas	1353	N.A.	Subsea Development - 5 subsea trees, 2 production manifolds.
Europa	MC 934	1213	3	Multi well subsea manifold.
Gemini	MC 292 - 90 miles SE of New Orleans, Louisiana	1036	3	Subsea development tied back to Viosca Knoll 900 platform. Wells tied back to a 4 slot cluster manifold.
Macaroni	Garden Banks 602	1128	4	4 well subsea manifold
Manatee	Green Canyon Block 155, 160 miles SW of New Orleans, Louisiana	591	N.A.	Subsea tieback to Bullwinkle Platform.
Mars	Mississippi Canyon Blocks 762, 763,806, 807, 850, & 851 - 130 miles SE of New Orleans, Louisiana	759	N.A.	Pipeline – 457 mm line (oil), 356 mm line (natural gas)
Mensa	Mississippi Canyon Blocks 686, 687, 730, 731 - 140 miles SE of New Orleans, Louisiana	1615	3	Wells connected to manifold, which is 101 km from platform.
Troika	Green Canyon Block 244, 150 miles offshore Louisiana	823	N.A.	Compact, eight slot subsea manifold - tied back to Bullwinkle platform – 23 km away.
Zinc	MC Blocks 354, 355, 398, 399 - 50 miles S of Grand Isle, Louisiana	445	N.A.	10 slot subsea template - tied back to Alabaster platform.

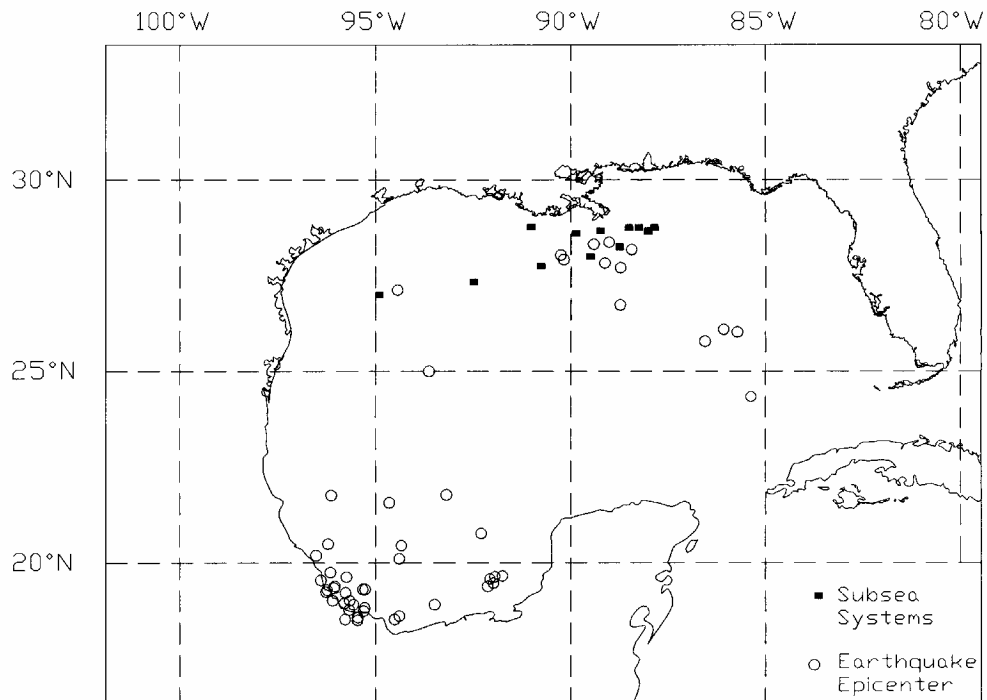
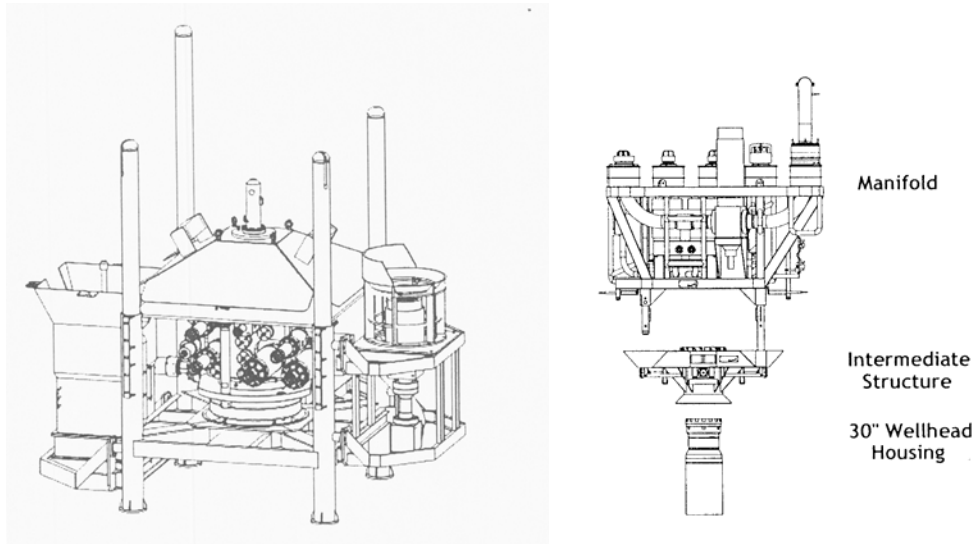


**FIG. 4.5. Deepwater Subsea Systems and Recorded Earthquake Epicenters in the Gulf of Mexico**

The Gemini subsea development, in a water depth of 1040 m, is located in the GOM lease block Mississippi Canyon 292, approximately 90 miles southeast of New Orleans (Coleman and Isenmann 2000). This system consists of a horizontally configured subsea tree and manifold with three production wells. The manifold assembly is a four slot cluster manifold, weighing roughly 41 metric tons, supported on the sea floor by the three 914 mm diameter conductors. Fig. 4.6 illustrates the subsea tree assembly and manifold used for the Gemini project (Beer and Jeffries 2000).



**(a) Subsea Tree Assembly**

**(b) Manifold and Intermediate Structure**

**FIG. 4.6. Gemini Subsea Development (Beer and Jeffries 2000)**

The Zinc project, shown in elevation in Fig. 4.7, is located south of Louisiana in a water depth of 450 m, on an old bed of the Mississippi River. The seabed is a highly underconsolidated clay soil (Bednar 1993). Because of the weak soil conditions, the foundation consists of four piles sunk to a depth of 75 m below the mudline used for initial support of the template. Each pile has a 1372 mm diameter that tapers to 1067 mm at the top. This development consists of a template structure with overall length and width of 36 m by 23 m. The distance from the base to the top of the pigging valve is 17 m and the weight of the structure in water is 454 metric tons. The template includes six well slots.

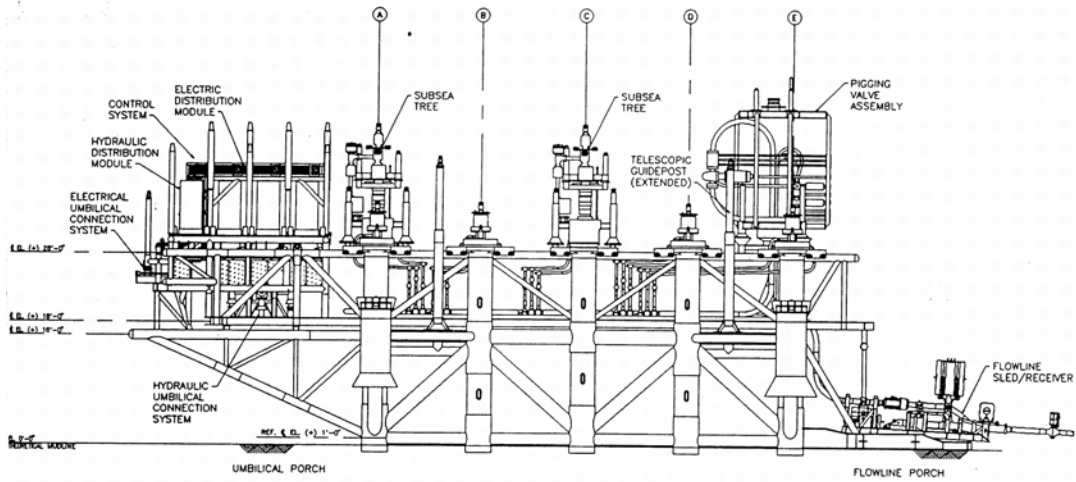


**FIG. 4.7. Zinc Template/Manifold – Elevation (Bednar 1993)**

## **5. STRUCTURAL MODELS AND ANALYSIS PROCEDURES**

### **5.1. INTRODUCTION**

The previous section contained a general description of the various types and functions of subsea systems and highlighted a few deepwater systems in the Gulf of Mexico. This section presents the details of a selected prototype subsea system, the development of the numerical model of this system, and the parametric study. The final section of this section outlines the details of the analysis procedures used to evaluate these systems.

### **5.2. DESCRIPTION OF ANALYTICAL MODEL**

#### **5.2.1. Prototype Structure**

One of the objectives for this research was to identify a prototype subsea system to evaluate the expected performance of subsea systems in the Gulf of Mexico under seismic loading. Although each subsea system is designed to meet the site and performance requirements, the basic geometry, structural member sizing, and loads are similar for each system type. The most significant differences are observed in the templates, manifolds, subsea wellheads and subsea trees. However, the foundation support system tends to be similar among subsea systems, such that a prototype for an analytical study may be defined.

The prototype system chosen for this study was derived from a Kvaerner advertisement for a single wellhead subsea Christmas tree in a trade magazine (see Fig. 5.1) (Kvaerner

2001). The subsea tree, designed for placement in water depths up to 3000 m, weighs approximately 30 metric tons, and has overall dimensions of 5 m by 3.8 m by 3.85 m. The foundation type selected for this prototype system, typical for subsea applications, consisted of a single casing, of 248,000 kPa steel, with an outside diameter of 762 mm diameter, embedded 30.5 m below the mudline (API 1996). Based on the dimensions provided in the Kvaerner advertisement, the center of gravity was assumed to be located at 60 percent of the subsea tree height above the mudline. The added mass of the system was conservatively estimated as 2.44 mtons by using the total enclosed volume of the wellhead to determine the weight of the displaced water volume.

The base case mudline strength of the soil was assumed to be 4.79 kPa and the strength gradient of the soil was assumed to be 0.48 kPa/m. Both of these are values typical of normally consolidated GOM clays (API 2000 a,b). The curve corresponding to soil type C, the weakest designation for soils, was selected in the API response spectra curve for the calculation of the soil casing stiffness values. In addition, the structural model was subjected to accelerations representative of Zones 1 and 2. As mentioned previously, these zones correspond to peak horizontal ground accelerations of 0.05 and 0.10g.

**3000 metres**

Kvaerner Oilfield Products delivers to Petrobras  
the world's first 3000m Subsea Xmas Tree

GLL 3000m Main Features:

Tree type:	Horizontal
Design Depth:	3000m
Pressure:	5000 PSI
Seals:	Metal
Weight:	30 Tonnes
Dimensions:	5m x 3,8m x 3,85m
Installation:	Guide-line less

For further information:  
[kop.sales@kvaerner.com](mailto:kop.sales@kvaerner.com)  
[www.kop.kvaerner.com](http://www.kop.kvaerner.com)

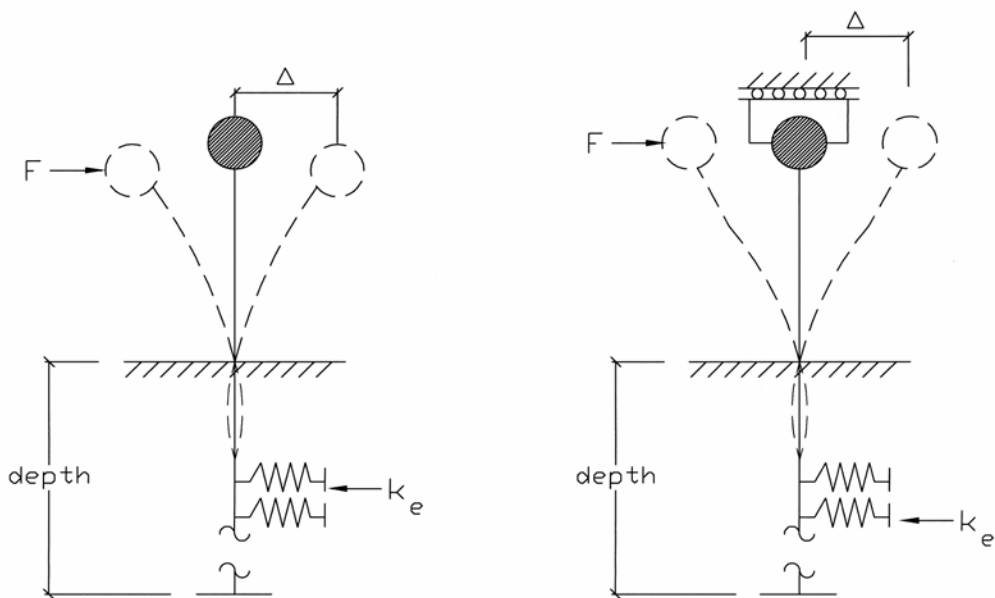
**BR PETROBRAS** **KVÆRNER**

**FIG. 5.1. Advertisement for Kvaerner Subsea Christmas Tree (Kvaerner 2001)**

### **5.2.2. Baseline Analytical Model**

The analytical model used for this study is based on the prototype structure, which is a simplified representation of the subsea tree. The model consists of a single casing embedded in clay soil, with the top portion of the casing cantilevered above the mudline,

supporting the lumped mass of the system at the top (see Fig. 5.2). The free-headed model represents structures supported by single casing foundations, and the fixed-headed model represents multi-casing structures, which are assumed to be essentially fixed against rotation since a single casing in a multi-casing structure cannot rotate freely due to the additional resistance provided the structure. The baseline model is fixed against vertical movement at the bottom of the casing. The lateral support conditions, provided by the soil surrounding the casing, are represented by a series of equivalent springs placed along the length of the casing located below the mudline. The foundation and support conditions are consistent with those of single wellhead subsea systems. A summary of the characteristics of the baseline model are listed in Table 5.1.



(a) Free-Headed Analytical Model

(b) Fixed-Headed Analytical Model

**FIG. 5.2. Free-Headed and Fixed-Headed Analytical Models**

**TABLE 5.1. Characteristics of the Baseline Analytical Model**

<b>Parameter</b>	<b>Units</b>	<b>Zone 1</b>	<b>Zone 2</b>
Soil-Casing Stiffness	kN/mm	2.07	1.95
Casing Outside Diameter	mm	762	
Casing Wall Thickness	mm	25.4	
Mass	mton	31.4	
Height Above Mudline	m	2.44	
Mudline Strength	kPa	4.79	
Strength Gradient	kPa/m	0.48	

The equation of motion, as stated in Section 2, is used to describe the structural response to earthquake loading. Eq. 5.2 and 5.3 are both variations of the basic expression for the equation of motion, Eq. 5.1, shown below.

$$f_I + f_D + f_S = 0 \quad (5.1)$$

$$m\ddot{u}(t) + c\dot{u}(t) + ku(t) = -m\ddot{u}_g(t) \quad (5.2)$$

$$\ddot{u}(t) + 2\zeta\omega_n\dot{u}(t) + \omega_n^2u(t) = -\ddot{u}_g(t) \quad (5.3)$$

Where all the variables were previously defined in Section 2.2. As illustrated in Eq. 5.1, the equation of motion consists of three primary force components, which are described above. The total mass,  $m$ , of the system is the sum of the mass of the structure, mass of the attached appurtenances or equipment, mass of the fluid contained within the system, and the added mass caused by the movement of the system through the water. The equivalent linear viscous damping in the structure is 5 percent (API 2000 a,b). The

spring stiffness coefficient,  $k$ , and the natural frequency,  $\omega_n$ , are related to the stiffness of the casing supporting the structure, as well as the stiffness properties of soil.

Subsea systems are subject to a number of different lateral loads during normal operating conditions, including currents, loads caused by connecting pipelines and risers, and earthquake loads. The magnitude of the riser loads is dependent upon the motion of the topsides structure attached to the riser, and indirectly on the depth of water in which the subsea system is submerged. The magnitude of the loads caused by the connection of a subsea structure to a pipeline is dependent upon the magnitude of the movement of the pipeline during normal conditions, as well as during the earthquake loading. Determining the magnitude of these loads for the prototype system is beyond the scope of this research, therefore lateral loads caused by attached risers and pipelines were not considered in this study. API-RP2A recommends that the force due to currents and waves be calculated using the following expression:

$$F = \frac{C_d w A}{2g} U |U| + \frac{C_m w}{g} V \frac{\delta U}{\delta t} \quad (5.4)$$

Where:

- $C_D$  = Drag coefficient
- $C_m$  = Inertia coefficient
- $U$  = Component of the velocity vector of the water normal to the axis of the member (m/s)
- $w$  = Weight density of water (N/m<sup>2</sup>)
- $g$  = Gravitational acceleration (m/s<sup>2</sup>)

$$\begin{aligned}
 A &= \text{Projected area normal to the cylinder axis (m)} \\
 \frac{\delta U}{\delta t} &= \text{Component of local acceleration vector normal to the axis of the} \\
 &\quad \text{member (m/s}^2\text{)}
 \end{aligned}$$

This expression is a variation of Morison's Equation, stated previously in Section 2.2 (Dean and Borgman 1986). This study includes the consideration of current loads only, because subsea systems are submerged in deep water, meaning that the acceleration vector in Eq. 5.4 is equal to zero (API 2000 a,b). The shape coefficient,  $C_d$ , is equal 1.5 for the sides of buildings and 0.5 for cylindrical sections. According to Jones (1985), when the actual current velocity at the installation site is unknown, the suggested design current velocity for pipelines in deepwater locations is 0.91 m/s. API-RP2A states that the surface circulatory current velocities in the Gulf of Mexico range between 0.91 and 1.83 m/s.

Table 5.2 presents a brief summary of the results obtained using Eq. 5.4 for the baseline analytical model. It was assumed that the current acts on a solid area 3.85 m wide and 5 m high and that the force is applied at the center of this area. The stresses applied to the casing due to the current load are also presented in Table 5.2. As indicated, the calculated current force and subsequent casing stresses are not large with respect to the allowable stresses in this application. The shear stresses range from 0.42 to 1.70 percent of the allowable shear stress. The bending stresses range from 1.59 to 6.34 percent of the allowable bending stress. For this reason, the lateral forces caused by current flowing through and around the model are not included in this study.

**TABLE 5.2. Loadings and Stresses Due to Current with Specified Velocities**

Parameter	Units	Design Current Velocity (m/s)	
		0.91	1.83
Force due to Current	kN	12.4	49.6
Shear Stress	kPa	422	1,690
Allowable Shear Stress	kPa	99,300	99,300
Overturning Moment	kN-m	31.0	124
Bending Stress	kPa	2,960	11,800
Allowable Bending Stress	kPa	186,000	186,000

### 5.2.3. Modeling Parameters

After the baseline analytical prototype was defined, the model was varied to simulate the behavior of a number of different subsea structures, including single and multiple wellhead systems. By varying parameters such as geometry, fixity, and mass; the baseline analytical model was used to simulate the behavior of a number of different subsea structures for Zone 1 and 2 earthquake accelerations.

As described in Tables 5.3 through 5.8, these parameters are soil-casing stiffness, mass of the subsea system, casing sizes, height of the mass above the mudline, mudline strength, strength gradient of the soil, and rotational fixity of the casing. The baseline case models are denoted as Model CC. The range of values used in the variation in soil-casing stiffness are consistent with the range of stiffness values derived (as described in Section 5.3) for various casing sizes, accelerations, applied masses, mudline strengths, and soil strength gradients. Both the mudline strength and the strength gradient values

are varied over a range of  $\pm 10$  and  $\pm 20$  percent of the baseline value, respectively. The dimensions for the casing diameters and thickness are typical of deep water structural casings. A few of the critical cases (or cases giving upper and lower bound values) were modeled as fixed-head casings in order to assess the impact of earthquake loadings on systems with more than one casing foundation support (i.e. multiple wellhead systems). The fixed-headed model with characteristics corresponding to the baseline model is denoted as Model CCF.

**TABLE 5.3. Variation of Soil-Casing Stiffness**

Case	Soil-Casing Stiffness (kN/mm)
Baseline (CC)	2.07, 1.95
A1	2.46
A2	2.36
A3	2.76
A4	2.69
A5	2.99
A6	2.95
A7	3.56
A8	3.55
A9	4.01
A10	4.00

**TABLE 5.4. Variation of Casing Size**

<b>Case</b>	<b>Pile Size (Outer Dia., mm x Wall Thickness, mm)</b>
Baseline (CC)	762 x 25.4
B1	762 x 38.1
B2	762 x 50.8
B3	914 x 25.4
B4	914 x 38.1
B5	914 x 50.8

**TABLE 5.5. Variation of Mudline Strength**

<b>Case</b>	<b>Mudline Strength (kPa)</b>
Baseline (CC)	4.79
C1	3.83
C2	4.31
C3	5.27
C4	5.75

**TABLE 5.6. Variation of Strength Gradient**

<b>Case</b>	<b>Strength Gradient (kPa/m)</b>
Baseline (CC)	0.48
D1	0.37
D2	0.43
D3	0.53
D4	0.58

**TABLE 5.7. Variation of Mass and Height**

Case	Height (m)	Mass (mton)
Baseline (CC)	2.44	31.4
EA2	4.57	
EA3	6.10	
EA4	7.62	
EB1	2.44	13.6
EB2	4.57	
EB3	6.10	
EB4	7.62	
EC1	2.44	45.4
EC2	4.57	
EC3	6.10	
EC4	7.62	
ED1-1	2.44	68.0
ED2-1	4.57	
ED3-1	6.10	
ED4-1	7.62	

**TABLE 5.8. Variations for Fixed-Headed Casing Models**

Case	Height (m)	Mass (mton)
CCF	2.44	31.4
F1	4.57	13.6
F2	6.10	45.4
F3	7.62	68.0

#### 5.2.4. Details of the Time History Analysis Model

The characteristics of the model structure used for the time history analysis are similar to the baseline model characteristics outlined in Table 5.1. The model consists of a single casing embedded in clay with the lumped mass of the system cantilevered above the mudline (see Fig. 5.3). The casing is fixed against vertical displacement. The equivalent lateral soil-casing stiffness, calculated for the parametric study, is applied at

the mudline location on the SAP model. A critical damping ratio of five percent was included in the input. The acceleration record used for this analysis is taken from the 1940 El Centro, California earthquake (Richter magnitude 6.9) (COSMOS 2003). The time history record is shown in Fig. 5.4. The earthquake has a duration of 53.74 seconds and has a five percent critical damping ratio. The amplification zone for the earthquake is for periods less than about 1.0 seconds.

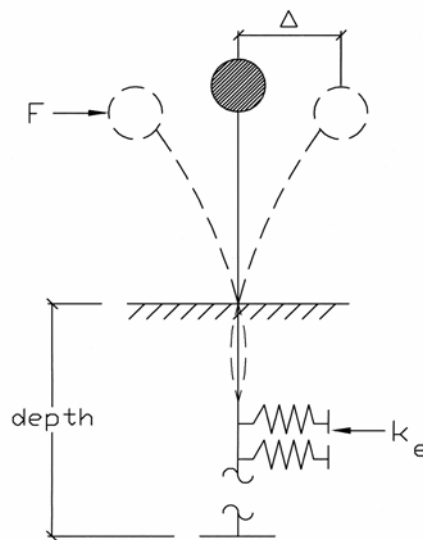


**FIG. 5.3. Lumped Mass Model for Time History Analysis**

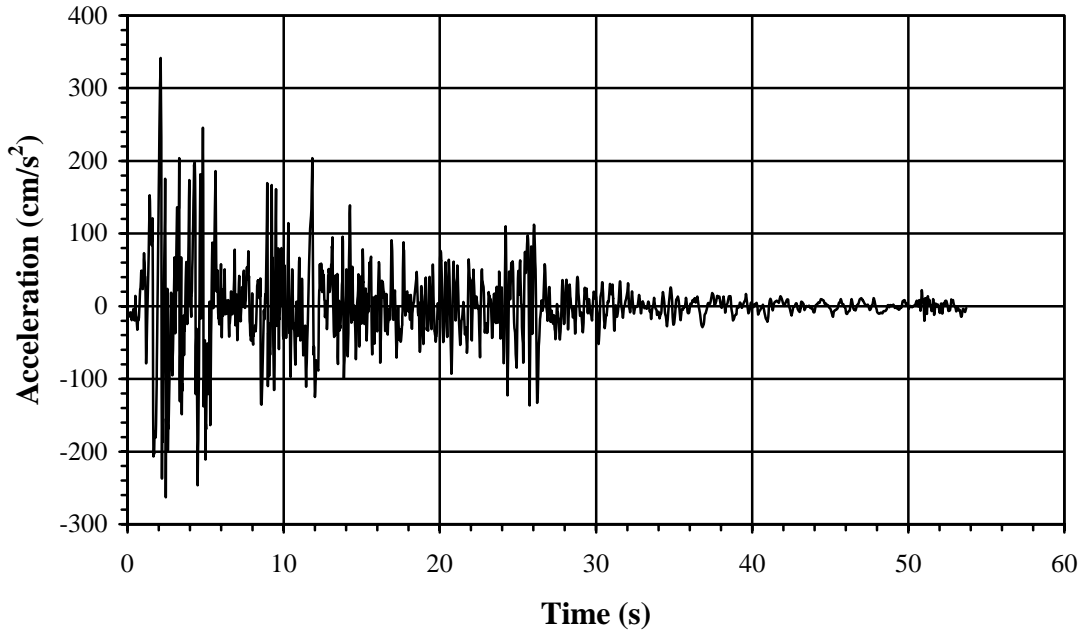


**FIG. 5.4. 1940 El Centro, California Earthquake Acceleration Record (COSMOS, 2003)**

### **5.3. ANALYSIS PROCEDURES**

#### **5.3.1. General**

The following subsections describe the procedures used to conduct the analyses for this study. For the parametric study, the impact of seismic loading on the prototype structures involved the utilization of three different steps.

1. The BMCOL76 program (BMCOL76 1981) and the API design spectra (API 2000 a,b) were used to determine the soil-casing stiffness values.
2. The soil-casing stiffness values were used with the API design response spectra to estimate the spectral acceleration values for the model under the design seismic loading.

3. The force and displacement values were obtained using the response spectra method.
4. The force values were used to calculate the stresses in the casing and deflection of the model for the design seismic loading.

For the time history analysis, the following steps were used:

1. The soil casing stiffness for the baseline model was obtained from the parametric study.
2. A time history analysis was conducted for the baseline model using the SAP2000 program (SAP2000 1999).
3. The force values obtained from the SAP2000 output were used to calculate the stresses in the casing. The deflection values were also obtained from the output.

### **5.3.2. Calculation of Equivalent Soil-Casing Stiffness**

The first step of the analysis was to determine the soil casing stiffness values for the model. The BMCOL76 program (BMCOL76 1981) computes deflections and reactions for an embedded casing (or pile) with specific geometry, loading conditions, and nonlinear soil resistance values. In this program, the soil-pile relationship is modeled as a beam-column on an inelastic foundation, which is detailed further in Section 2.2.3. Because the lateral response of the soil-casing is nonlinear, a linearized secant stiffness was determined using the design response spectra shown in Figure C2.3.6-2 of API-RP2A for a specified zone and soil type (API 2000 a,b). As shown in Table 5.4, the soil

$p$ - $y$  curves used in the model are based on Matlock's model for soft clay and are taken from Section 6.8.3 of API-RP2A.

In order to model the relationship between the soil and the casing using the BMCOL76 program, certain casing and soil properties are required. These properties include casing stiffness, embedment length, point of load application, fixity, and height of the casing above the mudline. Additional information includes the number of increments the length of the casing is to be divided into, and the length of each increment. The  $p$ - $y$  curves needed to evaluate the relationship between the pile and soil can be constructed using the load-deflection data for soft clays, as described in Table 5.9, and information on the lateral bearing capacity of the soil along the length of the pile, or casing (API 2000 a,b).

**TABLE 5.9. Values of  $p$ - $y$  Curve for Soft Clays (API 2000 a,b)**

$p/p_u$	$y/y_c$
0.00	0.00
0.50	1.00
0.72	3.00
1.00	8.00
1.00	$\infty$

Where:

- $p$  = Actual lateral resistance (kPa)
- $p_u$  = Lateral bearing capacity (kPa)
- $y$  = Actual lateral deflection (mm)
- $y_c$  =  $2.5 \cdot \varepsilon_c \cdot D$  = Lateral deflection related to  $\varepsilon_c$  (mm)
- $D$  = Pile diameter (mm)
- $\varepsilon_c$  = Strain which occurs at half of the maximum stress on laboratory undrained compression tests of undisturbed soil samples (assumed to be taken as 0.01 for this study)

The lateral bearing capacity is calculated using the following expressions (API 2000 a,b).

$$p_u = 3c + \gamma X + \frac{JcX}{D} \quad \text{for } 0 \leq X < X_R \quad (5.5)$$

$$p_u = 9c \quad \text{for } X \geq X_R \quad (5.6)$$

Where:

- $c$  = Undrained shear strength for undisturbed clay soil samples (kPa)
- $D$  = Pile diameter (mm)
- $\gamma$  = Effective unit weight of soil (assumed to be 12.2 for this study) (MN/m<sup>3</sup>)
- $J$  = Dimensionless empirical constant determined by field testing with values ranging between 0.25 and 0.5 (A value of 0.5 is reasonable for GOM clays) (API 2000 a,b)
- $X$  = Depth below the surface of the soil (mm)
- $X_R$  = Depth below the surface of the soil to the bottom of the resistance zone (mm). When the strength of the soil varies with depth, this term is obtained by plotting the two equations above and finding the intersection of these lines.

Finally, a series of different lateral loads were applied to the casing for each BMCOL76 model in order to construct the force versus displacement curve used to determine the soil-casing stiffness. For this study, there were seven points on the curve, corresponding to specified boundary loads of magnitudes 0, 44.5, 111, 222, 445, 667, and 890 kN. An example of the force versus displacement curves used for the parametric study is shown in Fig. 5.5.

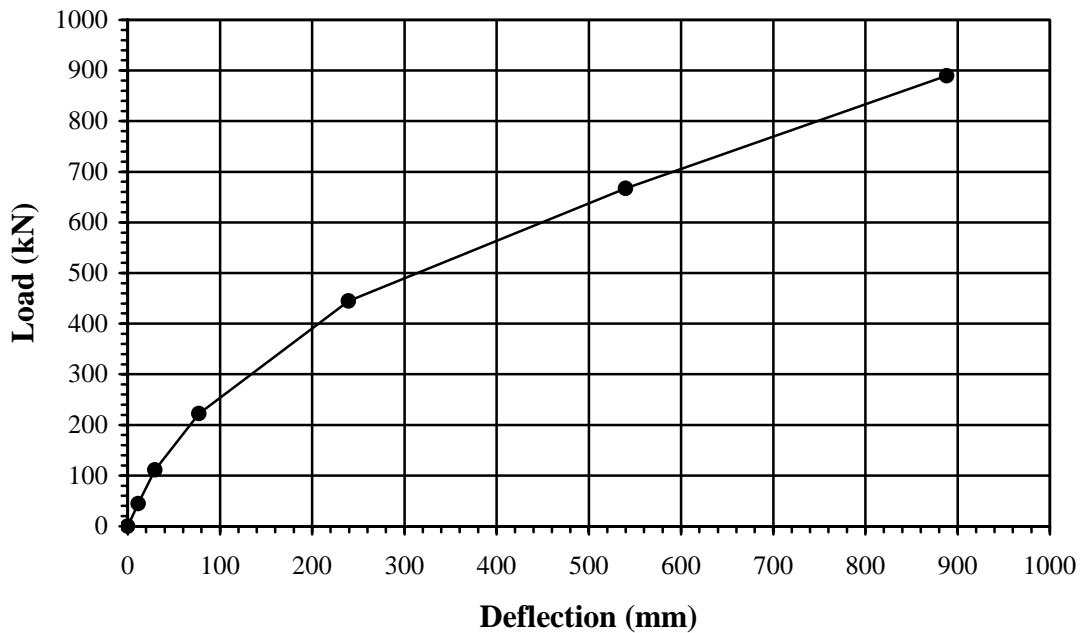


**FIG. 5.5. Force Versus Displacement Curve**

For each model, the deflection values found using BMCOL76 were used to construct a force versus displacement curve. This curve was used to determine the soil secant stiffness values. The following steps were used to determine the stiffness values:

1. An arbitrary data point on the force versus displacement curve was initially selected to calculate the overall stiffness value,  $k$ , of the casing, as shown in Eq. 5.7.
2. With this stiffness value, Eqs. 5.8 and 5.9 were used to determine the natural frequency and period, based on a single-degree-of-freedom (SDOF) system.

$$k = \frac{F}{d} \quad (5.7)$$

$$\omega = \sqrt{\frac{k}{m}} \quad (5.8)$$

$$T = \frac{2\pi}{\omega} \quad (5.9)$$

Where:

- $F$  = Lateral Force (kN)
- $d$  = Displacement (mm)
- $k$  = Soil-Casing Stiffness (kN/mm)
- $m$  = Lumped mass of the system (mton)
- $\omega$  = Natural frequency of the structure (rad/s)
- $T$  = Period of the structure (s)

3. The next step was to calculate the ratio  $S_A/G$ , where  $S_A$  is the spectral acceleration and  $G$  is the ratio of the effective horizontal ground acceleration to gravitational acceleration (g) (API 2000 a,b). The value of  $S_A/G$  was obtained from the normalized response spectra from API-RP2A, shown in Fig. 5.6, based on the period,  $T$ .
4. The spectral acceleration was then determined by multiplying  $S_A/G$  by the value of  $G$ , given in API-RP2A, based on the seismic zone.
5. Finally, a new force value was obtained using Eq. 5.10.

$$F = m * S_A \quad (5.10)$$

6. From the force-displacement curve, the corresponding displacement value for the new force was then obtained.

A number of iterations of this process were performed until the calculated soil casing values were within a specified tolerance of  $\pm 0.01$  percent.

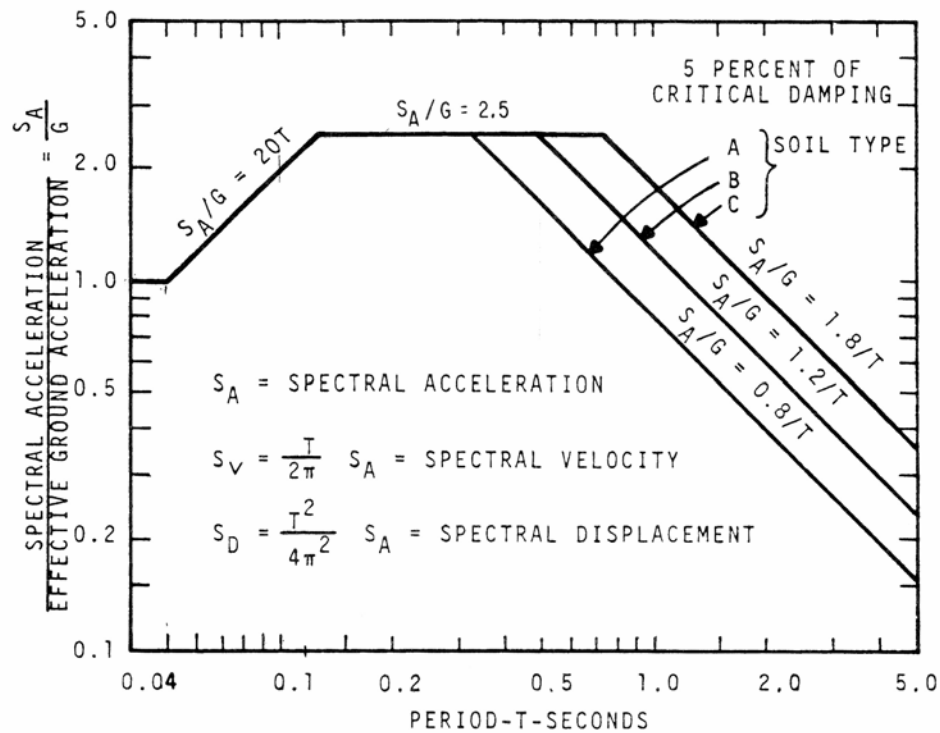


**FIG. 5.6. API Design Spectra (API 2000 a,b)**

Once the soil casing equivalent lateral stiffness values and the natural period were known, maximum spectral acceleration, displacement, and stress values corresponding to a particular analysis model were determined using the response spectrum in API-

RP2A (API 2000 a,b). The spectral acceleration,  $S_A$ , of the system was calculated as stated in the previous paragraph.

### **5.3.3. Time History Analysis Method**

The SAP2000 analysis program was used to conduct the linear time history analysis for this study (SAP2000 1999). The analytical model was constructed using most of the same parameters used for the baseline analytical model in the parametric study (see Sections 5.2.2 and 5.2.4). However, the lateral soil-casing stiffness value was derived using the displacement of the casing at the mudline instead of the top of the casing model. The resulting displacements and response of the structure were computed by the SAP2000 program after the model information and a file containing the El Centro earthquake acceleration record were defined. The SAP2000 program presents these results in the form of data files that contain the accelerations for each time step in the record. As with the parametric study, the shear forces were calculated by multiplying the mass of the model by the acceleration values. The maximum moment and displacement values corresponding to the maximum shear force were then obtained using the BMCOL76 program.

### **5.3.4. Calculation of Force and Stress Values**

The final step for the parametric study and time history analysis involved determining the stresses and displacements that the casing of the model experiences under earthquake

loading. For the results, the maximum shear forces, overturning moments and corresponding stresses were calculated to evaluate the performance of each model. This evaluation also included determining the maximum displacement values for each model. The shear forces, overturning moments, and stresses were calculated using Eqs. 5.11 to 5.13.

$$F = m * S_A \quad (5.11)$$

$$f_v = \frac{F}{A} \quad (5.12)$$

$$f_b = \frac{Mc}{I} \quad (5.13)$$

Where:

- $F$  = Shear force (kN)
- $S_A$  = Spectral Acceleration ( $m/s^2$ )
- $f_v$  = Shear stress (kPa)
- $A$  = Area of structural element ( $m^2$ )
- $M$  = Overturning moment (kN-m)
- $f_b$  = Bending stress (kPa)
- $I$  = Moment of inertia of structural element ( $mm^4$ )
- $c$  = Distance from extreme edge to the centroid of structural element (mm)

Because the length of the moment arm for the maximum overturning moment typically occurred below the mudline, most of the moment and displacement values for the models in the parametric study were obtained from the BMCOL76 program. However, for models A1 to A10, where the soil-casing stiffness was varied independent of the other model properties, obtaining the correct maximum moment and displacement values

using BMCOL76 program was more difficult. This is because there were several different variations in soil and casing properties that could produce the designated stiffness values. To approximate the maximum moment and displacement values for these models, Eq. 5.14 and 5.15 were used.

$$S_D = \frac{T^2}{4\pi^2} S_A \quad (5.14)$$

$$M = F * d \quad (5.15)$$

Where:

$$\begin{aligned} d &= \text{Length of the moment arm (m)} \\ T &= \text{Period of the casing (seconds)} \end{aligned}$$

Finally, the stresses obtained from these analyses were compared to the allowable stresses, as defined by API-RP2A Working Stress Design for offshore structures (API 2000 a). An increase of 70 percent is permitted for the evaluation of stresses caused by earthquake loading. In other words, the stresses caused by earthquake loading must be less than or equal to 70 percent of the allowable stresses. The expressions used to determine the allowable axial compressive stresses, shear stresses, and bending stresses are as follows:

$$F_a = \frac{\left[1 - \frac{(Kl/r)^2}{2C_c^2}\right] F_y}{5/3 + \frac{3(Kl/r)}{8C_c} - \frac{(Kl/r)^3}{8C_c^3}} \quad \text{for } Kl/r < C_c \quad (5.16)$$

$$F_a = \frac{12\pi^2 E}{23(Kl/r)^2} \quad \text{for } Kl/r \geq C_c \quad (5.17)$$

$$F_b = 0.75F_y \quad (5.18)$$

$$f_v = 0.4F_y \quad (5.19)$$

where:

- $F_a$  = Allowable axial stress (kPa)
- $K$  = Effective length factor, defined as 1.0 for piles in API-RP2A
- $l$  = Unbraced length of the member (m)
- $r$  = Radius of gyration (m)
- $C_c = \left[ \frac{2\pi^2 E}{F_y} \right]^{.05}$
- $F_y$  = Yield stress (kPa)
- $F_b$  = Allowable bending stress (kPa)
- $f_v$  = Allowable shear stress (kPa)

Eq. 5.20 is used to determine the shear stress ratio (SSR). Since only the stresses induced by earthquake loading are considered in this study, the SSR should be less than or equal to 0.7.

$$SSR = \frac{f_{\text{vcal}}}{f_v} \leq 0.7 \quad (5.20)$$

Where:

$$f_{vcal} = \text{Calculated shear stress (kPa)}$$

Eqs. 5.21 to 5.23 are used to calculate the combined axial and bending stress ratio (CSR) for the casing. Since only the stresses caused by earthquake loading are considered in this study, the CSR must be less than or equal to 0.7. According to API-RP2A, cylindrical members should be designed to satisfy the expressions in Eqs. 5.21 and 5.22. However, Eq. 5.23 can be substituted for these two expressions when the ratio of the axial stress to the allowable axial stress is less than or equal to 0.15.

$$CSR = \frac{f_a}{F_a} + \frac{C_m \sqrt{f_{bx}^2 + f_{by}^2}}{\left(1 - \frac{f_a}{F'_e}\right) F_b} \leq 0.7 \quad (5.21)$$

$$CSR = \frac{f_a}{0.6F_y} + \frac{\sqrt{f_{bx}^2 + f_{by}^2}}{F_b} \leq 0.7 \quad (5.22)$$

$$CSR = \frac{f_a}{F_a} + \frac{\sqrt{f_{bx}^2 + f_{by}^2}}{F_b} \leq 0.7 \quad \text{for } \frac{f_a}{F_a} \leq 0.15 \quad (5.23)$$

Where:

- $F_a$  = Allowable axial stress (kPa)
- $K$  = Effective length factor, defined as 1.0 for piles in API-RP2A
- $l$  = Unbraced length of the member (m)
- $r$  = Radius of gyration (m)
- CSR = Combined stress ratio

## **6. ANALYTICAL RESULTS**

### **6.1. INTRODUCTION**

The results from the parametric study and the time history analysis are presented in this section. The results generated from the baseline analytical model are presented first, followed by the results of the parametric study (for the free-headed casing models) from varying the soil casing stiffness, casing size, mudline strength and strength gradient of the soil, mass height above the mudline, and mass, respectively. In addition, the results for the fixed-headed casing models are presented. A summary of the parametric study results are presented in Section 6.2.9. Finally, the time history analysis results are presented in Section 6.3.

### **6.2. PARAMETRIC STUDY**

#### **6.2.1. Results for the Baseline Model**

Table 6.1 presents the data obtained from the analysis of the baseline prototype model. The properties of this model, labeled as model CC, are based on the properties of the selected prototype structure and typical site conditions in the GOM. The calculations performed to obtain this data are presented in Appendix A.

The calculated period for the Zone 1 subsea model is approximately four percent less than the period obtained from the Zone 2 model. As expected, the displacement and

stress values obtained from the Zone 2 model are approximately double those obtained from the Zone 1 model, because the PGA for Zone 2 is twice as large as the PGA for Zone 1. It should be noted that both the CSR and SSR values are smaller than the 70 percent allowable increase. Finally, the CSR for the Zone 2 model is approximately 1.7 times greater than the CSR obtained from the Zone 1 model. Additional data for the baseline model is presented in Table 6.1.

**TABLE 6.1. Baseline Model (CC) Results**

Parameter	Units	Zone 1	Zone 2
$k_{\text{soil}}$ (Soil-Casing Spring)	kN/mm	2.07	1.95
Height Above the Mudline	m	2.44	2.44
Mudline Strength	kPa	4.79	4.79
Strength Gradient for Soil	kPa/m	0.48	0.48
T	s	0.77	0.80
$S_A/G$	-	2.33	2.26
Displacement	mm	17.3	33.8
Shear Force	kN	35.8	69.5
Shear Stress	kPa	609	1183
Overturning Moment	kN-m	87.3	170
Bending Stress	kPa	17,000	33,300
SSR	-	0.012	0.024
CSR	-	0.13	0.22

### 6.2.2. Variation of Soil-Casing Stiffness

The first modeling parameter evaluated in this study was the soil-casing stiffness. The values considered for the soil-casing stiffness encompass almost the complete the range of stiffness values determined for the remaining casing models used in this study. Because the stiffness values were selected as incremental values, the design spectra in

API-RP2A (API 2000 a,b) was used only to calculate the displacements and stresses (see Section 5). For these cases only, the maximum bending moment is calculated using a moment arm distance which extends from the mudline to the center of gravity of the mass.

The results obtained from varying the soil-casing stiffness values are presented in Tables 6.2 and 6.3. The relationship between stresses, displacements and periods with respect to changes in the stiffness values are shown graphically in Figs. 6.1 to 6.4. As expected, the period of the casing model decreases nonlinearly as the stiffness parameter increases. In addition, there is a similar nonlinear relationship between the soil-casing stiffness and observed displacements. However, Figs. 6.3 and 6.4 show that the shear and bending stresses increase until the stiffness value is approximately 2.63 kN/mm or greater, at which point there is no change in either shear or bending stresses. This indicates that an increase in the stiffness parameter beyond this point will not cause a significant change in the bending and shear stress values. Finally the CSR values for this variable ranged between 0.06 and 0.13.

**TABLE 6.2. Response Spectra Calculations for Variation of Soil-Casing Stiffness**

Zone	Model No.	$k_{soil}$ , (kN/mm)	T (s)	$S_A/G$	$S_A$ ( $m/s^2$ )	Displacement (mm)
1	A1	0.53	1.54	1.17	0.57	34.3
	A2	0.70	1.33	1.35	0.66	29.7
	A3	0.88	1.19	1.51	0.74	26.6
	A4	1.75	0.84	2.14	1.05	18.8
	CC	2.07	0.77	2.33	1.14	17.3
	A5	2.63	0.69	2.50	1.23	14.6
	A6	3.50	0.59	2.50	1.23	11.0
2	A7	4.38	0.53	2.50	1.23	8.79
	A1	0.53	1.54	1.17	1.15	68.7
	A2	0.70	1.33	1.35	1.33	59.5
	A3	0.88	1.19	1.51	1.48	53.2
	A3	1.75	0.84	2.14	2.10	37.6
	CC	1.95	0.80	2.26	2.22	35.6
	A5	2.63	0.69	2.50	2.45	29.3
	A6	3.50	0.59	2.50	2.45	22.0
A7	4.38	0.53	2.50	2.45	17.6	

**TABLE 6.3. Force and Stress Values for Variation of Soil-Casing Stiffness.**

Zone	Model No.	Shear Force (kN)	Shear Stress (kPa)	Overtopping Moment (kN-m)	Bending Stress (kPa)	SSR	CSR
1	A1	18.0	614	44.0	4,200	0.006	0.06
	A2	20.8	709	50.8	4,850	0.007	0.06
	A3	23.3	793	56.8	5,420	0.008	0.07
	A4	32.9	1,120	80.3	7,670	0.011	0.08
	A5	38.5	1,310	93.8	8,960	0.013	0.08
	A6	38.5	1,310	93.8	8,960	0.013	0.08
	A7	38.5	1,310	93.8	8,960	0.013	0.08
2	A1	36.1	1,230	88.0	8,400	0.012	0.08
	A2	41.7	1,420	102	9,700	0.014	0.09
	A3	46.6	1,590	114	10,800	0.016	0.09
	A4	65.9	2,240	161	15,300	0.023	0.12
	A5	77.0	2,620	188	17,900	0.026	0.13
	A6	77.0	2,620	188	17,900	0.026	0.13
	A7	77.0	2,620	188	17,900	0.026	0.13

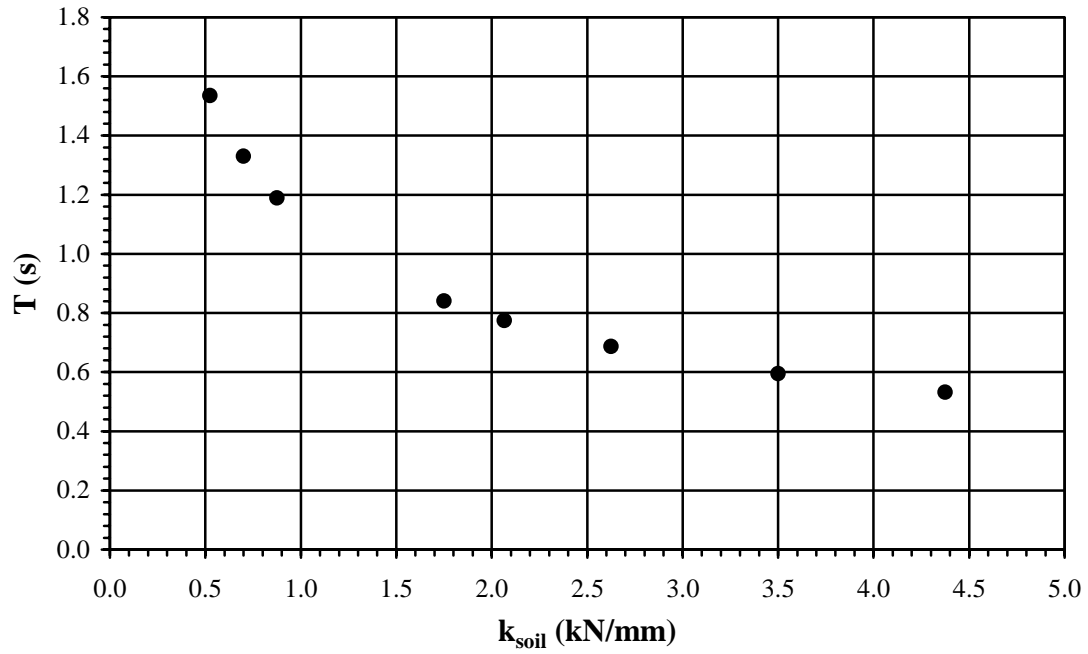


**FIG. 6.1. Change in Period Due to Variation of Soil-Casing Stiffness**

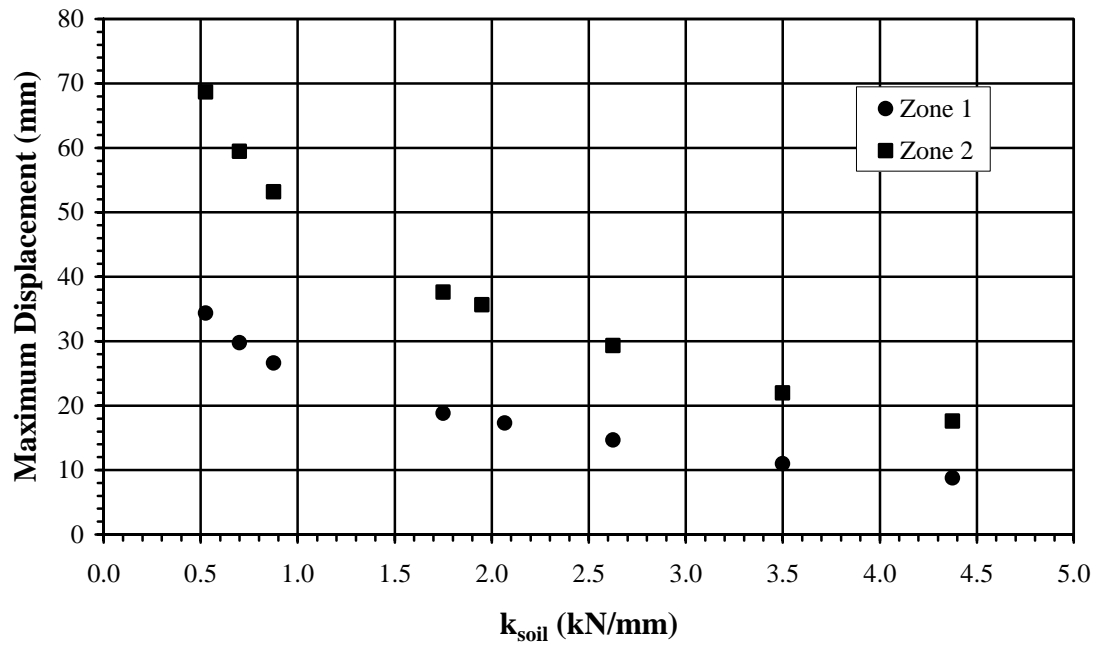


**FIG. 6.2. Change in Displacement Due to Variation of Soil-Casing Stiffness**

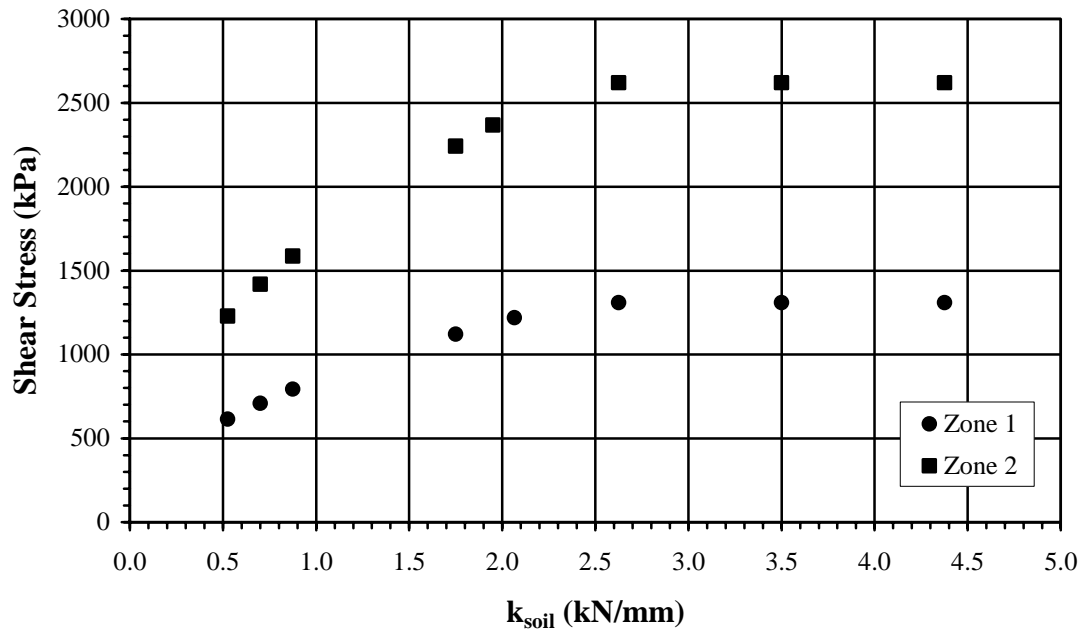


**FIG. 6.3. Change in Shear Stress Due to Variation of Soil-Casing Stiffness**

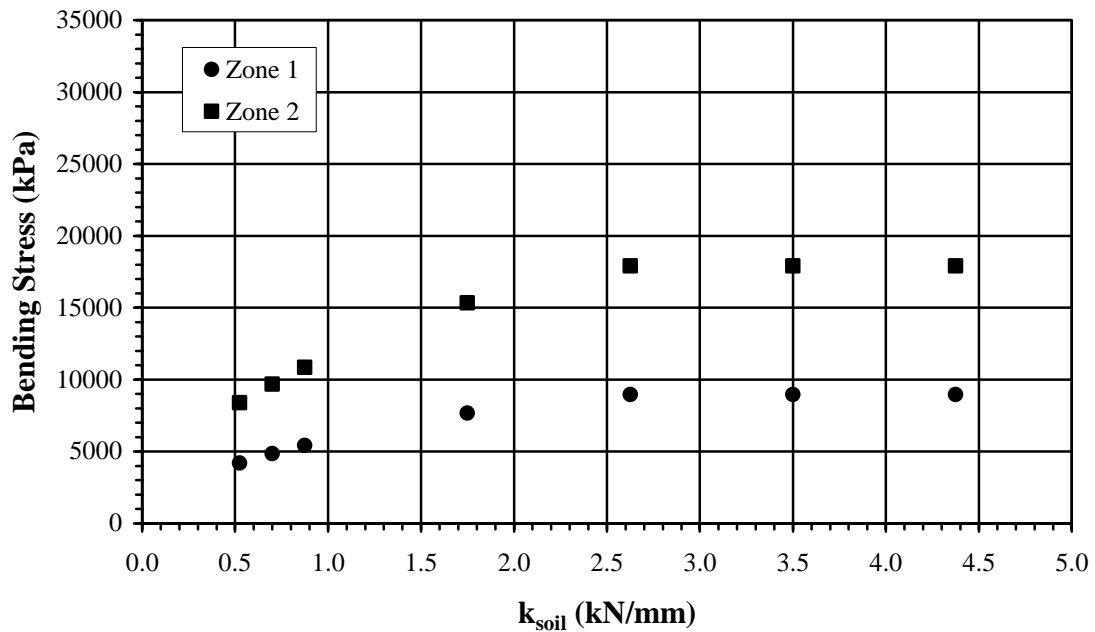


**FIG. 6.4. Change in Bending Stress Due to Variation of Soil-Casing Stiffness**

### 6.2.3. Variation of Casing Size

The dimensions chosen to evaluate the impact of varying casing size are consistent with diameter and wall thicknesses typically used subsea pile applications. The soil-casing stiffness values, maximum bending moments, and displacements were obtained using the BMCOL76 analysis program, while the shear forces were calculated based on the design spectra from API-RP2A (API 2000 a,b). Tables 6.4 and 6.5 present the results obtained from the study for this parameter. The variation of period, displacement and stress values with respect to the change in casing sizes are shown in Figs. 6.5 to 6.8.

As expected, the period, maximum tip deflection, and stress values decrease as the area of steel increases. These values decrease because increasing the area of steel increases the stiffness of the casing. There is approximately a 50 percent difference between the shear and bending stress values obtained from the smallest and largest casing sizes. Both the SSR and CSR values obtained for this parameter were less than 0.7. The SSR values for the model B5, the largest casing size, are roughly 50 percent of those obtained from the baseline model. The CSR values obtained for model B5 are approximately 45 percent less than the CSR values obtained for the baseline model.

**TABLE 6.4. BMCOL76 and Response Spectra Calculations for Variations of Casing Size**

Zone	Model No.	Casing Size (Outer Dia. x Wall Thick.) (mm)	T (s)	S <sub>A</sub> /G	S <sub>A</sub> (m/s <sup>2</sup> )	Displacement (mm)
1	CC	762 x 25.4	0.77	2.33	1.14	17.3
	B1	762 x 38.1	0.71	2.50	1.23	15.6
	B2	762 x 50.8	0.67	2.50	1.23	14.4
	B3	914 x 25.4	0.64	2.50	1.23	14.1
	B4	914 x 38.1	0.59	2.50	1.23	11.9
	B5	914 x 50.8	0.56	2.50	1.23	10.6
2	CC	762 x 25.4	0.80	2.26	2.22	33.8
	B1	762 x 38.1	0.72	2.49	2.44	31.2
	B2	762 x 50.8	0.68	2.50	2.45	27.9
	B3	914 x 25.4	0.65	2.50	2.45	28.2
	B4	914 x 38.1	0.59	2.50	2.45	23.7
	B5	914 x 50.8	0.56	2.50	2.45	21.8

**TABLE 6.5. Resulting Force and Stress Values for Variation of Casing Size**

Zone	Model No.	Shear Force (kN)	Shear Stress (kPa)	Overtopping Moment (kN-m)	Bending Stress (kPa)	SSR	CSR
1	CC	69.5	2,370	178	17,000	0.012	0.13
	B1	76.6	1,770	201	13,500	0.009	0.10
	B2	77.0	1,360	208	11,000	0.007	0.08
	B3	77.0	2,170	207	13,500	0.011	0.10
	B4	77.0	1,470	218	9,890	0.007	0.07
	B5	77.0	1,120	226	8,010	0.006	0.06
2	CC	35.8	1,220	349	33,300	0.024	0.22
	B1	38.5	888	401	26,900	0.018	0.17
	B2	38.5	678	416	22,000	0.014	0.14
	B3	38.5	1,080	414	27,000	0.022	0.18
	B4	38.5	734	436	19,800	0.015	0.13
	B5	38.5	558	452	16,000	0.011	0.10

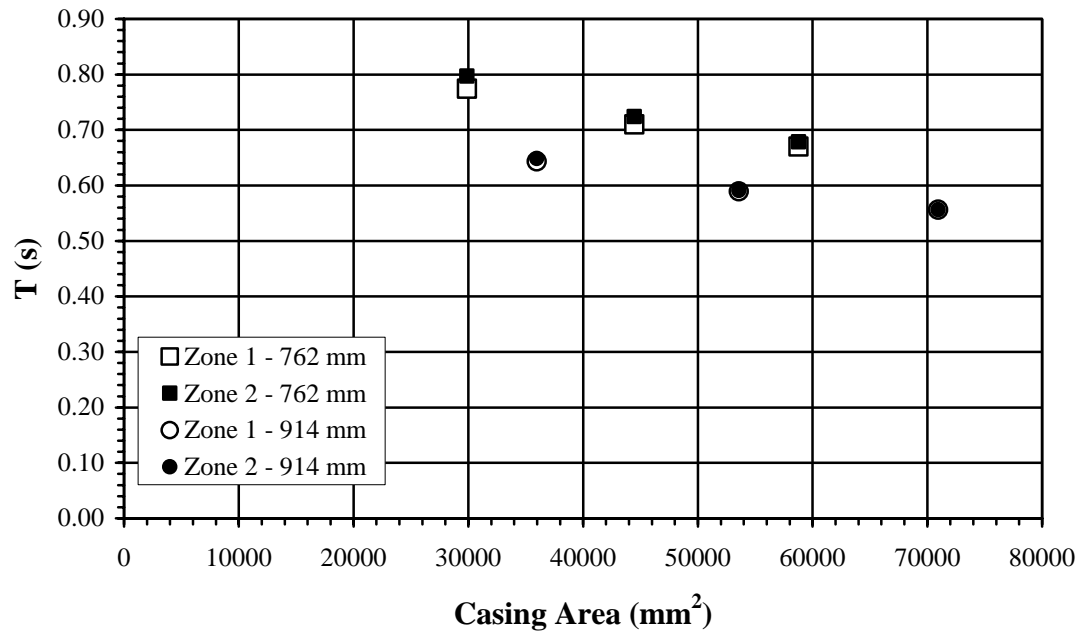


FIG. 6.5. Change in Period Due to Variation of Casing Size

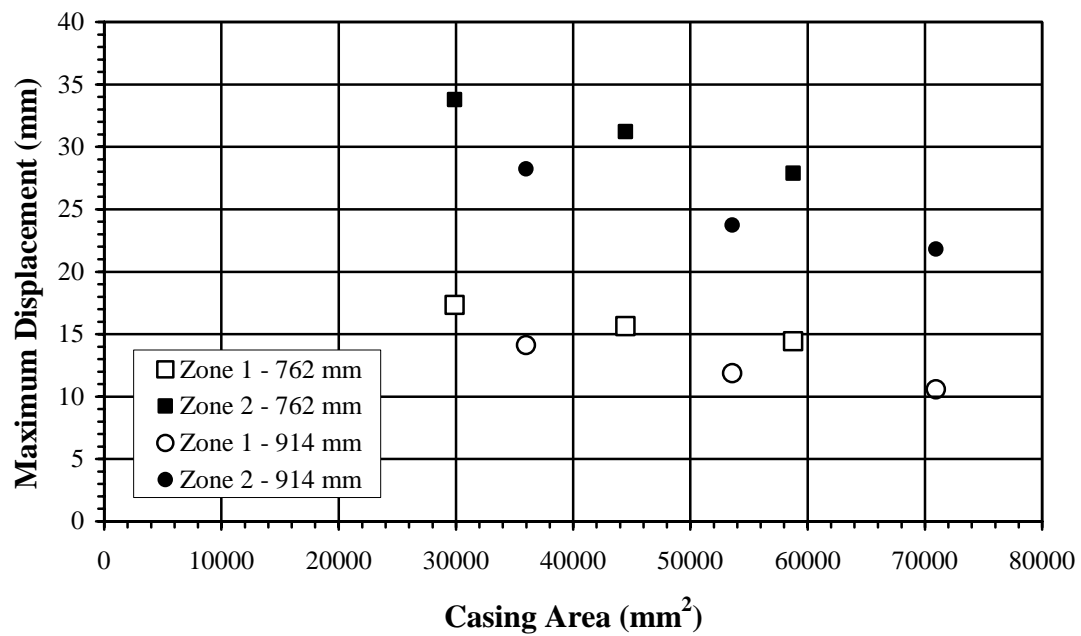


FIG. 6.6. Change in Deflections Due to Variation of Casing Size

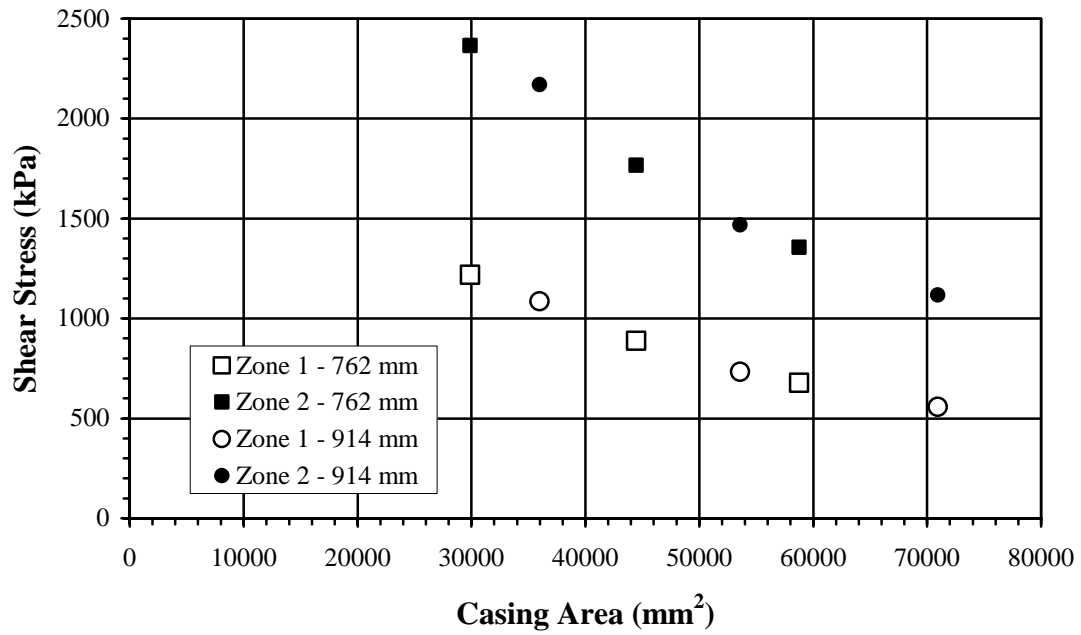


FIG. 6.7. Change in Shear Stress Due to Variation of Casing Size

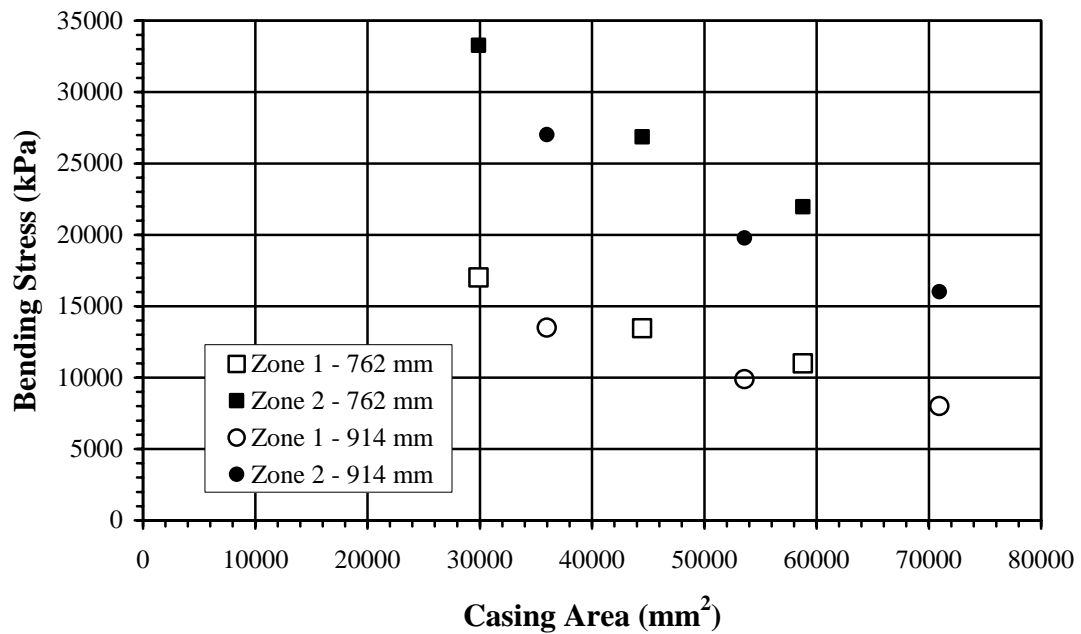


FIG. 6.8. Change in Bending Stress Due to Variation of Casing Size

#### **6.2.4. Variation of Mudline Strength and Strength Gradient of the Soil**

The effects of varying the mudline strength of the soil and the strength gradient of the soil along the length of the casing below the mudline were studied. The mudline strength and strength gradient values were varied  $\pm 10$  percent and  $\pm 20$  percent relative to the baseline model values. The results are presented in Tables 6.6 to 6.9 and Figs. 6.9 to 6.16.

As the mudline strength increases, the period of the structure decreases approximately four percent for the Zone 1 PGA and five percent for the Zone 2 PGA. Similarly, increasing the strength gradient values from 0.38 kPa/m (D1/D1) up to 0.57 kPa/m (D4/D4) resulted in a nearly linear decrease of approximately six percent in the model period. Increasing the value of either parameter caused small decreases in the deflection values obtained for the range of mudline strength and strength gradient values examined. The shear stresses of acting on the piles increased between five and seven percent over the range of values examined in this study. The bending stress and displacement values for both parameters do not show a definitive pattern corresponding with the variation values. This may be caused by the change in the length of the moment arm as the strength gradient and mudline strength are varied, so that even as the shear forces increase, the maximum bending moments could decrease or increase, depending on the length of the moment arm. The SSR and CSR values for both parameters were less than 0.7 and were relatively unaffected by the changes in the mudline strength and the strength gradient of the soil.

**TABLE 6.6. BMCOL76 and Response Spectra Calculations for Variation of Mudline Strength**

Zone	Model No.	Mudline strength (kPa)	T (s)	S <sub>A</sub> /G	S <sub>A</sub> (m/s <sup>2</sup> )	Displacement (mm)
1	C1	3.83	0.79	2.27	1.11	18.4
	C2	4.31	0.78	2.30	1.13	14.7
	CC	4.79	0.77	2.33	1.14	17.3
	C3	5.27	0.77	2.35	1.15	14.5
	C4	5.75	0.76	2.38	1.17	14.3
2	C1	3.83	0.82	2.20	2.16	34.6
	C2	4.31	0.81	2.23	2.19	28.5
	CC	4.79	0.80	2.26	2.22	33.8
	C3	5.27	0.79	2.29	2.24	28.1
	C4	5.75	0.78	2.32	2.27	27.9

**TABLE 6.7. Force and Stress Values for Variation of Mudline Strength**

Zone	Model No.	Shear Force (kN)	Shear Stress (kPa)	Overtopping Moment (kN-m)	Bending Stress (kPa)	SSR	CSR
1	C1	34.9	1,190	178	17,000	0.012	0.13
	C2	35.4	1,200	170	16,200	0.012	0.12
	CC	35.8	1,220	178	17,000	0.012	0.13
	C3	36.2	1,230	171	16,300	0.012	0.12
	C4	36.6	1,250	172	16,400	0.013	0.12
2	C1	67.7	2,300	346	33,000	0.023	0.21
	C2	68.6	2,340	329	31,400	0.024	0.21
	CC	69.5	2,370	349	33,300	0.024	0.22
	C3	70.4	2,400	333	31,700	0.024	0.21
	C4	71.3	2,430	335	31,900	0.024	0.21

**TABLE 6.8. BMCOL76 and Response Spectra Calculations for Variation of Strength Gradient**

Zone	Model No.	Strength gradient for soil (kPa/m)	T (s)	S <sub>A</sub> /G	S <sub>A</sub> (m/s <sup>2</sup> )	Displacement (mm)
1	D1	0.38	0.80	2.26	1.11	17.8
	D2	0.43	0.78	2.29	1.12	17.6
	CC	0.48	0.77	2.33	1.14	17.3
	D3	0.53	0.76	2.36	1.16	17.1
	D4	0.57	0.75	2.39	1.17	16.9
2	D1	0.38	0.82	2.18	2.14	36.9
	D2	0.43	0.81	2.22	2.18	36.3
	CC	0.48	0.80	2.26	2.22	33.8
	D3	0.53	0.78	2.29	2.25	35.1
	D4	0.57	0.77	2.33	2.28	34.6

**TABLE 6.9. Force and Stress Values for Variation of Strength Gradient**

Zone	Model No.	Shear Force (kN)	Shear Stress (kPa)	Overturning Moment (kN-m)	Bending Stress (kPa)	SSR	CSR
1	D1	34.8	1,180	175	16,700	0.012	0.13
	D2	35.3	1,200	169	16,100	0.012	0.12
	CC	35.8	1,220	178	17,000	0.012	0.13
	D3	36.3	1,230	172	16,400	0.012	0.13
	D4	36.7	1,250	174	16,600	0.013	0.13
2	D1	67.2	2,290	341	32,500	0.023	0.21
	D2	68.4	2,330	328	31,300	0.023	0.20
	CC	69.5	2,370	349	33,300	0.024	0.22
	D3	70.6	2,400	336	32,000	0.024	0.21
	D4	71.7	2,440	339	32,300	0.025	0.21

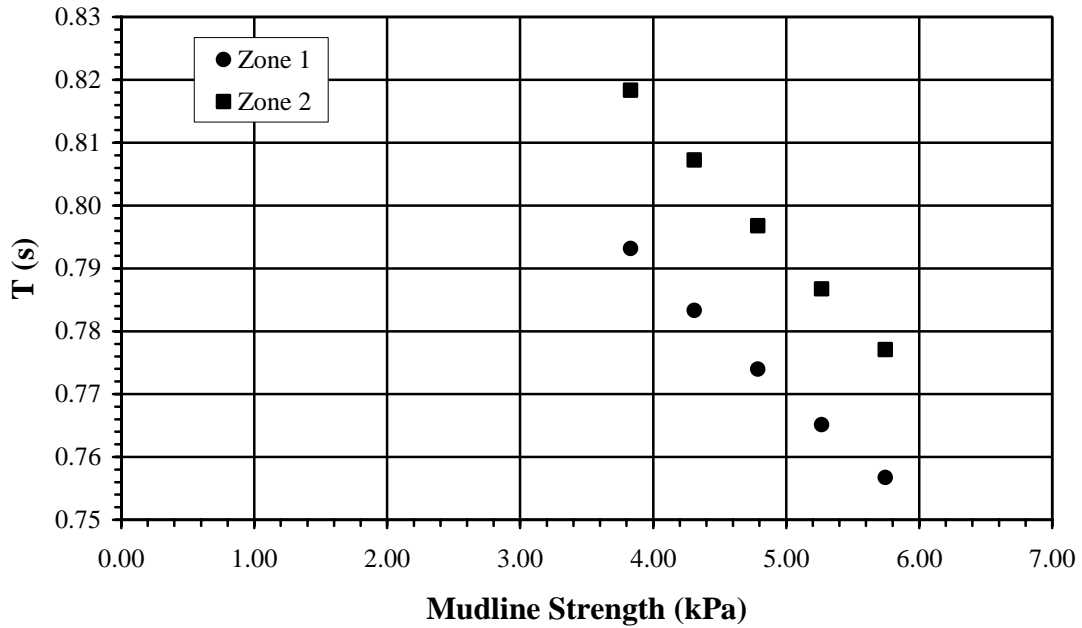


**FIG. 6.9. Change in Period Due to Variation of Mudline Strength**

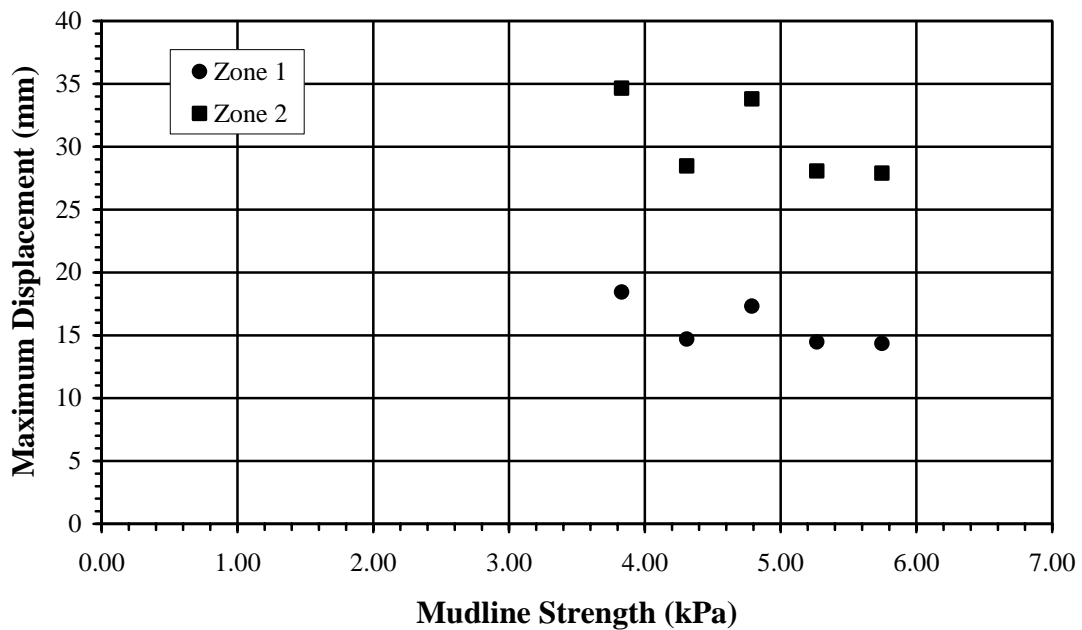


**FIG. 6.10. Change in Deflection Due to Variation of Mudline Strength**

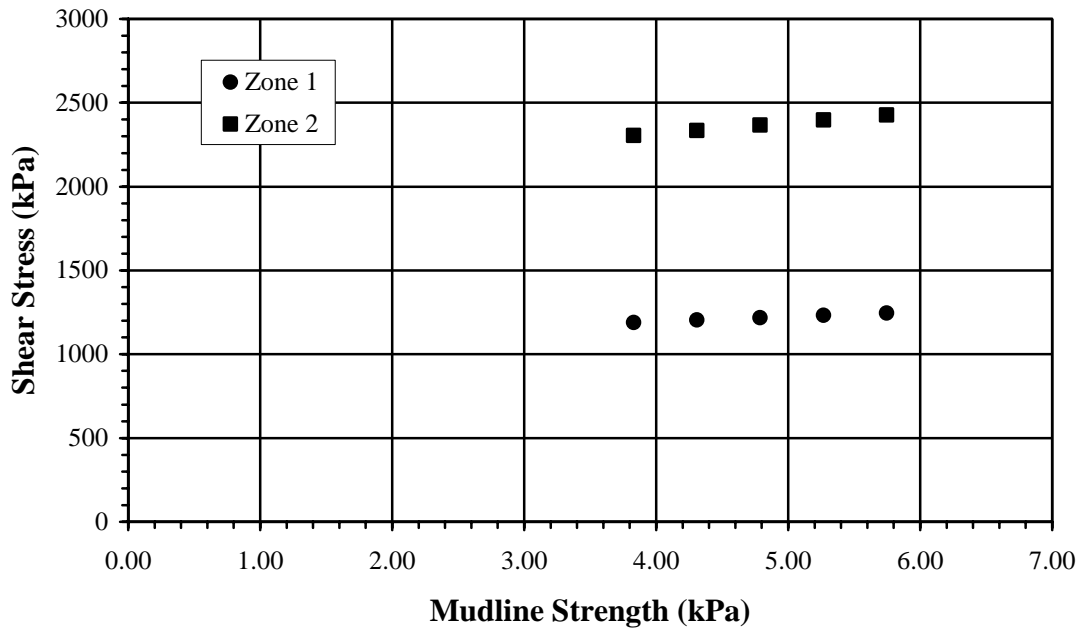


**FIG. 6.11. Change in Shear Stress Due to Variation of Mudline Strength**

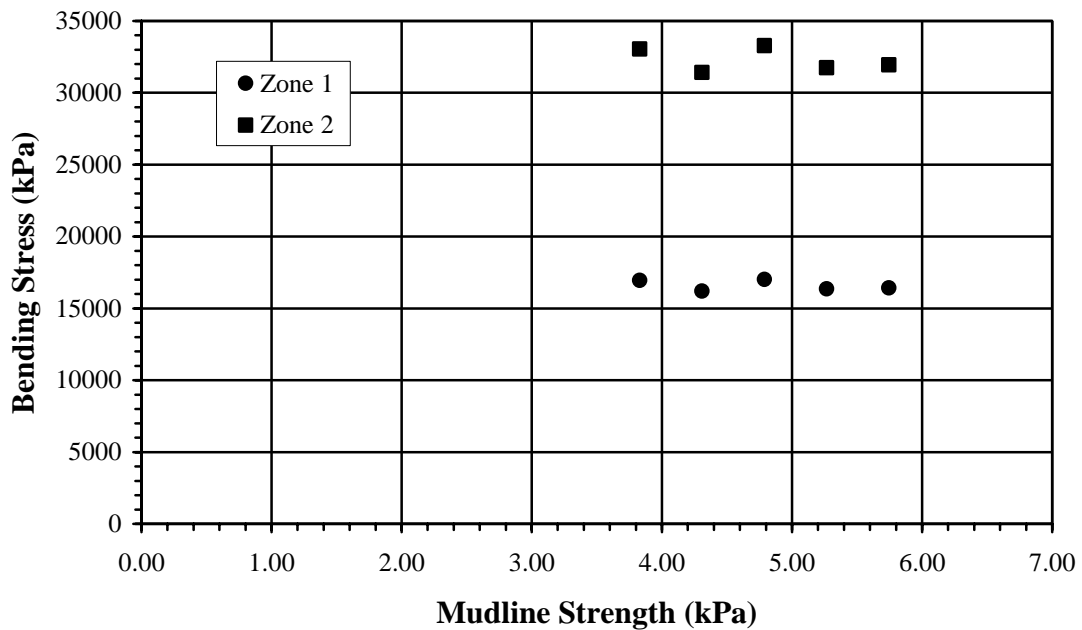


**FIG. 6.12. Change in Bending Stress Due Variation of Mudline Strength**

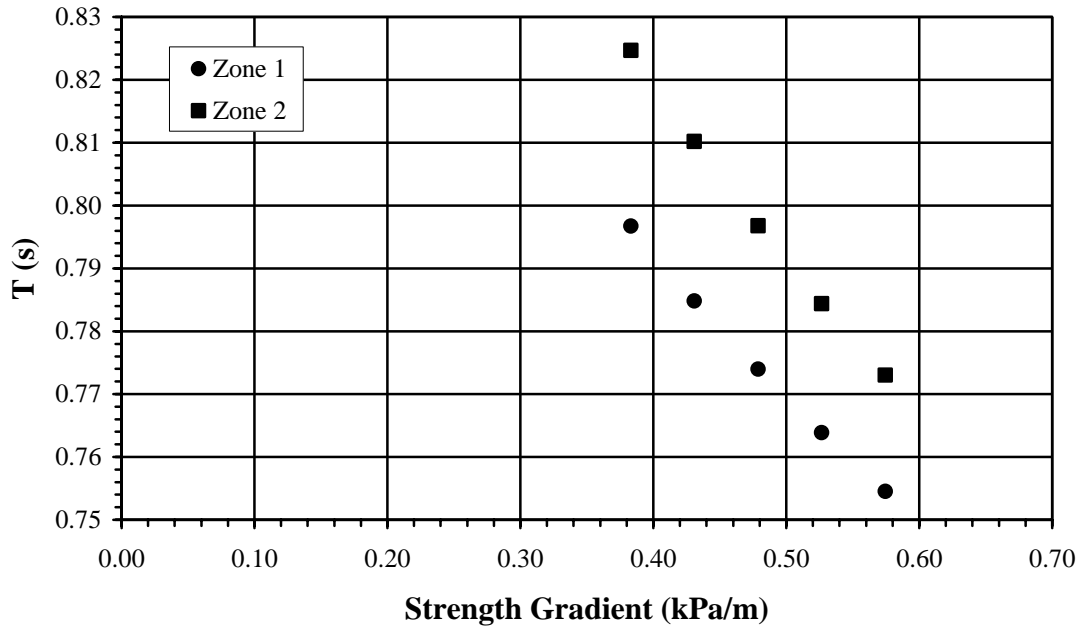


**FIG. 6.13. Change in Period Due to Variation of Strength Gradient**

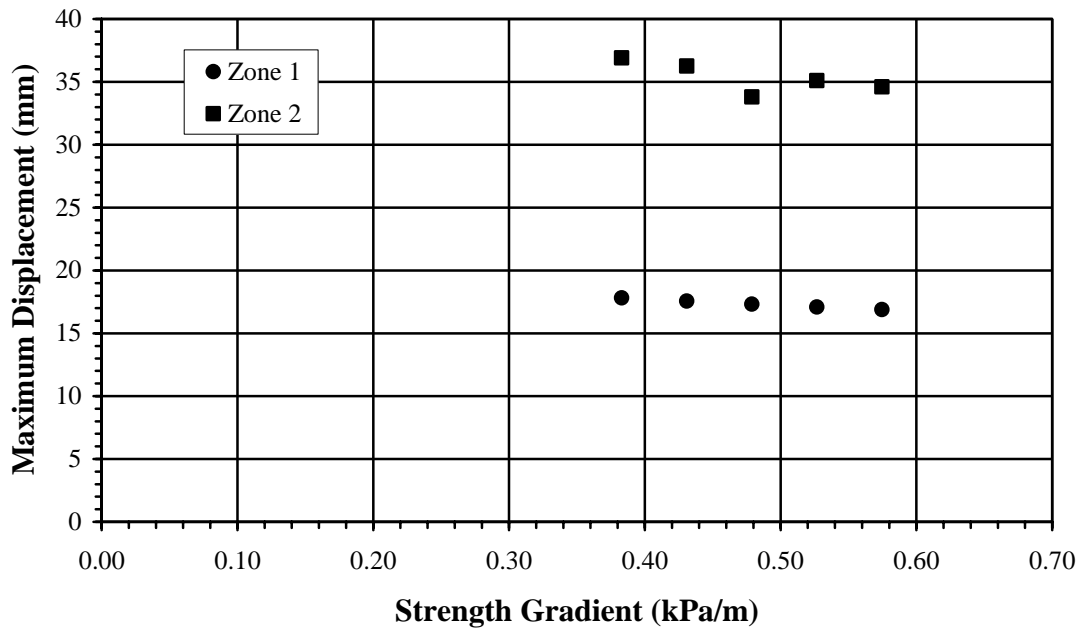


**FIG. 6.14. Change in Deflection Due to Variation of Strength Gradient**

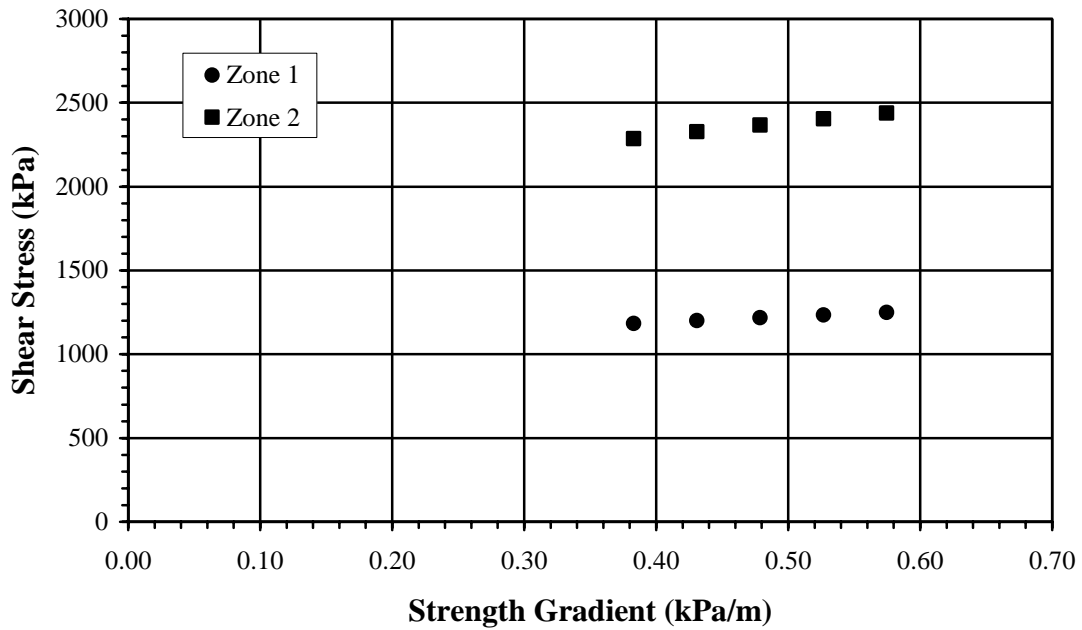


**FIG. 6.15. Change in Shear Stress Due to Variation of Strength Gradient**

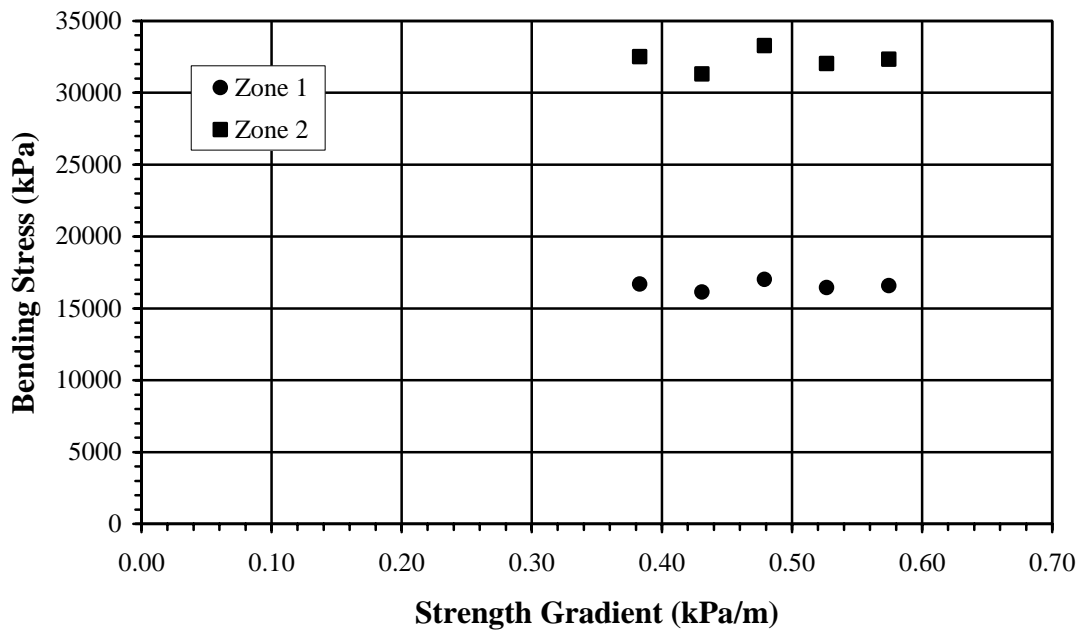


**FIG. 6.16. Change in Bending Stress Due Variation of Strength Gradient**

### 6.2.5. Variation of Mass Height Above the Mudline

This section contains the results obtained from varying the distance of the center of gravity for the lumped mass of the subsea model above the mudline. The values chosen for this parameter were based on dimensions that are typical of subsea applications. The results obtained for the analyses used to evaluate this parameter are presented in Tables 6.10 and 6.11 and Figs. 6.17 to 6.20.

The maximum bending stresses occurred below the mudline and the maximum shear stresses were observed at points along the portion of the casing above the mudline. As the height of the mass above the mudline increases, the period and deflection values of the model also increase. As the height of the casing increased from 2.44 m to 7.62 m, the maximum observed bending stress values increased approximately eight percent for the Zone 1 accelerations and 10 percent the Zone 2 accelerations. However, as the height of the casing increased, the observed shear stress values decreased approximately 60 percent. This is due to the decrease in the  $S_A$  values as the mass height above the mudline increased. Both the SSR and CSR values obtained for this parameter were less than 0.7. Finally, the SSR values decreased approximately 42 percent for Zones 1 and 2, while the CSR values remained relatively unchanged.

**TABLE 6.10. BMCOL76 and Response Spectra Calculations for Variation of Mass Height**

Zone	Model No.	Mass (mtons)	Height (m)	T (s)	S <sub>A</sub> /G	S <sub>A</sub> (m/s <sup>2</sup> )	Displacement (mm)
1	CC	31.4	2.44	0.77	2.33	1.14	17.3
	EA2		4.57	1.00	1.80	0.88	22.4
	EA3		6.10	1.18	1.53	0.75	26.4
	EA4		7.62	1.37	1.31	0.64	30.6
2	CC		2.44	0.80	2.26	2.22	33.8
	EA2		4.57	1.02	1.76	1.73	44.0
	EA3		6.10	1.19	1.52	1.49	54.1
	EA4		7.62	1.37	1.31	1.29	61.1

**TABLE 6.11. Resulting Force and Stress Values for Height Variations.**

Zone	Model No.	Shear Force (kN)	Shear Stress (kPa)	Overtopping Moment (kN-m)	Bending Stress (kPa)	SSR	CSR
1	CC	35.8	1220	178	17,000	0.012	0.13
	EA2	27.7	942	187	17,900	0.009	0.13
	EA3	23.5	800	190	18,200	0.008	0.14
	EA4	20.2	688	191	18,300	0.007	0.14
2	CC	69.5	2,370	349	33,300	0.024	0.22
	EA2	54.3	1,850	368	35,100	0.019	0.23
	EA3	46.7	1,590	378	36,100	0.016	0.23
	EA4	40.4	1,380	382	36,500	0.014	0.24

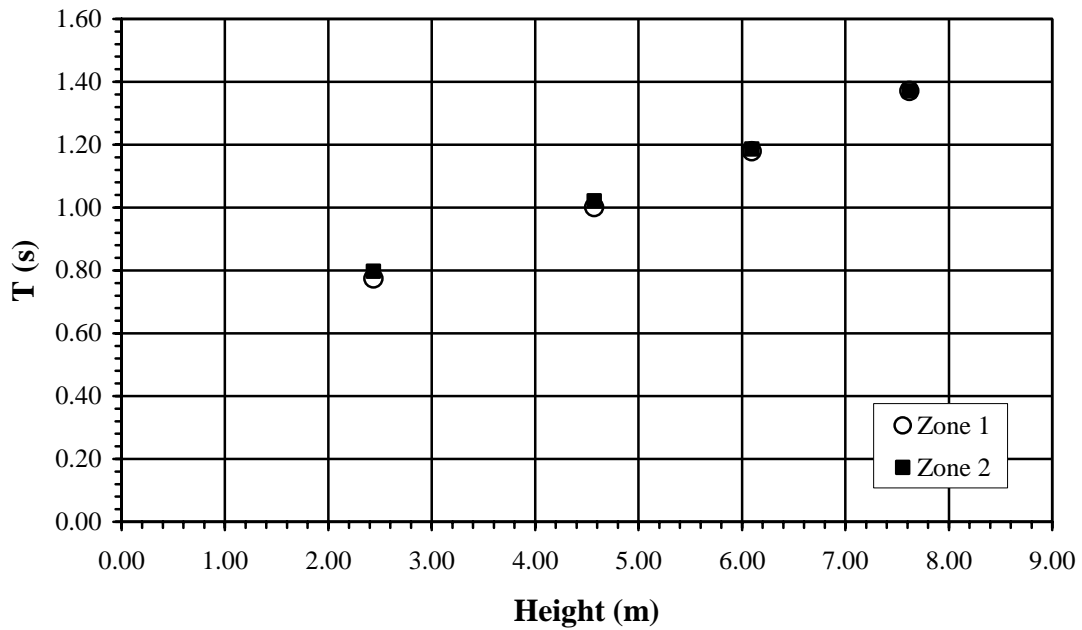


**FIG. 6.17. Change in Period Due to Variation of Mass Height**

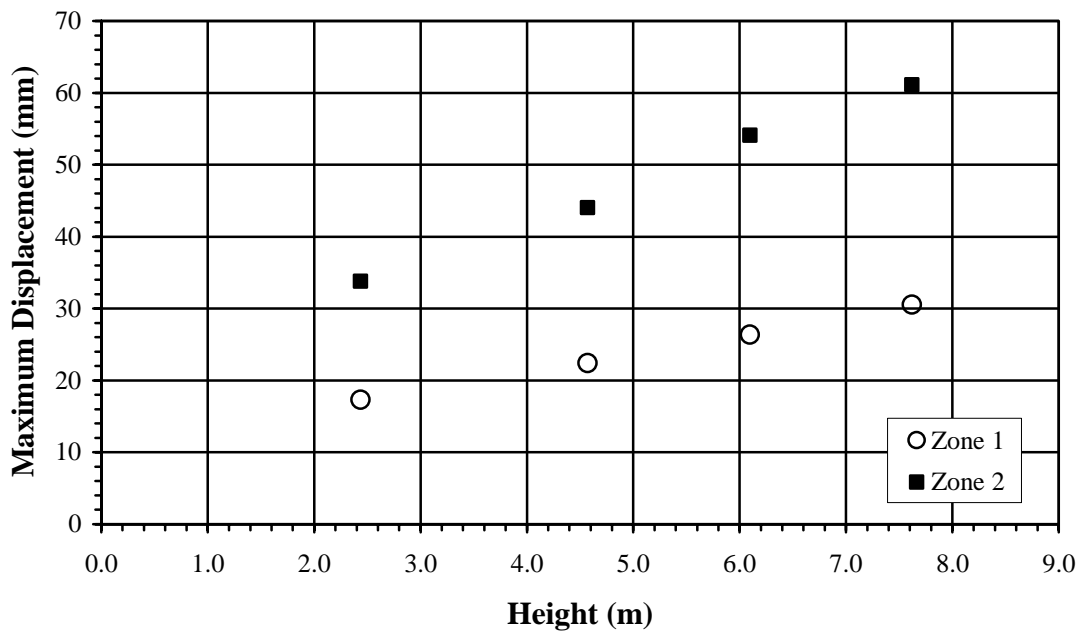


**FIG. 6.18. Change in Displacement Due to Variation of Mass Height**

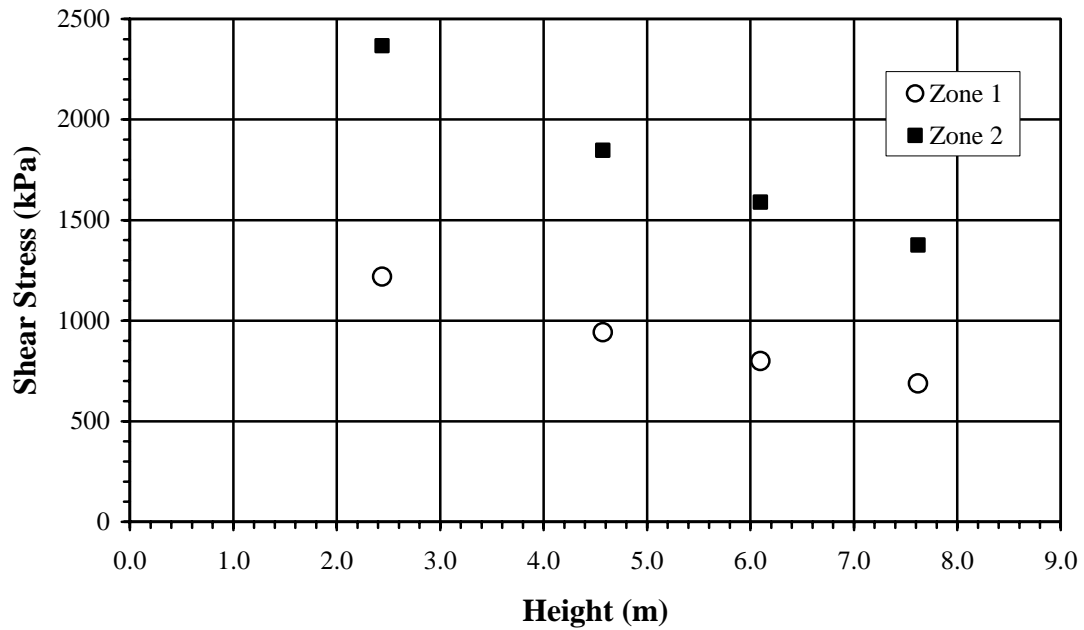


**FIG. 6.19. Change in Shear Stress Due to Variation of Mass Height**

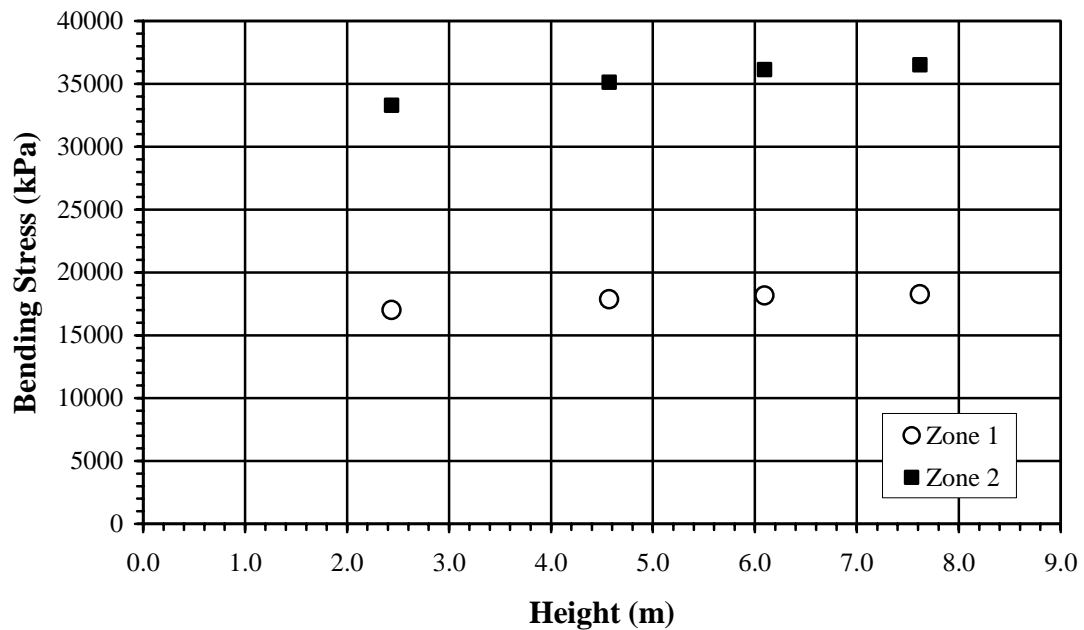


**FIG. 6.20. Change in Bending Stress Due to Variation of Mass Height**

### 6.2.6. Variation of Mass

This section contains the results obtained from the variation of the mass parameter of the baseline model. The values selected for this parameter were typical of some of the weights supported by subsea structures. The results obtained from the analysis of these models are presented in Tables 6.12 and 6.13 and Figs. 6.21 to 6.24.

The period of the model increased as the mass of the model increased, which is expected because the value of the period is related to value of the mass of the model. Although the spectral acceleration of the model decreased, the displacement, shear and bending stresses increased due to the increase in the mass. In addition these values appear to increase at a more constant rate only for mass values greater than 31.4 mtons, the second data point. Over the range of values used for this parameter variation, both the maximum shear and bending stress values were approximately three times greater than the minimum stress values. Figs. 6.21 to 6.24, show that when comparing the Zone 1 and 2 values of period, displacement, and stress a smaller difference occurs for smaller mass values. All of the CSR and SSR values obtained for this parameter were less than 0.7. The SSR values for Model ED1, with the largest mass, were approximately three times greater than those obtained from Model EB1, which had the smallest mass. In addition, the CSR values for Model ED1 were roughly 3.5 times larger than the corresponding values obtained for EB1.

**TABLE 6.12. BMCOL 76 and Response Spectra Calculations for Variation of Mass**

Zone	Model No.	Height (m)	Mass (mtons)	T (s)	S <sub>A</sub> /G	S <sub>A</sub> (m/s <sup>2</sup> )	Displacement (mm)
1	EB1	2.44	13.6	0.51	2.50	1.23	8.08
	CC		31.4	0.77	2.33	1.14	17.3
	EC1		45.4	0.93	1.93	0.95	20.8
	ED1		68.0	1.15	1.56	0.77	25.2
2	EB1		13.6	0.51	2.50	2.45	16.1
	CC		31.4	0.80	2.26	2.22	33.8
	EC1		45.4	0.97	1.86	1.83	41.3
	ED1		68.0	1.19	1.51	1.48	52.3

**TABLE 6.13. Force and Stress Values for Variation of Mass**

Zone	Model No.	Shear Force (kN)	Shear Stress (kPa)	Overtopping Moment (kN-m)	Bending Stress (kPa)	SSR	CSR
1	EB1	16.7	568	83.1	7,930	0.006	0.06
	CC	35.8	1,220	178	17,000	0.012	0.13
	EC1	43.0	1,460	214	20,500	0.015	0.16
	ED1	52.1	1,770	259	24,700	0.018	0.21
2	EB1	33.4	1,140	166	15,900	0.011	0.10
	CC	69.5	2,370	349	33,300	0.024	0.22
	EC1	82.9	2,820	423	40,300	0.028	0.27
	ED1	101	3,430	530	50,600	0.035	0.35

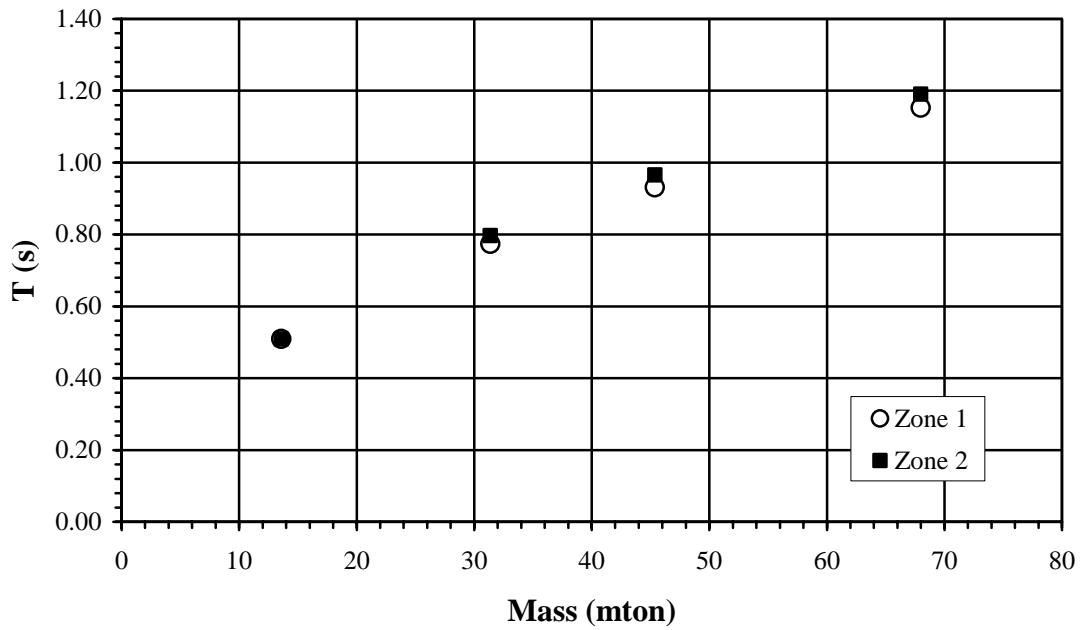


FIG. 6.21. Change in Period Due to Variation of Mass

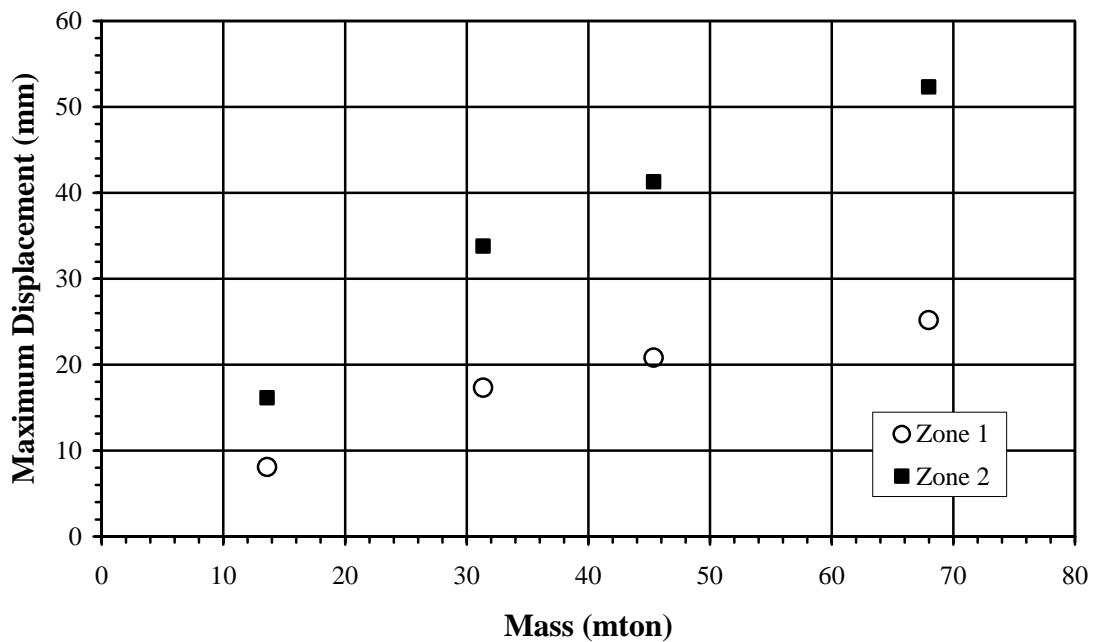
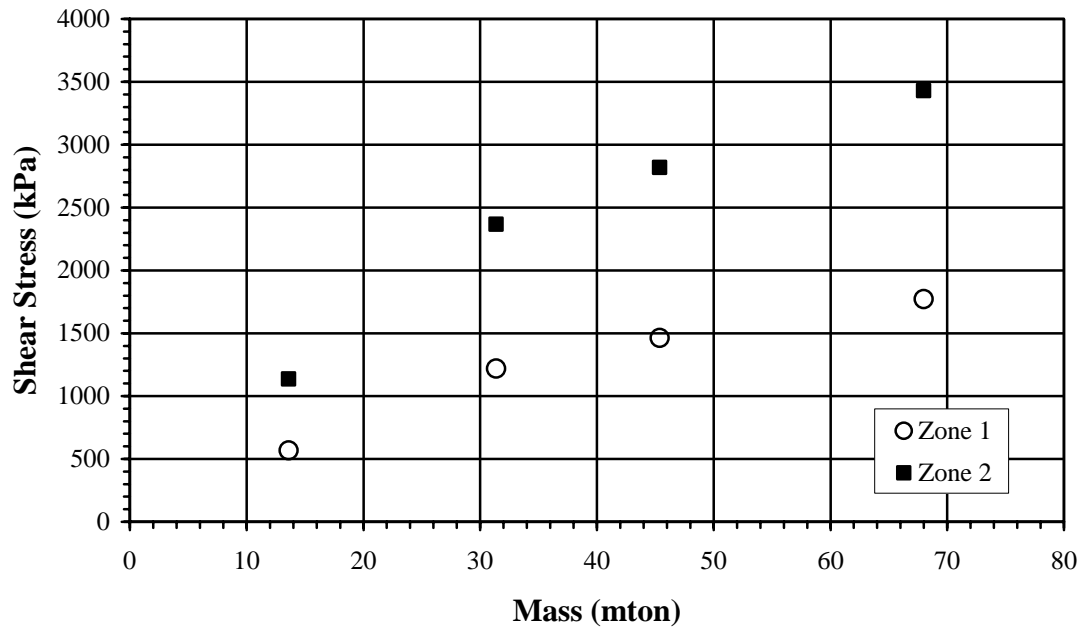
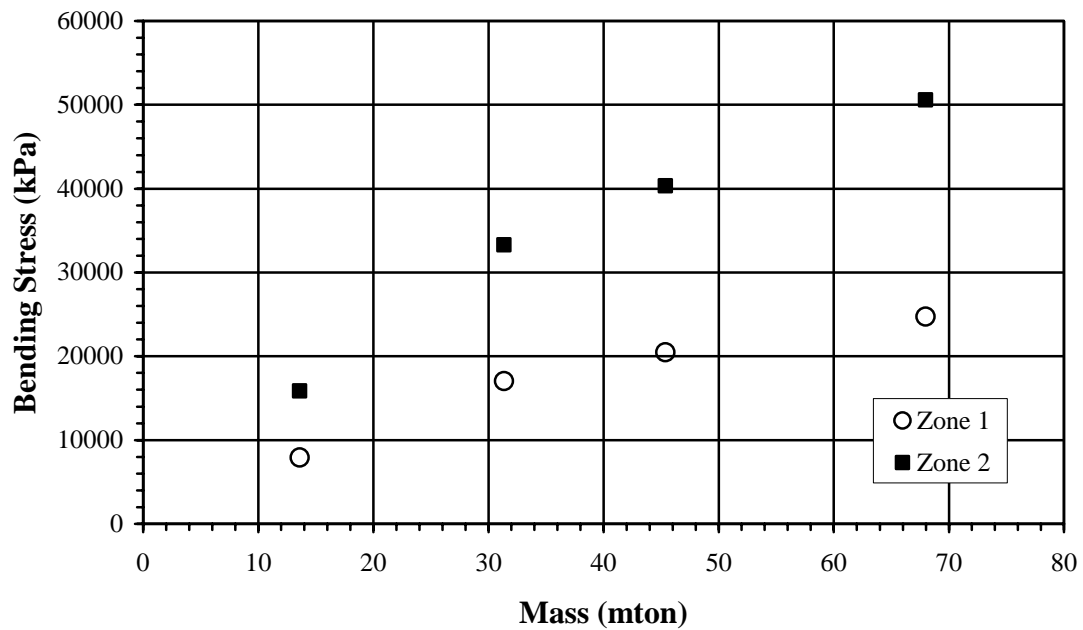


FIG. 6.22. Change in Displacement Due to Variation of Mass



**FIG. 6.23. Change in Shear Stress Due to Variation of Mass**



**FIG. 6.24. Change of Bending Stress Due to Variation of Mass**

### **6.2.7. Variation of Mass and Height of Mass Above the Mudline**

This section contains the results obtained from the combined variation of the height and mass of the model. These two parameters were selected for combined variation because the most significant changes in the response of the casing model were caused by the variation of these parameters separately. In all cases, the casing size and soil parameters were maintained to match the baseline model. The results obtained from the subsequent analyses are presented in Tables 6.14 and 6.15 and Figs. 25 to 28.

The period values for Model ED4 were approximately four times larger than the smallest value, obtained from the analyses of Model EB1. Figs. 6.25 and 6.26 show an approximately linear relationship for the period and displacement values versus the height of the casing. The results shown in Fig. 6.27 indicate that amount of change in the shear stress values increased as the mass of the model increased. Although the bending stresses increased as the height of the casing increased, the impact of the variation of mass was more critical. The SSR and CSR values obtained for this parameter were less than 0.7. Finally, the CSR values obtained from Model ED4 were approximately 4.0 times greater than the values obtained from Model EB1.

**TABLE 6.14. BMCOL76 and Response Spectra Calculations for Variation of Mass and Height**

Zone	Model No.	Mass (mtons)	Height (m)	T (s)	S <sub>A</sub> /G	S <sub>A</sub> (m/s <sup>2</sup> )	Displacement (mm)
1	EB1	13.6	2.44	0.51*	2.50	1.23	8.08
	EB2		4.57	0.66	2.50	1.23	13.5
	EB3		6.10	0.78	2.32	1.14	17.4
	EB4		7.62	0.90	1.99	0.98	20.1
	CC	31.4	2.44	0.77	2.33	1.14	17.3
	EA2		4.57	1.00	1.80	0.88	22.4
	EA3		6.10	1.18	1.53	0.75	26.4
	EA4		7.62	1.37	1.31	0.64	30.6
	EC1	45.4	2.44	0.93	1.93	0.95	20.8
	EC2		4.57	1.20	1.50	0.73	26.9
	EC3		6.10	1.42	1.27	0.62	31.6
	EC4		7.62	1.65	1.09	0.54	36.7
	ED1	68.0	2.44	1.15	1.56	0.77	25.2
	ED2		4.57	1.47	1.22	0.60	32.9
	ED3		6.10	1.74	1.04	0.51	38.8
	ED4		7.62	2.02	0.89	0.44	44.9
2	EB1	13.6	2.44	0.51*	2.50	2.45	16.1
	EB2		4.57	0.66	2.50	2.45	27.0
	EB3		6.10	0.78	2.32	2.27	34.7
	EB4		7.62	0.90	1.99	1.96	40.2
	CC	31.4	2.44	0.80	2.26	2.22	33.8
	EA2		4.57	1.02	1.76	1.73	44.0
	EA3		6.10	1.19	1.52	1.49	54.1
	EA4		7.62	1.37	1.31	1.29	61.1
	EC1	45.4	2.44	0.97	1.86	1.83	41.3
	EC2		4.57	1.25	1.45	1.42	52.9
	EC3		6.10	1.45	1.24	1.22	62.6
	EC4		7.62	1.67	1.08	1.06	73.2
	ED1	68.0	2.44	1.19	1.51	1.48	52.3
	ED2		4.57	1.54	1.17	1.14	65.9
	ED3		6.10	1.81	1.00	0.98	76.9
	ED4		7.62	2.08**	0.87	0.85	89.8

\* Minimum Period

\*\* Maximum Period

**TABLE 6.15. Force and Stress Values for Variation of Mass and Height**

Zone	Model No.	Shear Force (kN)	Shear Stress (kPa)	Overturning Moment (kN-m)	Bending Stress (kPa)	SSR	CSR
1	EB1	16.7	568	83.1	7,930	0.012	0.06
	EB2	16.7	568	113	10,800	0.009	0.07
	EB3	15.5	526	125	11,900	0.008	0.08
	EB4	13.3	453	126	12,000	0.007	0.08
	CC	35.8	1,220	178	17,000	0.006	0.13
	EA2	27.7	942	187	17,900	0.006	0.13
	EA3	23.5	800	190	18,200	0.005	0.14
	EA4	20.2	688	191	18,300	0.005	0.14
	EC1	43.0	1,460	214	20,500	0.015	0.16
	EC2	33.3	1,130	225	21,500	0.011	0.17
	EC3	28.2	961	228	21,800	0.010	0.18
	EC4	24.3	826	229	21,900	0.008	0.18
	ED1	52.1	1,770	259	24,700	0.018	0.21
	ED2	40.8	1,390	275	26,300	0.014	0.23
	ED3	34.6	1,180	280	26,700	0.012	0.23
	ED4	29.8	1,010	281	26,800	0.010	0.24
2	EB1	33.4	1,140	166	15,900	0.024	0.10
	EB2	33.4	1,140	225	21,500	0.019	0.13
	EB3	30.9	1,050	250	23,900	0.016	0.15
	EB4	26.6	906	252	24,000	0.014	0.15
	CC	69.5	2,370	349	33,300	0.011	0.22
	EA2	54.3	1,850	368	35,100	0.011	0.23
	EA3	46.7	1,590	378	36,100	0.011	0.23
	EA4	40.4	1,380	382	36,500	0.009	0.24
	EC1	82.9	2,820	423	40,300	0.028	0.27
	EC2	64.3	2,190	440	42,000	0.022	0.28
	EC3	55.1	1,880	450	43,000	0.019	0.29
	EC4	48.1	1,640	457	43,600	0.016	0.30
	ED1	101	3,430	530	50,600	0.035	0.35
	ED2	77.8	2,650	542	51,800	0.027	0.36
	ED3	66.4	2,260	549	52,400	0.023	0.37
	ED4	57.7	1,960	557	53,100	0.020	0.38

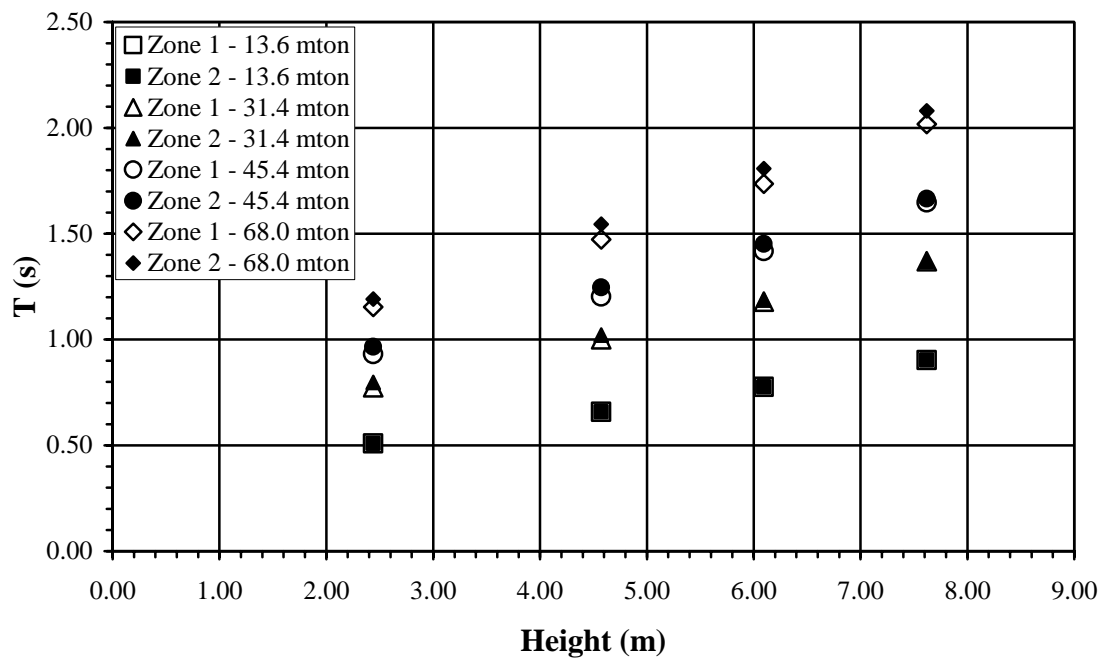


FIG. 6.25. Change in Period Due to Variation of Mass and Height

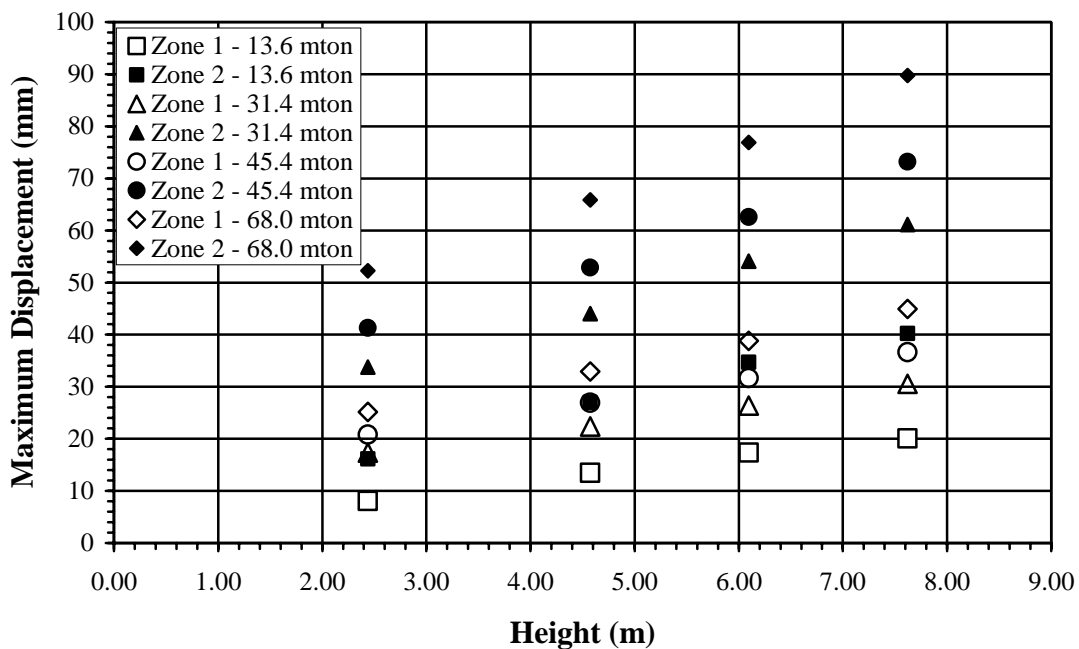


FIG. 6.26. Change in Displacement Due to Variation of Mass and Height

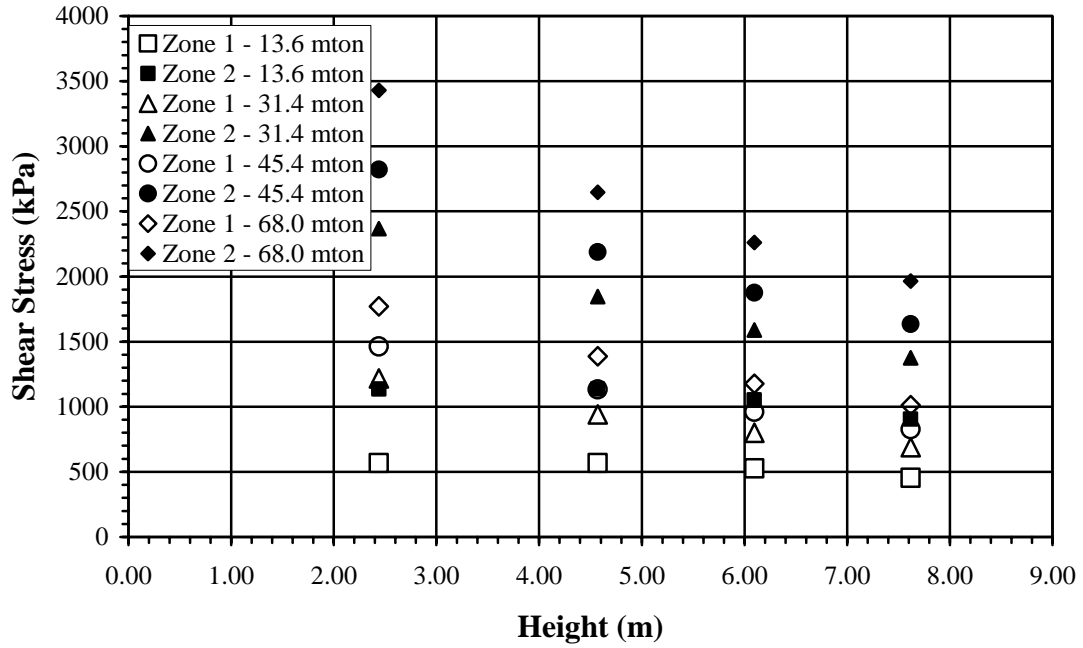


FIG. 6.27. Change in Shear Stress Due to Variation of Mass and Height

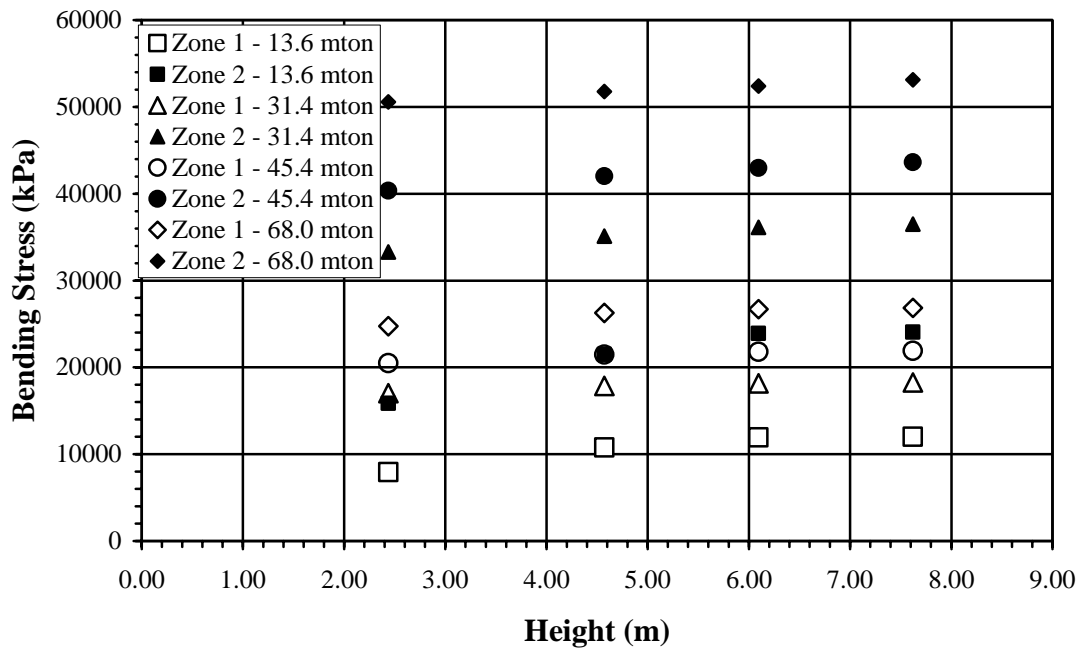


FIG. 6.28. Change in Bending Stress Due to Variation of Mass and Height

### 6.2.8. Fixity Variation

This section deals with the data generated by the analyses of the models with fixed-headed casings. The top of the casings were fixed against rotation to simulate the lateral resistance provided to an individual casing that is part of a multi-casing foundation. Tables 6.16 and 6.17, along with Figs. 6.29 to 6.32, outline the results obtained from these models. In addition, Figs. 6.29 to 6.32 include results from free-headed casing models with comparable characteristics to the fixed-headed models.

Analysis of Model CCF yielded period values that were about half of the period values obtained from the baseline model. Although the displacement of the model typically increased as the height of the cantilever increased for the free-headed models, the displacement values decreased as the height increased for the fixed-headed models. The same behavior was observed in the range of bending stress values obtained for the fixed-headed and free-headed models. However, the shear stresses from the fixed-headed casings decreased as the height increased, although these values were significantly higher than the stresses obtained from the comparable free-headed models. Although the CSR and SSR values obtained are below the limiting ratio of 0.7. The SSR values obtained from Model CCF were approximately ten percent higher than the ratios obtained from the baseline model. The CSR values obtained from the fixed headed models were approximately 1.4 to 1.8 times greater than the values obtained from the corresponding free-headed models. The increase in these values is primarily due to the increased bending stresses caused by fixing the casing against rotation.

**TABLE 6.16. BMCOL76 and Response Spectra Calculations for Fixed-Headed Casing**

Zone	Model No.	Mass (mtons)	Height (m)	T (s)	S <sub>A</sub> /G	S <sub>A</sub> (m/s <sup>2</sup> )	Displacement (mm)
1	CCF	31.4	2.44	0.45	2.50	1.23	7.02
	F1	68.0	4.57	0.81	2.22	1.09	31.3
	F2		6.10	0.94	1.92	0.94	27.2
	F3		7.62	1.07	1.68	0.82	23.8
2	CCF	31.4	2.44	0.46	2.50	2.45	13.4
	F1	68.0	4.57	0.84	2.15	2.11	64.4
	F2		6.10	0.95	1.89	1.85	55.2
	F3		7.62	1.08	1.67	1.64	48.1

**TABLE 6.17. Force and Stress Values for Fixed-Headed Casing**

Zone	Model No.	Shear Force (kN)	Shear Stress (kPa)	Overturning Moment (kN-m)	Bending Stress (kPa)	SSR	CSR
1	CCF	38.5	1,310	198	18,900	0.013	0.14
	F1	74.0	2,520	547	52,200	0.025	0.36
	F2	64.1	2,180	474	45,200	0.022	0.33
	F3	56.1	1,910	415	39,600	0.019	0.31
2	CCF	76.9	2,610	397	37,900	0.026	0.24
	F1	144	4,890	1,090	104,000	0.049	0.64
	F2	126	4,280	944	90,100	0.043	0.57
	F3	112	3,790	831	79,300	0.038	0.52

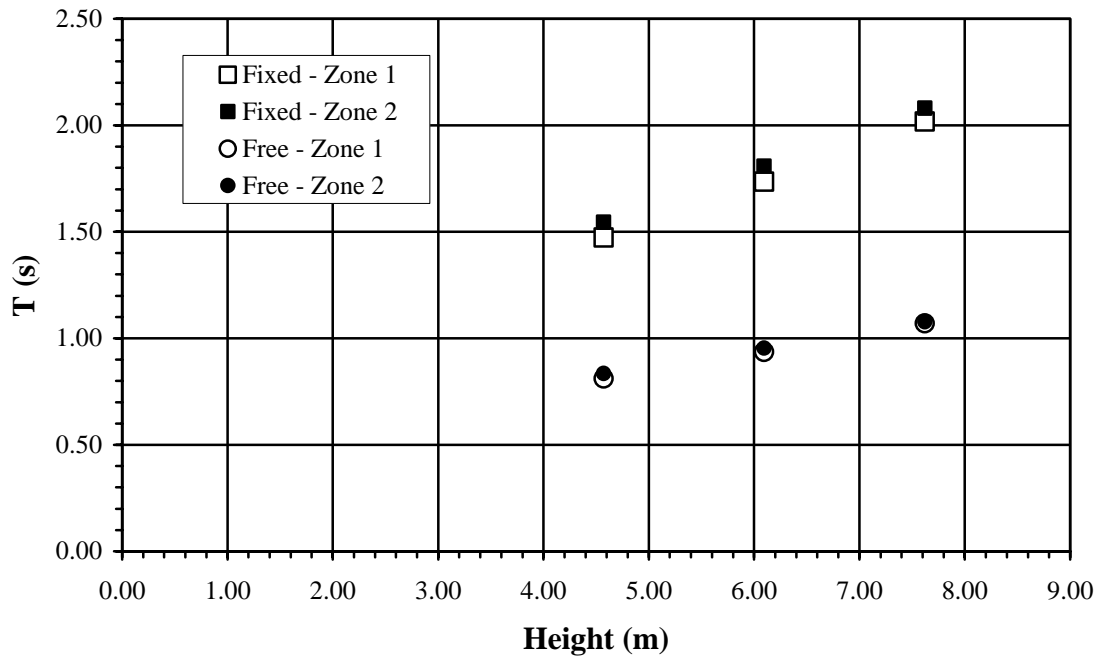


**FIG. 6.29. Comparison of Period Values Obtained from Free-Headed and Fixed-Headed Casings**

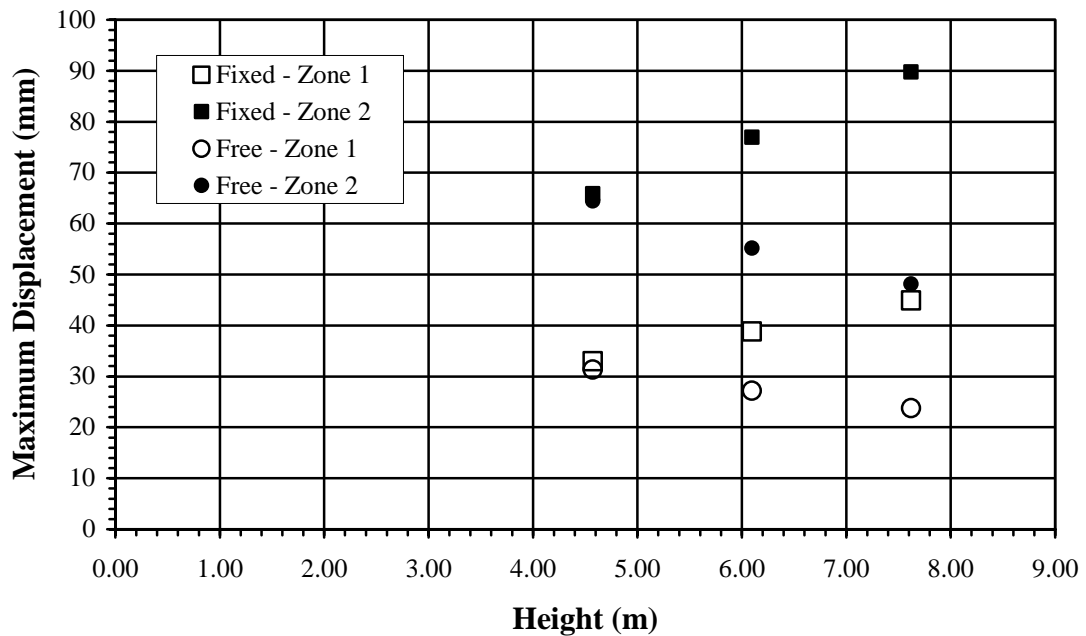


**FIG. 6.30. Comparison of Displacement Values Obtained from Free-Headed and Fixed-Headed Casings**

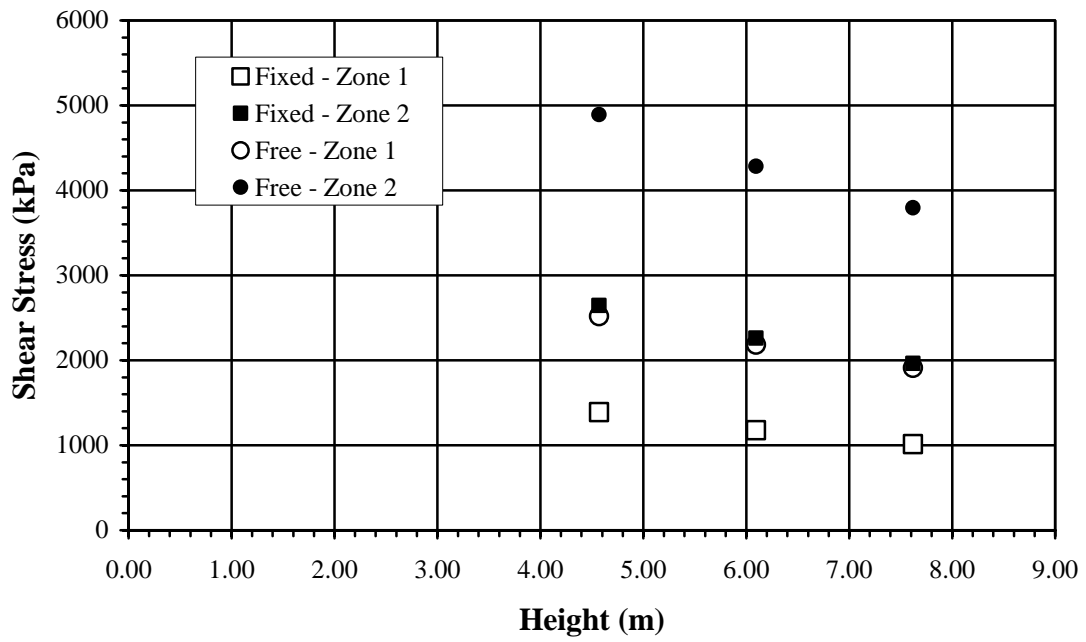


**FIG. 6.31. Comparison of Shear Stress Values Obtained from Free-Headed and Fixed-Headed Casings**

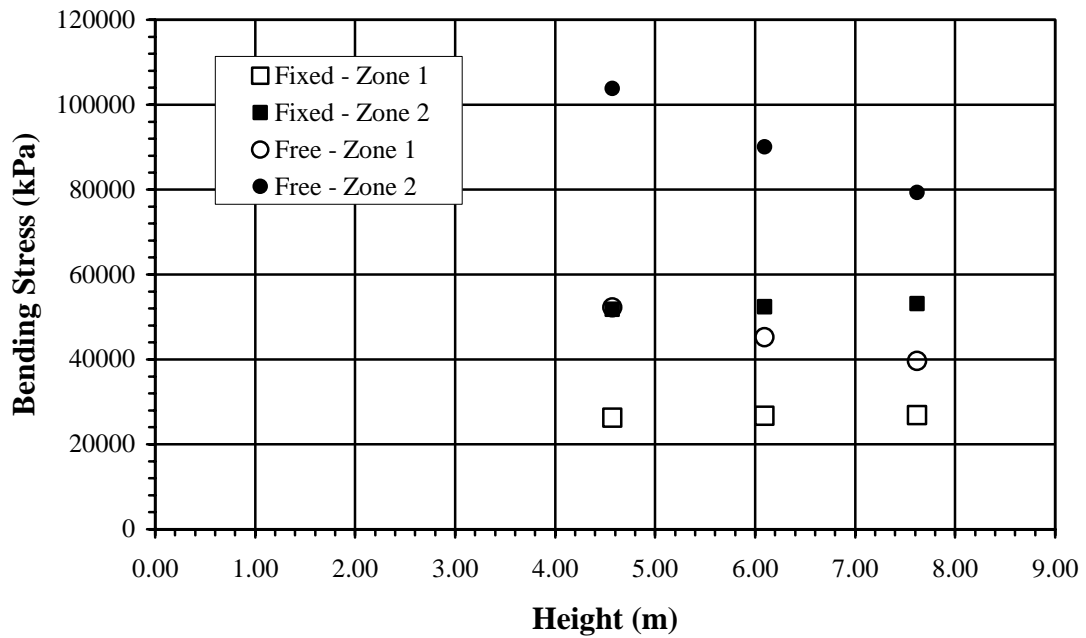


**FIG. 6.32. Comparison of Bending Stress Values Obtained from Free-Headed and Fixed-Headed Casings**

### 6.2.9. Summary of Parametric Study Results

A summary of the results obtained from the parametric study models is provided in this section. Table 6.18 presents the maximum and minimum results obtained from the parametric study of the free-headed casing models. The maximum period values for both Zones 1 and 2 are approximately 4.5 times larger than the minimum value. The largest SSR values are approximately five times greater than the smallest values obtained from the parametric study. Finally the maximum CSR values are 6 (Zone 1) and 16 (Zone 2) times greater than the minimum values.

**TABLE 6.18. Summary of Results for Parameter Variation**

Parameter	Zone 1		Zone 2	
	Minimum	Maximum	Minimum	Maximum
T (s)	0.45	2.02	0.46	2.08
Spectral Acceleration (m/s <sup>2</sup> )	0.44	1.23	0.85	2.45
Displacement (mm)	7.02	44.9	13.4	89.8
Shear Stress (kPa)	307	1,770	906	3,430
Bending Stress (kPa)	3,330	40,800	6,650	81,100
SSR	0.005	0.025	0.009	0.049
CSR	0.04	0.36	0.06	0.64

Tables 6.19 to 6.26 present summaries of the period, displacement and stress values obtained from the analyses performed for this study. Figs. 6.33 to 6.36 depict the variation of these results with respect the each parameter. As shown in these tables and figures, the parameter variations which caused the greatest changes in the response of the model were the combined height and mass parameters, as well as the fixity parameter. As compared with the other parameters, changes in the mudline strength and

strength gradient of the soil caused the least amount of variation in the period, stress and displacement of the model. The greatest variation in the displacement values were caused by the manipulation of the mass and height parameters, and the greatest variation in the shear and bending stresses were observed in the fixed-headed models.

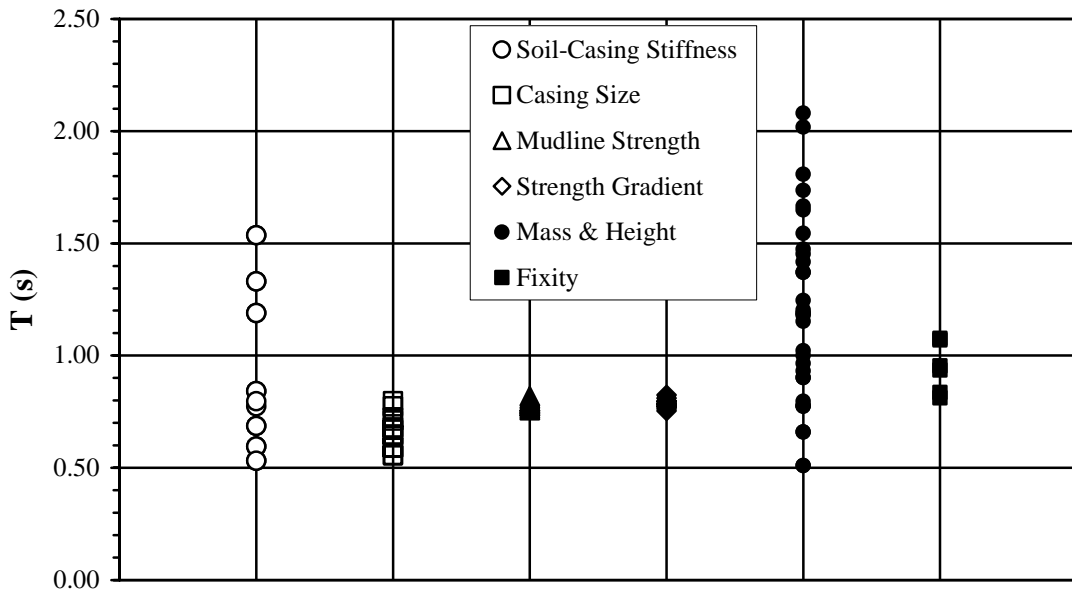


**FIG. 6.33. Range of Period Values for Parameter Variations – Free Headed Pile**

**TABLE 6.19. Summary of Period Data from Parametric Study – Fixed-Headed Pile**

Model No.	Mass (mton)	Height (m)	T (s)	
			Zone 1	Zone 2
F1	31.4	2.44	0.45	0.46
F2	68.0	4.57	0.81	0.84
F3		6.10	0.94	0.95
F4		7.62	1.07	1.08

**TABLE 6.20. Summary of Period Data from Parametric Study – Free-Headed Pile**

Model No.	Variable	Units	Parameter Value	T (s)		
				Zone 1	Zone 2	
CC	Control Case	-	-	0.77	0.80	
A1	Soil-Casing Spring	kN/mm	0.53	1.54	1.54	
A2			0.70	1.33	1.33	
A3			0.88	1.19	1.19	
A4			1.75	0.84	0.84	
A5			2.63	0.69	0.69	
A6			3.50	0.60	0.60	
A7			4.38	0.53	0.53	
B1	Pile Size (Outer Dia. by Wall Thick.)	mm	762 x 38.1	0.71	0.72	
B2			762 x 50.8	0.67	0.68	
B3			914 x 25.4	0.64	0.65	
B4			914 x 38.1	0.59	0.59	
B5			914 x 50.8	0.56	0.56	
C1	Strength Gradient	kPa	0.38	0.80	0.83	
C2			0.43	0.79	0.81	
C3			0.53	0.76	0.78	
C4			0.58	0.76	0.77	
D1	Mudline Strength	kPa/m	3.83	0.79	0.82	
D2			4.31	0.78	0.81	
D3			5.27	0.77	0.79	
D4			5.75	0.76	0.78	
E1	Mass & Height	mtons, m	31.4	4.57	1.00	1.02
E2				6.10	1.18	1.19
E3				7.62	1.37	1.37
E4			13.6	2.44	0.51	0.51
E5				4.57	0.66	0.66
E6				6.10	0.78	0.78
E7				7.62	0.90	0.90
E8			45.4	2.44	0.93	0.97
E9				4.57	1.20	1.25
E10				6.10	1.42	1.45
E11				7.62	1.65	1.67
E12			68.0	2.44	1.15	1.19
E13				4.57	1.47	1.54
E14				6.10	1.74	1.81
E15				7.62	2.02	2.08

**TABLE 6.21. Summary of Deflection Data from Parametric Study – Free-Headed Pile**

Model No.	Variable	Units	Parameter Value	Displacement (mm)		
				Zone 1	Zone 2	
CC	Control Case	-	-	17.3	33.8	
A1	Soil-Casing Spring	kN/mm	0.53	34.3	68.7	
A2			0.70	29.7	59.7	
A3			0.88	26.6	53.2	
A4			1.75	18.8	37.6	
A5			2.63	14.6	29.3	
A6			3.50	11.0	22.0	
A7			4.38	8.79	17.6	
B1	Pile Size (Outer Dia. by Wall Thick.)	mm	762 x 38.1	15.6	31.2	
B2			762 x 50.8	14.4	27.9	
B3			914 x 25.4	14.1	28.2	
B4			914 x 38.1	11.9	23.7	
B5			914 x 50.8	10.6	21.8	
C1	Strength Gradient	kPa	0.38	17.8	36.9	
C2			0.43	17.6	36.3	
C3			0.53	17.1	35.1	
C4			0.58	16.9	34.6	
D1	Mudline Strength	kPa/m	3.83	18.4	34.6	
D2			4.31	14.7	28.5	
D3			5.27	14.5	28.1	
D4			5.75	14.3	27.9	
E1	Mass & Height	mtons, m	31.4	4.57	22.4	44.0
E2				6.10	26.4	54.1
E3				7.62	30.6	61.1
E4			13.6	2.44	8.10	16.1
E5				4.57	13.5	27.0
E6				6.10	17.3	34.7
E7				7.62	20.1	40.2
E8			45.4	2.44	20.8	41.3
E9				4.57	26.9	52.9
E10				6.10	31.6	62.6
E11			68.0	7.62	36.7	73.2
E12				2.44	25.2	52.3
E13				4.57	32.9	65.9
E14				6.10	38.8	76.9
E15				7.62	44.9	89.8

**TABLE 6.22. Summary of Deflection Data from Parametric Study – Fixed-Headed Pile**

Model No.	Mass (mton)	Height (m)	Displacement (mm)	
			Zone 1	Zone 2
F1	31.4	2.44	7.02	13.4
F2	68.0	4.57	31.3	64.4
F3		6.10	27.2	55.2
F4		7.62	23.8	48.1

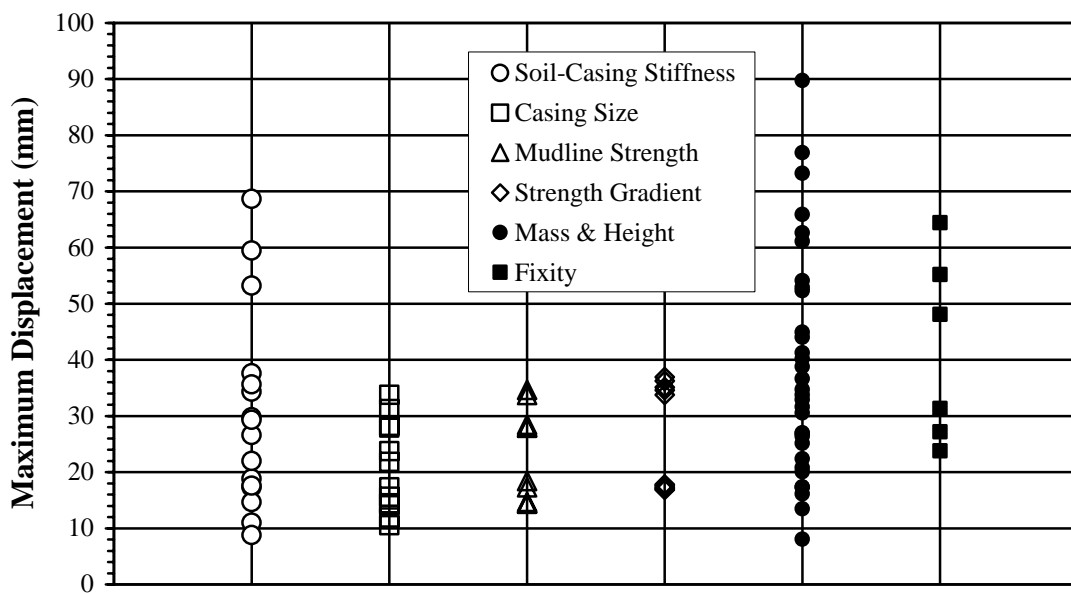


**FIG. 6.34. Range of Maximum Displacement Values for Parameter Variations**

**TABLE 6.23. Summary of Shear Stresses from Parametric Study – Free-Headed Pile**

Model No.	Variable	Units	Parameter Value	Shear Stress (kPa)		
				Zone 1	Zone 2	
CC	Control Case	-	-	1,220	2,370	
A1	Soil-Casing Spring	kN/mm	0.53	614	1,230	
A2			0.70	709	1,420	
A3			0.88	793	1,590	
A4			1.75	1,120	2,240	
A5			2.63	1,310	2,620	
A6			3.50	1,310	2,620	
A7			4.38	1,310	2,620	
B1			Pile Size (Outer Dia. by Wall Thick.)	mm	762 x 38.1	888
B2	762 x 50.8	678			1,360	
B3	914 x 25.4	1,080			2,170	
B4	914 x 38.1	734			1,470	
B5	914 x 50.8	558			1,120	
C1	Strength Gradient	kPa	0.38	1,180	2,290	
C2			0.43	1,200	2,330	
C3			0.53	1,230	2,400	
C4			0.58	1,250	2,440	
D1	Mudline Strength	kPa/m	3.83	1,190	2,300	
D2			4.31	1,200	2,340	
D3			5.27	1,230	2,400	
D4			5.75	1,250	2,430	
E1	Mass & Height	mtons, m	31.4	4.57	942	1,850
E2				6.10	800	1,590
E3				7.62	688	1,380
E4			13.6	2.44	568	1,140
E5				4.57	568	1,140
E6				6.10	526	1,050
E7				7.62	453	906
E8			45.4	2.44	1,460	2,820
E9				4.57	1,130	2,190
E10				6.10	961	1,880
E11				7.62	826	1,640
E12			68.0	2.44	1,770	3,430
E13				4.57	1,390	2,650
E14				6.10	1,180	2,260
E15				7.62	1,010	1,960

**TABLE 6.24. Summary of Shear Stresses from Parametric Study – Fixed-Headed Pile**

Model No.	Mass (mton)	Height (m)	Displacement (mm)	
			Zone 1	Zone 2
F1	31.4	2.44	1,310	2,610
F2	68.0	4.57	2,520	4,890
F3		6.10	2,180	4,280
F4		7.62	1,910	3,790

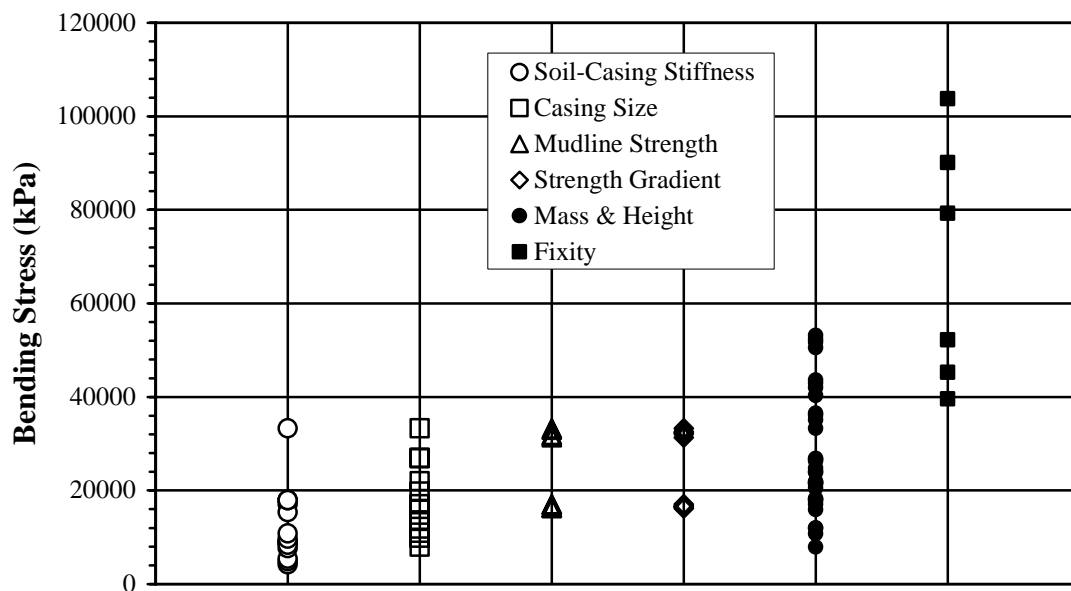


**FIG. 6.35. Range of Shear Stress Values for Parameter Variations**

**TABLE 6.25. Summary of Bending Stresses from Parametric Study – Free-Headed Pile**

Model No.	Variable	Units	Parameter Value	Bending Stress (kPa)		
				Zone 1	Zone 2	
CC	Control Case	-	-	17,000	33,300	
A1	Soil-Casing Spring	kN/mm	0.53	4,200	8,400	
A2			0.70	4,850	9,700	
A3			0.88	5,420	10,800	
A4			1.75	7,670	15,300	
A5			2.63	8,960	17,900	
A6			3.50	8,960	17,900	
A7			4.38	8,960	17,900	
B1	Pile Size (Outer Dia. by Wall Thick.)	mm	762 x 38.1	13,500	26,900	
B2			762 x 50.8	11,000	22,000	
B3			914 x 25.4	13,500	27,000	
B4			914 x 38.1	9,890	19,800	
B5			914 x 50.8	8,010	16,000	
C1	Strength Gradient	kPa	0.38	16,700	32,500	
C2			0.43	16,100	31,300	
C3			0.53	16,400	32,000	
C4			0.58	16,600	32,300	
D1	Mudline Strength	kPa/m	3.83	17,000	33,000	
D2			4.31	16,200	31,400	
D3			5.27	16,300	31,700	
D4			5.75	16,400	31,900	
E1	Mass & Height	mtons, m	31.4	4.57	17,900	35,100
E2				6.10	18,200	36,100
E3				7.62	18,300	36,500
E4			13.6	2.44	7,930	15,900
E5				4.57	10,800	21,500
E6				6.10	11,900	23,900
E7				7.62	12,000	24,000
E8			45.4	2.44	20,500	40,300
E9				4.57	21,500	42,000
E10				6.10	21,800	43,000
E11				7.62	21,900	43,600
E12			68.0	2.44	24,700	50,600
E13				4.57	26,300	51,800
E14				6.10	26,700	52,400
E15				7.62	26,800	53,100

**TABLE 6.26. Summary of Bending Stresses from Parametric Study – Fixed-Headed Pile**

Model No.	Mass (mton)	Height (mton)	Displacement (mm)	
			Zone 1	Zone 2
F1	31.4	2.44	18,900	37,900
F2	68.0	4.57	52,200	104,000
F3		6.10	45,200	90,100
F4		7.62	39,600	79,300

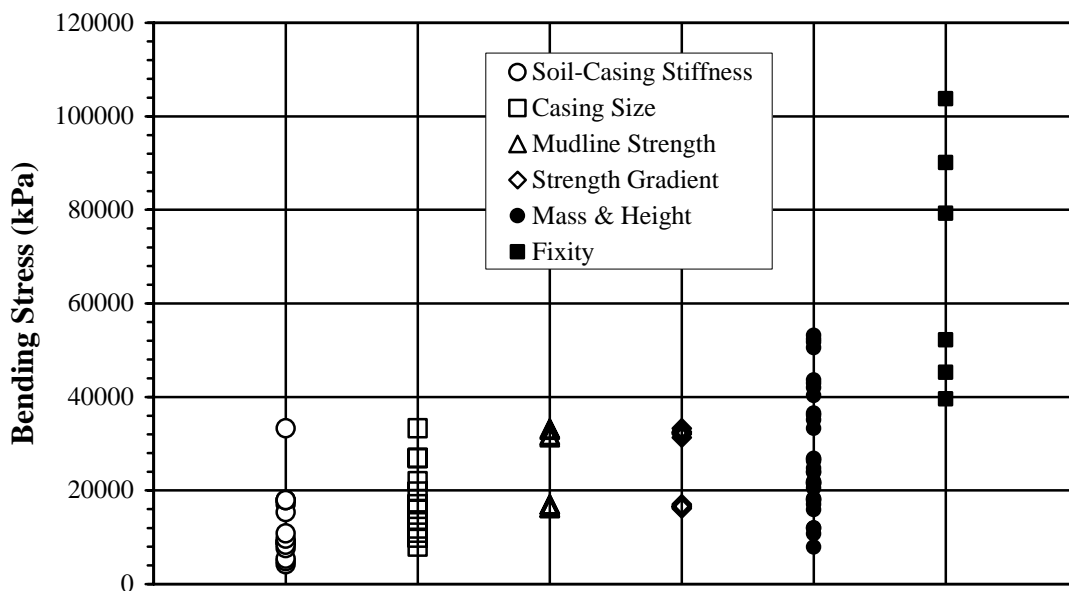


**FIG. 6.36. Range of Bending Stress Values for Parameter Variations**

### 6.3. TIME HISTORY ANALYSIS RESULTS

The results obtained from the time history analysis of the baseline model using the acceleration record from the 1940 El Centro, California earthquake, shown in Fig. 6.37, are presented in this section. It should be noted that the acceleration record was not scaled to fit the design spectra. The SAP2000 program was used to determine the

acceleration and shear force values experienced by the model for the El Centro ground accelerations (SAP2000 1999). As with the parametric study, the maximum moment and displacement values were determined by using the BMCOL76 program (BMCOL76 1981), as discussed in Section 5.3.3. Table 6.27 outlines the maximum accelerations, forces, stresses and displacements experienced by the casing for the applied ground motions. The response spectrum corresponding to the El Centro record, along with the Zones 1 and 2 API design spectra are shown in Fig 6.38. The line intersecting the spectra where the period is equal to 0.74 seconds shows that El Centro accelerations are approximately six times greater than the Zone 1 accelerations and three times greater than the Zone 2 accelerations. Figs. 6.39 and Figs. 6.40 display the acceleration and shear force values with respect to time. These results indicate that the CSR and SSR values are less than the limiting ratio of 0.7.

**TABLE 6.27. Time History Analysis Results (SAP2000 1999)**

<b>Parameter</b>	<b>Value</b>
T (s)	0.74
Maximum Acceleration (cm/s <sup>2</sup> )	653
Maximum Displacement (mm)	137
Maximum Shear Force (kN)	205
Maximum Shear Stress (kPa)	6,980
Maximum Bending Moment (kN-m)	1,230
Maximum Bending Stress (kPa)	117,000
Maximum SSR	0.070
Maximum CSR	0.66

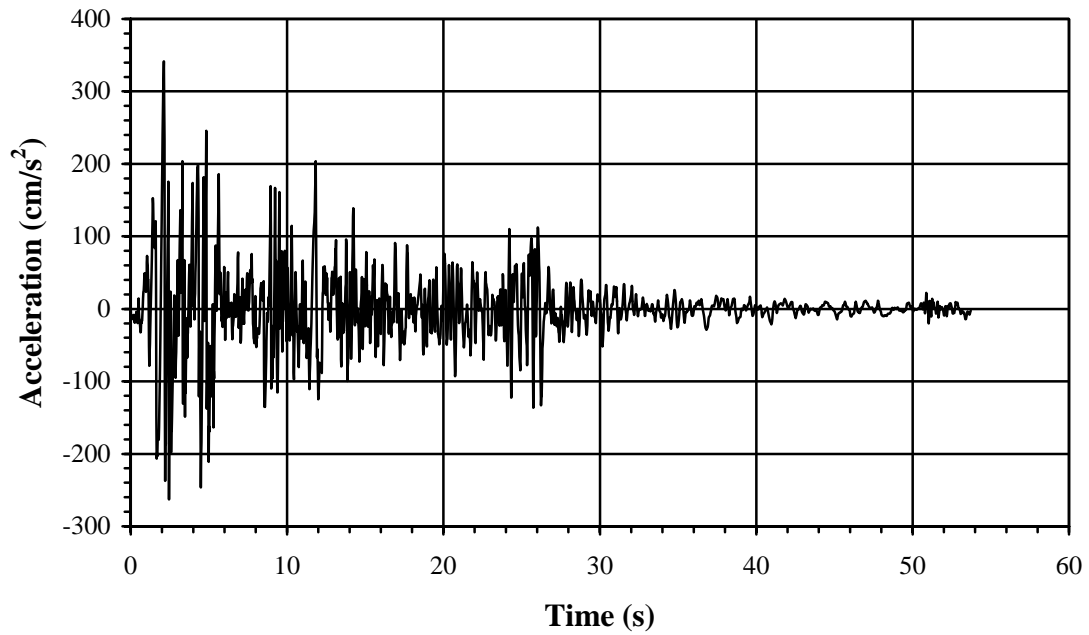


**FIG. 6.37. Acceleration Record from 1940 El Centro, CA Earthquake**

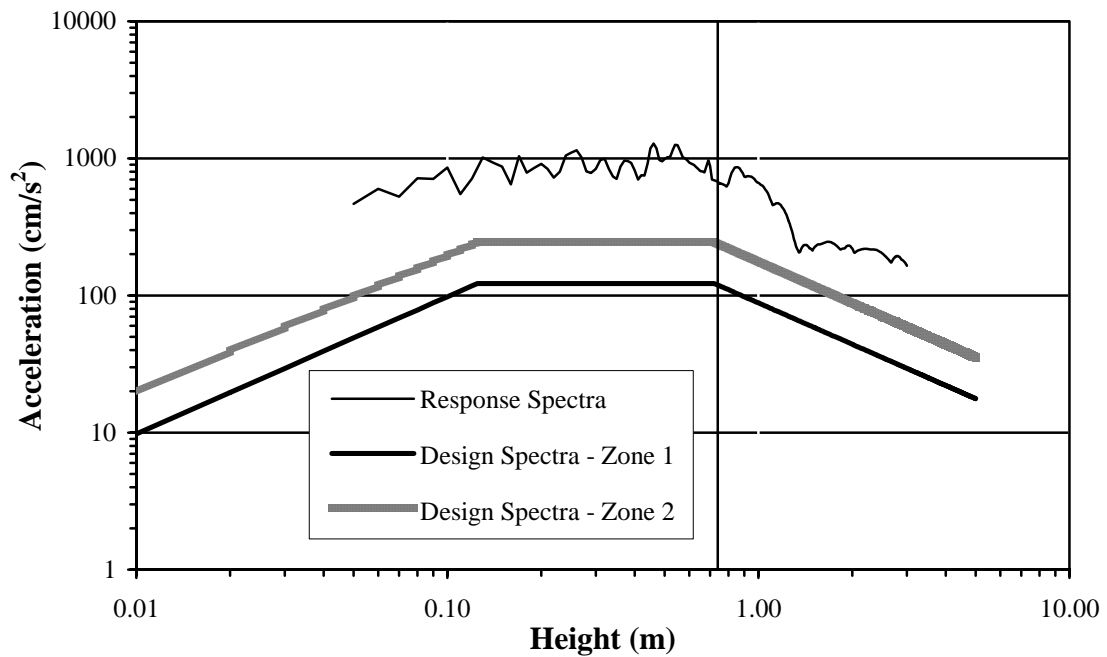


**FIG. 6.38. Response Spectra and API Design Spectra**

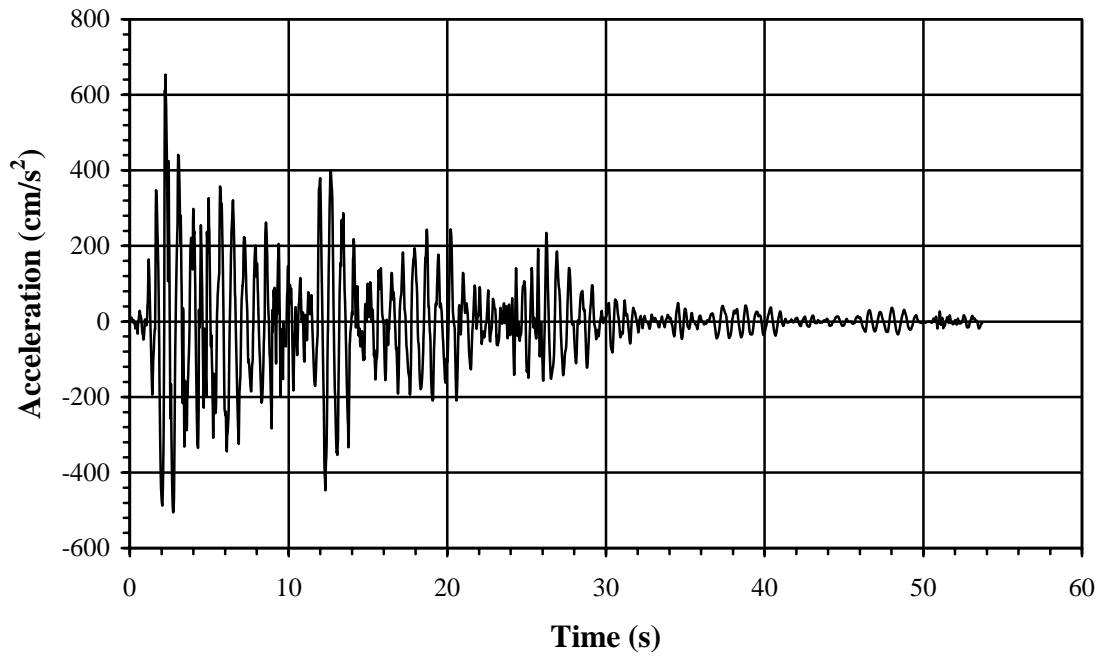


**FIG. 6.39. Accelerations Obtained from Time History Analysis**

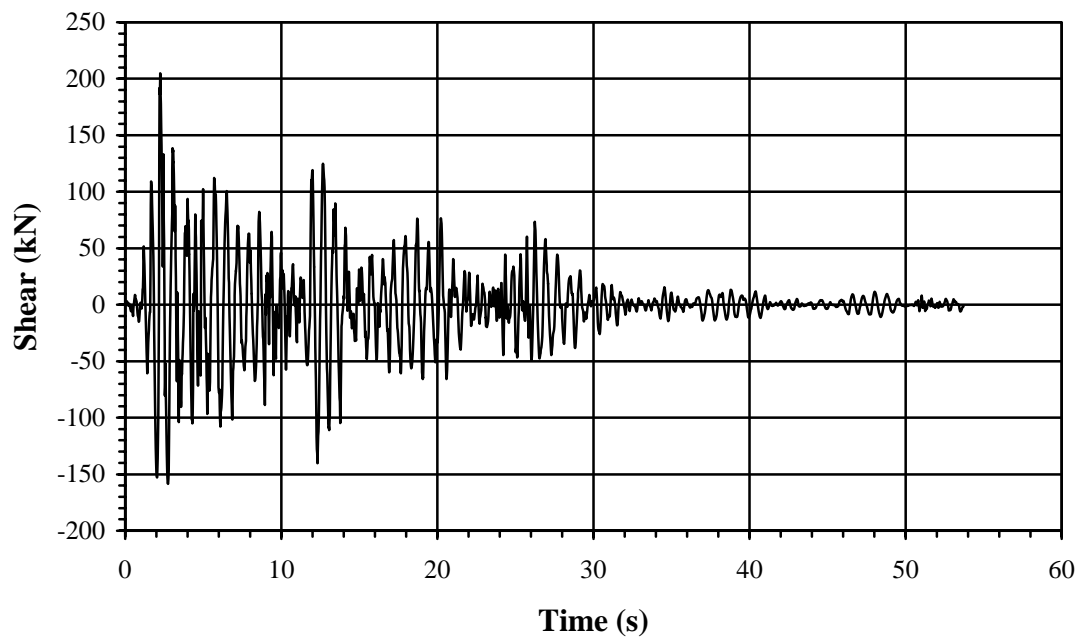


**FIG. 6.40. Shear Forces Obtained from Time History Analysis**

#### 6.4. CONCLUSION

The results from this study show that the height, mass, and fixity of the SDOF model have the greatest effect on the response of the model to earthquake loading. In general, increasing the mass and height of the model caused the stress and displacement values to increase. Fixing the casing against rotation at the mass location caused the stress values to increase. As the height of the casing increased, the bending stress decreased. As expected, increasing the casing sizes caused the stresses and displacement values to decrease. Variation of the mudline strength and strength gradient parameters, within the ranges used in this study, did not cause significant changes in the stresses or displacements.

The SSR values obtained from both the parametric study and time history analysis were typically very small. The maximum CSR values obtained from the parametric study and the time history analysis approach 0.7, however, these values never exceed this limit. The stresses induced by Zones 1 and 2 accelerations are not substantial in comparison to other possible lateral loads applied to subsea systems, such as riser loads. Finally, the maximum displacement value obtained from the time history analysis is about 30 percent larger than the maximum value obtained from the parametric study.

## 7. SUMMARY AND CONCLUSIONS

### 7.1. SUMMARY

The number of deepwater subsea systems in the GOM continues to increase due to technological advances and the ever increasing demand for energy. Since the GOM is rather benign for earthquake potential, API does not require that offshore structures in this region be designed for earthquakes. As a result, questions have been raised regarding their seismic vulnerability. Earthquake shaking, liquefaction potential, and soil sliding due to slope instability are three earthquake related factors that can impact the performance of subsea structures. The focus of this research was to evaluate the performance of these systems in deepwater environments in the GOM during potential earthquake shaking.

The first task of this study was to review available information on the seismicity of the GOM. As demonstrated by the seismic zone rating applied to this region, the seismic risk in the GOM is considered to be low. However, a number of earthquakes have been recorded in this region, most with Richter magnitude values greater than 3.0. The largest recorded event, which occurred in the Mississippi Fan area, had a Richter magnitude of 4.9. The second task of this research was to survey the range of systems used in subsea applications. These structures included subsea wellheads, subsea Christmas trees, templates and manifolds; all of which are supported by either single or multiple casing foundations, depending on the application and design requirements. In

addition, a survey of the deepwater subsea systems located in the Gulf of Mexico was conducted. Most of the systems included in this survey are located in the vicinity of the grouping of earthquake epicenters in the Mississippi Fan area.

The models, parametric study, and analysis procedures were based on the information gathered on subsea systems and earthquakes in the Gulf of Mexico. In addition, a survey of the current practices for the structural design of offshore structures provided critical information for the analyses. The prototype structure selected for this study was a single wellhead subsea Christmas tree embedded in clay soils typical of the Gulf of Mexico. The baseline analytical model was derived from the prototype structure, and the parameters chosen for variation included the mass, height, base fixity, and soil properties. The soil-casing stiffness, accelerations, and corresponding stresses were determined using the BMCOL76 program and the response spectra method. In addition, a time history analysis of the baseline analytical model was conducted using the ground motion record obtained from the 1940 El Centro, California earthquake.

## 7.2. CONCLUSIONS

The following conclusions were made based on the results of the study.

1. A review of the information available on the GOM, classified by API RP2A as a Zone 0 seismic risk area, confirms that the seismicity of this area is relatively low.
2. Model subsea wells were analyzed with Zone 1 and Zone 2 seismic accelerations to provide a conservative bound for Zone 0 area such as the Gulf of Mexico. In general, the stresses produced by the simulated earthquake loads are relatively negligible for the free-headed casing models in Zones 1 and 2 accelerations. As with the free-headed casing models, most of stress ratio values observed for the fixed-headed models were well within the allowable limits for the selected earthquake loads. Maximum CSR values obtained from the parametric study approach, but never exceed, the limiting ratio value of 0.7 for seismic loading. In addition, the displacements induced in the analytical models by these loads also seem to be within the range of values that could be reasonably expected to occur during the course of normal operating conditions. These conditions include pipeline shifting and movement caused from the tension in the attached risers.
3. The results from the parametric study indicate that the base fixity, mass, and height parameters have the greatest effect on the response of the subsea structure to lateral loading. Increasing the mass and height parameters of the free-headed casing models, which simulate the responses of single casing structures, generally caused

the stress and displacements due to lateral loading to increase. Although the shear and bending stresses obtained from the fixed-headed models were higher than those obtained from the corresponding free-headed models, the stress values decreased as the height of the casing increased above the mudline. The CSR values observed for the fixed-headed models ranged between 0.14 and 0.64. The range of CSR values obtained for the free-headed casing models was between 0.04 and 0.64.

4. The period, mass, height of the casing above the mudline, and base fixity dictate the magnitude of stress and displacement values observed in the casing. When the mass, height, and fixity remain unchanged; the stress and displacement values did not vary for period values between 0.125 and 0.72 seconds. For periods between 0.0 and 0.125 seconds, the stress and displacement values increase. Finally, these values decreased as the period increased above 0.72 seconds.
5. A time history analysis was completed to compare with the parametric analysis.

The El Centro earthquake ground motion was used; ground accelerations are 6X those for API Zone 1 and 3X those for Zone 2. Even with these conservative ground motions, the results show that the maximum SSR value obtained from the baseline free-headed casing model for the El Centro ground motion record falls well below the limiting stress ratio for earthquake loads. It should be noted that the maximum CSR value, 0.66, is close to the limiting ratio of 0.7. Although the largest displacement value is greater than the values obtained from the parametric study, this value should still fall within the range of allowable displacements for subsea structures.

### **7.3. RECOMMENDATIONS**

1. The impact of earthquake shaking on the integrity of a single and multiple casing foundation subsea structures is dependent upon a number of different factors that are specific to site and system requirements. Seismic risk for proposed projects should be investigated for specific site conditions and equipment constraints. Specific design information for a subsea system is critical in making a final assessment of the expected performance under site specific ground motions.
2. Based on the results from this study, earthquake shaking (within Zones 1 and 2 PGA values) should not dramatically impact the performance of deepwater subsea structures in the GOM. However, further research should be conducted to determine the impact of sliding soil due to soil instability on the performance of these structures in the GOM.

## REFERENCES

- American Petroleum Institute (API). (1996). "Recommended Practice for Design and Operation of Subsea Production Systems." *API-RP17A*, 2<sup>nd</sup> ed., Washington, D.C.
- American Petroleum Institute (API). (2000a). "Recommended Practice for Planning, Designing, and Constructing Fixed Offshore Platforms - Working Stress Design." *API-RP2A*, 21<sup>st</sup> ed., Washington D.C.
- American Petroleum Institute (API). (2000b). "Recommended Practice for Planning, Designing, and Constructing Fixed Offshore Platforms – Load and Resistance Factor Design." *API-RP2A*, 21<sup>st</sup> ed., Washington D.C.
- BMCOL76* (1981). The Earth Technology Corporation, Long Beach, CA.
- Bea, R.G. (1999). "Reliability Based Earthquake Design Guidelines for Marine Structures." *J. of Waterway, Port, Coastal, and Ocean Engrg.*, ASCE, 125(5), 219 - 231.
- Bednar, J.M. (1993). "The Zinc Subsea Production System: An Overview." *Proc. Offshore Technol. Conf., OTC 7283, Society of Petroleum Engineers, Houston, TX., May 217- 225.*
- Beer, P., Ribbeck, L. and Jeffries, A. (2000). "Gemini Subsea System Design." *Proc. Offshore Technol. Conf., OTC 11866, Society of Petroleum Engineers, Houston, TX., May 41-49.*
- Boore, D.M. and Smith, C.E. (1999). "Analysis of Earthquake Recordings Obtained from the Seafloor Earthquake Measurement System (SEMS) Instruments Deployed Off the Coast of Southern California." *Bulletin of the Seismological Society of America*, 89(1), 260-274.

- Boote, D. and Mascia, D. (1994). "Anti-seismic Design Methodologies Applied to Offshore Structures." *Marine, Offshore, and Ice Technology*, T. K. S. Murphy, P. A. Wilson, and P. Wadhams, eds., Computational Mechanics Publications, Southampton, 99-112.
- Boote, D., Mascia, D., and Caffarena, R. (1998). "Seismic Behaviour of Fixed Offshore Platforms." *17<sup>th</sup> Inter. Conf. Offshore Mechanics and Arctic Engr.*, OMAE98-0332, American Society of Mechanical Engineers, Lisbon, Portugal, July, 1-11.
- Bruschi, R., Gudmestad, O.T., Blaker, F., and Nadim, F. (1996). "Seismic Assessment for Offshore Pipelines." *J. of Infrastructure Systems*, 2(3), 145-151.
- Chan, H.S.Y. (1987). "Earthquake Response Spectrum Analysis of Offshore Platforms." *Engr. Structures*, 9, 272-276.
- Chopra, A.K. (1995). *Dynamics of Structures: Theory and Applications to Earthquake Engineering*, Upper Saddle River, NJ.
- Coleman, E. and Isenmann, G. (2000). "Overview of the Gemini Subsea Development." *Proc. Offshore Technol. Conf., OTC 11863, Society of Petroleum Engineers*, Houston, TX., May, 11-17.
- Consiglio Nazionale delle Ricerche (1984). "Norme tecniche per le costruzioni in zone sismiche." *Documento di studio a cura del Gruppo Nazionale per la Difesa dai Terremoti*.
- Consortium of Organizations for Strong Motion Observation Systems (COSMOS). (2003). COSMOS Virtual Data Center, "El Centro, CA 1940 05 18 2037 PST." <<http://db.cosmos-eq.org/scripts/event.plx?evt=88>>. (July 10, 2003).

- Cox, W.R. and McCann, J.W. (1986). "Analysis of Laterally Loaded Piles." *Planning and Design of Fixed Offshore Platforms*, B. McClelland and M.D. Reifel, eds., Van Nostrand Reinhold Company, New York, 801-832.
- Crouse, C.B. (1996). "Seismic Exposure and Site Response Characteristics for Offshore Platform Design." *Proc. Offshore Technol. Conf., OTC 8105, Society of Petroleum Engineers*, Houston, TX., May, 757-761.
- SAP2000. (1999). Computers and Structures, Inc., 1995 University Avenue, Berkeley, CA.
- Dean, R.G. and Borgman, L.E., (1986). "Wind and Wave Forces." *Planning And Design of Fixed Offshore Platforms*, B. McClelland and M.D. Reifel eds., Van Nostrand Reinhold Company, New York, 317-363.
- Deluca, M. (2002). "Thinking Big, Delving Deeper." *Offshore Engineer*, April, 23-33.
- Frohlich, C. (1982). "Seismicity of the Central Gulf of Mexico." *Geology*, 10, 103-106.
- GEODAS. (1998). National Geophysical Data Center, 325 Broadway, Boulder, CO.
- Goodfellow Associates (1990). *Applications of Subsea Systems*, Pennwell Publishing Company, Tulsa, OK.
- Han, R.P.S., and Xu, H. (1996). "Simple and Accurate Added Mass Model for Hydrodynamic Fluid-Structure Interaction Analysis." *J. of the Franklin Institute*, 333B(6), 929-945.
- Ibrahim, A.K., Carye, J., Latham, G. and Buffler, R. T. (1981). "Crustal Structure in the Gulf of Mexico from OBS Refraction and Multichannel Reflection Data." *American Association of Petroleum Geologists Bulletin*, 65, 1207-1229.

- Jones, W.T. (1985). "Deepwater Pipeline Environmental Design Conditions." *Proc. International Offshore Mechanics and Arctic Engr. Symposium*, Dallas, TX, February, 451- 466.
- Kershenbaum, N.Y, Choi, and H.S., Mebarkia, S.A. (1998). "Subsea Pipeline Behavior Under Seismic Impact." *Proc. 8<sup>th</sup> Inter. Offshore and Polar Engr. Conf., International Society of Offshore and Polar Engineering*, Montreal, Canada, May, 86- 93.
- Kvaerner (2001). "Advertisement in Offshore." *Offshore*. December, 61 (12), 31.
- Liaw, C.Y. and Reimer, R.B. (1975). "Hydrodynamic Interaction Effects on the Cylindrical Legs of Deepwater Platforms." *Proc. Offshore Technol. Conf., OTC 2324, Society of Petroleum Engineers*, Houston, TX., May, 777-786.
- Matlock, H. (1970). "Correlations for Design of Laterally Loaded Piles in Soft Clay." *Proc. Offshore Technol. Conf., OTC 1204, Society of Petroleum Engineers*, Houston, TX., May, 577-594.
- McInturff, T.L., and Gist, G. N. (1993). "An Overview of the Zinc Subsea Tree and Wellhead System." *Proc. Offshore Technol. Conf., OTC 7284, Society of Petroleum Engineers*, Houston, TX., May, 227-234.
- McLaughlin, D.C. (1998). "Mensa Project: An Overview." *Proc. Offshore Technol. Conf., OTC 8576, Society of Petroleum Engineers*, Houston, TX., May, 9-20.
- Michalopoulos, A.P., Johnson, W.J., and Levadoux, J.N. (1984). "Seismic Design of Foundations for Offshore Structures." *Underwater Technology*, 10(1), 15-22.

- Minerals Management Service (MMS). (2003a). "East Breaks, Gulf of Mexico Region Lease Information." <<http://www.gomr.mms.gov/homepg/lseale/ng15-01.pdf>>. (July 14, 2003).
- Minerals Management Service (MMS). (2003b). "Desoto Canyon, Gulf of Mexico Region Lease Information." <<http://www.gomr.mms.gov/homepg/lseale/nh16-11.pdf>>. (July 14, 2003).
- Minerals Management Service (MMS). (2003c). "Green Canyon, Gulf of Mexico Region Lease Information." <<http://www.gomr.mms.gov/homepg/lseale/ng15-03.pdf>>. (July 14, 2003).
- Minerals Management Service (MMS). (2003d). "Garden Banks, Gulf of Mexico Region Lease Information." <<http://www.gomr.mms.gov/homepg/lseale/ng15-02.pdf>>. (July 14, 2003).
- Minerals Management Service (MMS). (2003e). "Mississippi Canyon, Gulf of Mexico Region Lease Information." <<http://www.gomr.mms.gov/homepg/lseale/nh16-03.pdf>>. (July 14, 2003).
- Nair, D. and Kallaby J. (1986). "Earthquake, Wave, and Other Dynamic Considerations." *Planning and Design of Fixed Offshore Platforms*, B. McClelland and M.D. Reifel, eds., Van Nostrand Reinhold Company, New York, 720-759.
- Newmark, N.M. and Hall, W.J. (1987). *Earthquake Spectra and Design*, M. S. Agbabian, ed., Earthquake Engineering Research Institute, Urbana-Champaign, IL.
- Offshore Technology (2002a). "Canyon Express Gas Field Mississippi Canyon, USA, Industry Projects." <<http://www.offshore-technology.com/projects/canyon/index.html>>. (January 14, 2002).

- Offshore Technology (2002b). "Hoover Diana Gulf of Mexico, Industry Projects." <<http://www.offshore-technology.com/projects/hoover/index.html>>. (January 14, 2002).
- Offshore Technology (2003c). "Manatee Gulf of Mexico, Industry Projects." <<http://www.offshore-technology.com/projects/manatee/index.html>>. (January 14, 2003).
- Offshore Technology (2003d). "Mensa Gulf of Mexico, Industry Projects." <<http://www.offshore-technology.com/projects/mensa/index.html>>. (January 14, 2003).
- Offshore Technology (2003e). "Troika Gulf of Mexico, Industry Projects." <<http://www.offshore-technology.com/projects/troika/index.html>>. (July 14, 2003).
- Rao, P.M. and O'Neill, M.W. (1997). "Important Consideration for Seismic-Resistant Design of Offshore Piles." *Proc. 7<sup>th</sup> Inter. Offshore and Polar Engr. Conf., International Society of Offshore and Polar Engineering*, Honolulu, HI, May, 745-752.
- Reese, L.C. and Wang, S.T. (1986). "Method of Analysis of Piles Under Lateral Loading." *Marine Geotechnology and Nearshore/Offshore Structures*, R.C. Chaney and H. Y. Fang, ed. Philadelphia, PA, 199-211.
- Shell Exploration and Production Company (SEPCo). (2002a). "Europa Subsea Development." <<http://www.shellus.com/sepco/where/offshore/europa.htm>>. (January 14, 2002).
- Shell Exploration and Production Company (SEPCo). (2002b). "Macaroni Subsea Development." <<http://www.shellus.com/sepco/where/offshore/europa.htm>>. (January 14, 2002).

Smith, C.E. (1997). "Dynamic Response of a Steel-Jacket Platform Subject to Measured Seafloor Earthquake Ground Accelerations.", *8<sup>th</sup> Inter. Conf. Behavior of Offshore Structures*, Netherlands, 197-211.

United States Geological Survey (USGS). (2002). "NEIC – Worldwide Earthquake Catalog Search." <[http://neic.usgs.gov/neis/epic/epic\\_rect.html](http://neic.usgs.gov/neis/epic/epic_rect.html)>. (June 10, 2002).

## **APPENDIX A**

### **SAMPLE CALCULATIONS**

#### **A.1. INTRODUCTION**

A sample of the calculations performed for the parametric study is presented in this appendix. The calculations shown below were conducted using the baseline model properties. Section A.2 describes the procedures used to determine the required input values for the BMCOL76 program. Section A.3 outlines the procedures used to calculate the period, soil-casing stiffness, and shear force values. Section A.4 presents the calculations used to determine the stresses and stress ratios.

#### **A.2. CALCULATION INPUT VALUES FOR BMCOL76**

This section deals with the calculation of the required input values for the BMCOL76 analysis. Table A.1 presents soil and casing properties for the baseline model and Table A.2 presents the  $p$ - $y$  curve values for soft clays (also shown in Section 5). A maximum embedded depth of 30.5 feet was assumed for the casing analysis. For this model, the quantity of  $y_c$  is equal to 19.1 mm (see Table A.2). Eqs. A.1 and A.2 were used to determine the lateral resistance of the soil along the casing length (refer to Section 5 for more details). The values obtained at the stations located at 0.0, 6.10, 12.2 and 30.5 m below the mudline are presented in Table A.3. These results were input into the BMCOL76 program where remaining resistance values were interpolated.

$$p_u = 3c + \gamma X + \frac{JcX}{D} \quad \text{for } 0 \leq X < X_R \quad (\text{A.1})$$

$$p_u = 9c \quad \text{for } X \geq X_R \quad (\text{A.2})$$

**TABLE A.1. Required Soil and Casing Properties for BMCOL76 Analysis**

Variable	
Casing Outside Diameter (mm)	762
Casing Wall Thickness (mm)	25.4
Height Above Mudline (m)	2.44
Soil Unit Weight (MN/m <sup>3</sup> )	12.2
Mudline Strength (kPa)	4.79
Strength Gradient (kPa/m)	0.48
J	0.5
$\epsilon_c$	0.01
Length Increment (m)	0.305
Young's Modulus (kPa)	$2.00 \times 10^8$
I (m <sup>4</sup> )	$3.99 \times 10^{-3}$
EI (kN-m <sup>2</sup> )	798,242

**TABLE A.2. P-y Curve Values for Soft Clays (API 2000 a,b)**

$p/p_u$	$y/y_c$
0.00	0.00
0.50	1.00
0.72	3.00
1.00	8.00
1.00	$\infty$

Where:

- $p$  = Actual lateral resistance (kPa)
- $p_u$  = Lateral bearing capacity (kPa)
- $y$  = Actual lateral deflection (mm)
- $y_c$  =  $2.5 * \epsilon_c * D$  = Lateral deflection related to  $\epsilon_c$  (mm)
- $D$  = Pile diameter (mm)
- $\epsilon_c$  = Strain which occurs at half of the maximum stress on laboratory undrained compression tests of undisturbed soil samples (assumed to be as 0.01 for this study)

**TABLE A.3. Lateral Soil Resistance Properties for BMCOL76 Input**

<b>Depth (m)</b>	<b><math>p_u</math> (Eq. A.1) (kPa)</b>	<b><math>p_u</math> (Eq. A.2) (kPa)</b>	<b><math>p_{u(min)}</math> (kPa)</b>
0.00	35.9	108	35.9
6.10	359	323	323
12.2	874	539	539
30.5	3,570	1,190	1,190

### **A.3. CALCULATION OF SOIL-CASING STIFFNESS**

This section presents the calculations used to determine the period, soil casing stiffness and shear forces for the baseline model. The following deflection values, shown in Table A.4, were taken from the BMCOL76 results file and a graph of the corresponding force-displacement curve is shown in Fig. A.1. Eqs. A.3 to A.5 (refer to Section 5 for more details) and the API design spectra shown in Fig. 5.5 are then used to calculate the soil-casing stiffness, period and shear force values. Note that the PGA values for Zones 1 and 2 are 0.05g and 0.10g, respectively. As shown in Tables A.5 and A.6, a number of interpolations were performed until the soil-casing stiffness values converged. A summary of the results obtained from these calculations are presented in Table A.7.

$$\omega = \sqrt{\frac{k}{m}} \quad (\text{A.3})$$

$$T = \frac{2\pi}{\omega} \quad (\text{A.4})$$

$$F = m * S_A \quad (\text{A.5})$$

**TABLE A.4. Deflections Obtained from BMCOL76**

Force (kN)	Maximum Tip Displacement (mm)
0.00	0.00
44.5	11.4
111	29.5
222	77.3
445	240
667	540
890	888

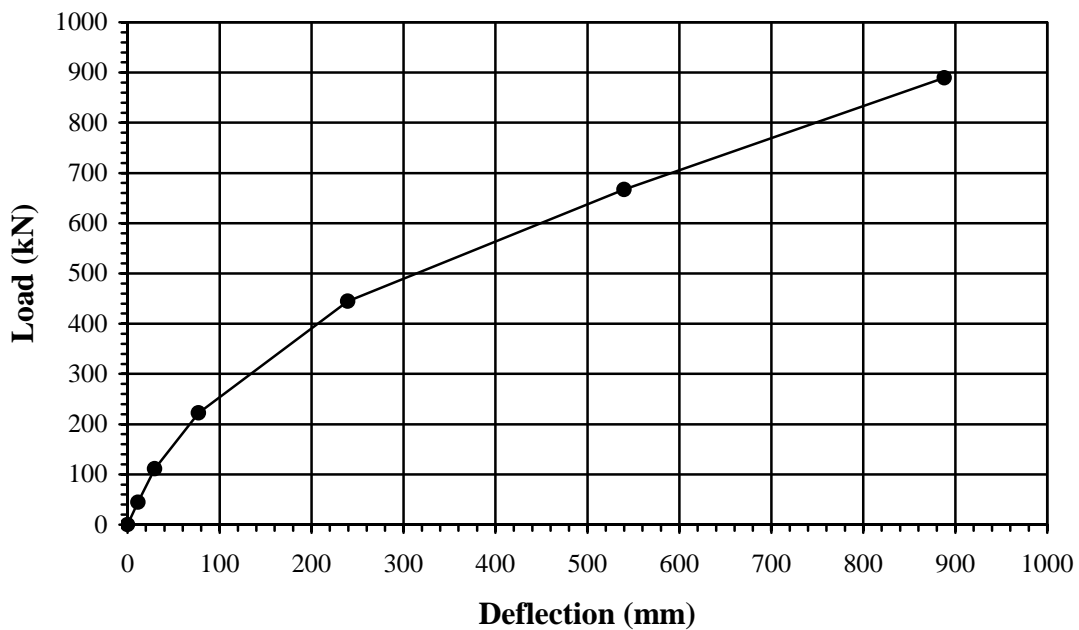


**FIG. A.1. Force-Displacement Curve for Baseline Analytical Model.**

**TABLE A.5. Soil-Casing Calculations for Zone 1**

Iteration	Force (kN)	Disp. (mm)	k	$\omega$ (rad/s)	T (s)	$S_A/G$	$S_A$	$F_{m^*a}$ (kN)
1	445	342	1.30	6.43	0.98	1.84	0.90	28.4
2	28.4	13.7	2.07	8.12	0.77	2.32	1.14	35.8
3	35.8	17.3	2.07	8.11	0.77	2.32	1.14	35.8

Where:

$$G = 0.49 \text{ (m/s}^2\text{)}$$

**TABLE A.6. Soil-Casing Calculations for Zone 2**

Iteration	Force (kN)	Disp. (mm)	k	$\omega$ (rad/s)	T (s)	$S_A/G$	$S_A$ (m/s <sup>2</sup> )	$F_{m^*a}$ (kN)
1	445	342	1.30	6.43	0.98	1.84	1.81	56.81
2	56.8	28.5	2.00	7.97	0.79	2.28	2.24	70.39
3	70.4	36.1	1.95	7.88	0.80	2.26	2.22	69.6
4	69.5	35.6	1.95	7.88	0.80	2.26	2.22	69.6
5	69.6	35.7	1.95	7.88	0.80	2.26	2.22	69.6

Where:

$$G = 0.98 \text{ (m/s}^2\text{)}$$

**TABLE A.7. Summary of Results from Soil-Casing Calculations**

Parameter	Zone 1	Zone 2
k	2.07	1.95
T	0.77	0.80
$S_A$ (m/s <sup>2</sup> )	1.14	2.26
Shear Force	35.8	69.6

#### A.4. CALCULATION OF STRESSES AND DISPLACEMENTS

This section presents the stress and stress ratio calculations. In order to determine the final bending moment and maximum tip displacement, the baseline model is reanalyzed in the BMCOL76 program, using shear force value obtained from the previous section.

The maximum displacements and bending moments were obtained from the results of the analysis. The shear and bending stresses are calculated using Eqs. A.6 and A.7 and the allowable axial, shear and bending stresses are calculated using Eqs. A.8 to A.11 (see Section 5 for more details). The steel casing has a material yield strength of 248,000 kPa. The shear stress ratio (SSR) is calculated using Eq. A.12 and the CSR is calculated using Eqs. A.13 to A.15. The results of these calculations are shown in Table A.8. Figs. A.2 to A.7 depict the displacement, shear force and bending moment profiles along the length of the casing. Note that a 70 percent increase in the allowable stresses is permitted for the seismic loading.

$$f_v = \frac{F}{A} \quad (\text{A.6})$$

$$f_b = \frac{Mc}{I} \quad (\text{A.7})$$

$$F_a = \frac{\left[1 - \frac{(Kl/r)^2}{2C_c^2}\right] F_y}{5/3 + \frac{3(Kl/r)}{8C_c} - \frac{(Kl/r)^3}{8C_c^3}} \quad \text{for } Kl/r < C_c \quad (\text{A.8})$$

$$F_a = \frac{12\pi^2 E}{23(Kl/r)^2} \quad \text{for } Kl/r \geq C_c \quad (\text{A.9})$$

$$F_b = 0.75F_y \quad (\text{A.10})$$

$$f_v = 0.4F_y \quad (\text{A.11})$$

$$SSR = \frac{f_{vcal}}{f_v} \leq 1.0 \quad (\text{A.12})$$

$$CSR = \frac{f_a}{1.7 * F_a} + \frac{C_m \sqrt{f_{bx}^2 + f_{by}^2}}{1.7 * (1 - \frac{f_a}{F'_e}) F_b} \leq 1.0 \quad (\text{A.13})$$

$$CSR = \frac{f_a}{1.7 * (0.6F_y)} + \frac{\sqrt{f_{bx}^2 + f_{by}^2}}{1.7 * F_b} \leq 1.0 \quad (\text{A.14})$$

$$CSR = \frac{f_a}{1.7 * F_a} + \frac{\sqrt{f_{bx}^2 + f_{by}^2}}{1.7 * F_b} \leq 1.0 \quad \text{for } \frac{f_a}{F_a} \leq 0.15 \quad (\text{A.15})$$

**TABLE A.8. Summary of Displacement and Stress Results**

<b>Parameter</b>	<b>Zone 1</b>	<b>Zone 2</b>
Displacement (mm)	17.3	33.8
Shear Stress (kPa)	609	1,183
Overturning Moment (kN-m)	87.3	170
Bending Stress (kPa)	17,000	33,300
Shear Stress Ratio	0.012	0.024
CSR	0.048	0.073

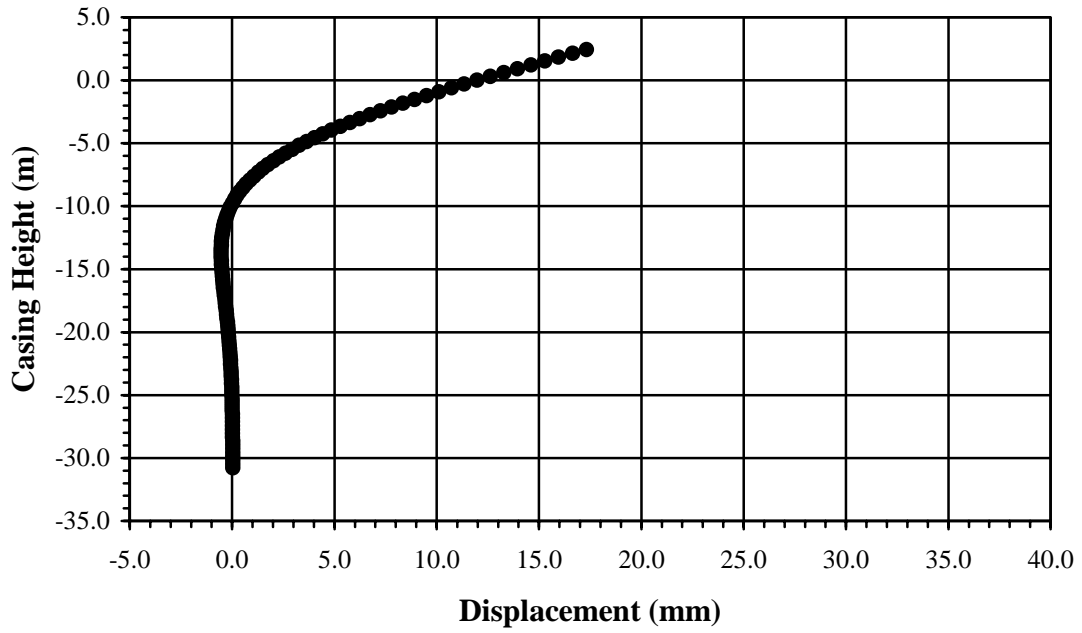


**FIG. A.2. Zone 1 Casing Displacement Profile**

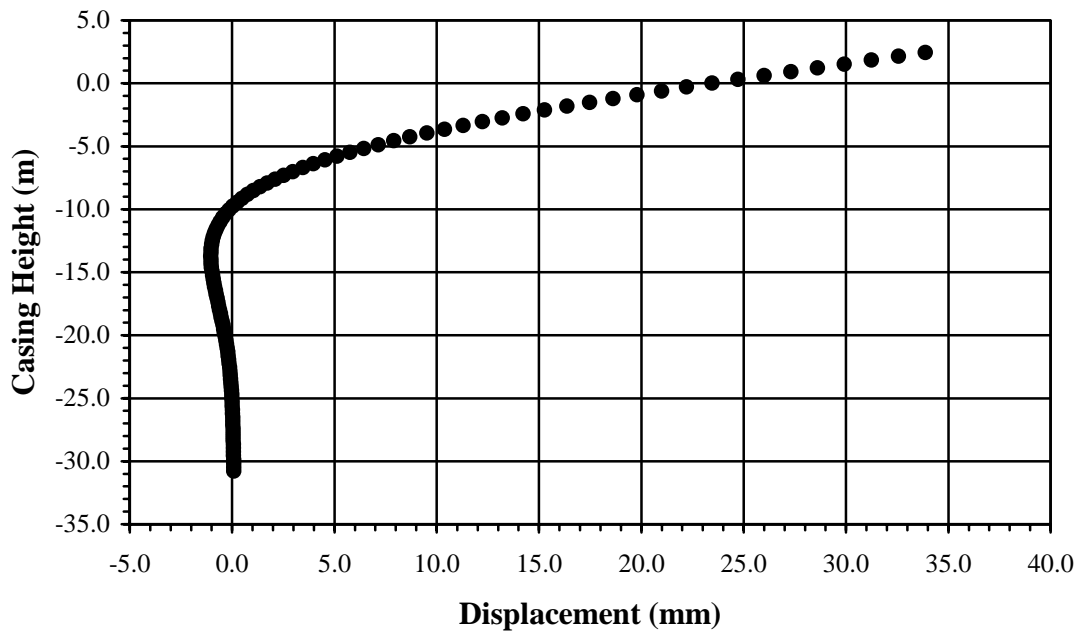


**FIG. A.3. Zone 2 Casing Displacement Profile**

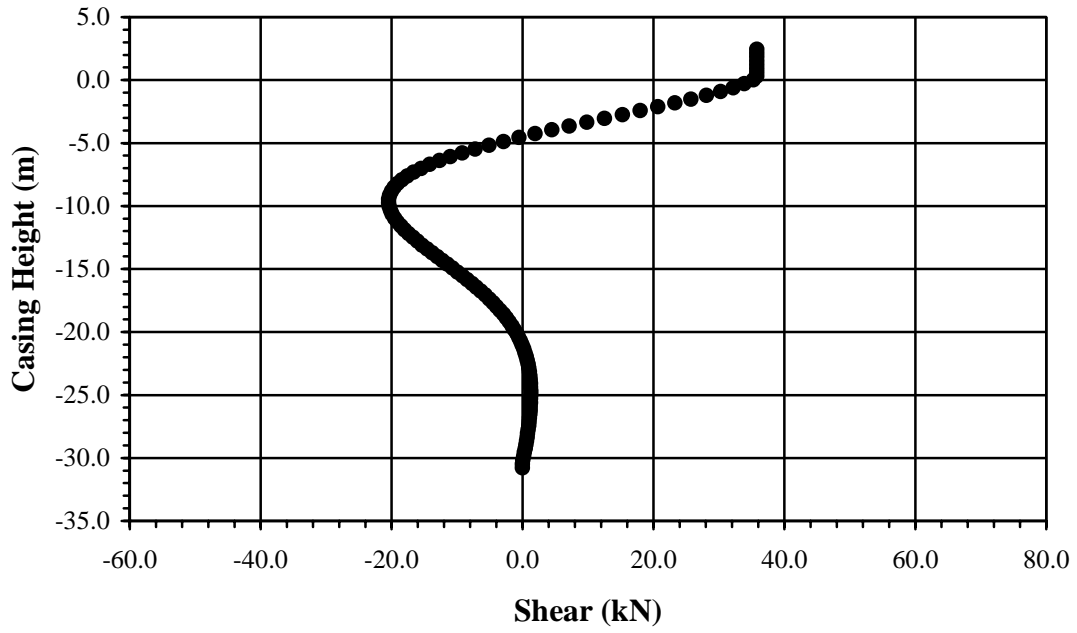


**FIG. A.4. Zone 1 Casing Shear Profile**

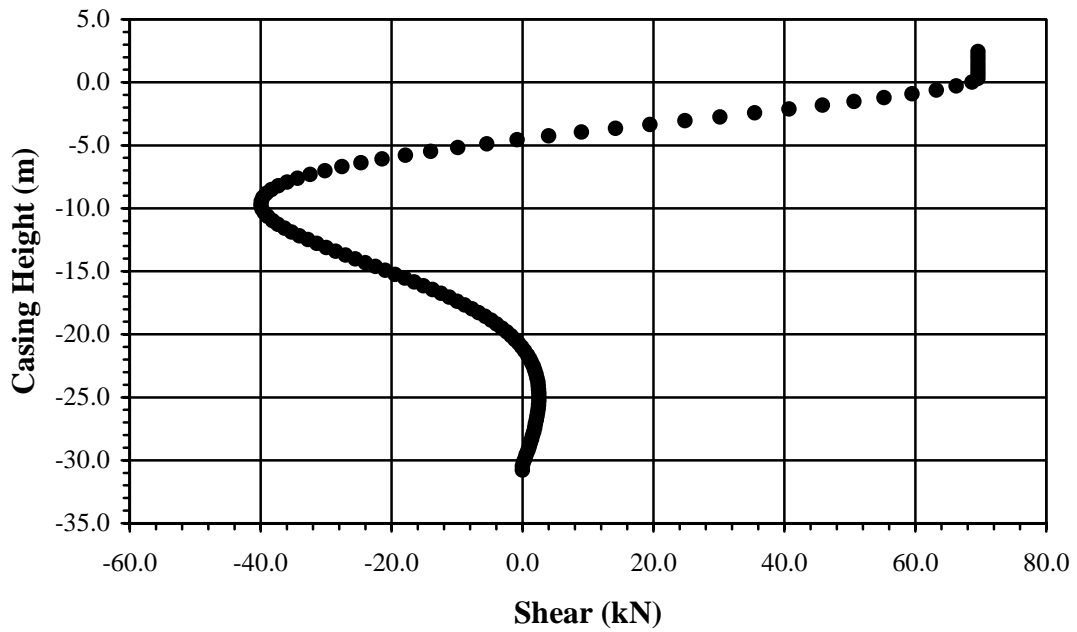


**FIG. A.5. Zone 2 Casing Shear Profile**

